NACA

RESEARCH MEMORANDUM

EFFECT OF COMPRESSIBILITY AND CAMBER AS DETERMINED FROM AN INVESTIGATION OF THE NACA 4-(3)(08)-03 AND 4-(5)(08)-03 TWO-BLADE PROPELLERS UP TO FORWARD MACH NUMBERS OF 0.925

By Melvin M. Carmel, Francis G. Morgan, Jr.,
and Domenic A. Coppolino

Langley Aeronautical Laboratory
Langley Air Force Base, Va.

NATIONAL ADVISORY COMMITTEE
FOR AERONAUTICS
WASHINGTON
June 29, 1950

NATIONAL ADVISORY COMMITTEE FOR AERONAUTICS

RESEARCH MEMORANDUM

EFFECT OF COMPRESSIBILITY AND CAMBER AS DETERMINED FROM AN INVESTIGATION OF THE NACA 4-(3)(08)-03 AND 4-(5)(08)-03 TWO-BLADE PROPELLERS UP TO FORWARD MACH NUMBERS OF 0.925

By Melvin M. Carmel, Francis G. Morgan, Jr., and Domenic A. Coppolino

SUMMARY

Tests of the NACA 4-(3)(08)-03 and NACA 4-(5)(08)-03 two-blade propellers were conducted in the Langley 8-foot high-speed tunnel for blade angles between 40° and 65° and through a Mach number range up to 0.925.

The results show that if the outboard sections of a propeller are the thinnest, the design of propellers in the supercritical Mach number range should incorporate loading distributions which are concentrated at the tip sections. The characteristics of the NACA 4-(5)(08)-03 propeller at maximum efficiency are superior to those for the NACA 4-(3)(08)-03 propeller for take-off and climb operation; they are about the same for high-speed operation. The trend of the force-test results is accurately reflected in the wake results presented in this paper.

INTRODUCTION

A limited analysis of the effects of compressibility on the NACA 4-(5)(08)-03 propeller is presented in reference 1. A similar analysis of the effects of design camber comparing the NACA 4-(3)(08)-03 and NACA 4-(5)(08)-03 propellers is presented in reference 2. Only force-test results were presented in these papers.

Wake measurements were taken behind these propellers in order to provide an insight into their elemental characteristics, and section-thrust-coefficient curves obtained from these measurements are presented

herein. Low-speed characteristics of propellers have already been thoroughly investigated and, therefore, this paper is presented with high-speed propeller characteristics as a prime consideration. A further analysis of the force-test results for both the NACA 4-(3)(08)-03 and NACA 4-(5)(08)-03 propellers is also included herein.

SYMBOLS

b	blade width, feet
c_{l_d}	section design lift coefficient
C_P	power coefficient $\left(\frac{P}{\rho n^3 D^5}\right)$
C_T	thrust coefficient $\left(\frac{T}{\rho n^2 D^4}\right)$
D	propeller diameter, feet
b/D	blade-width ratio
h	maximum thickness of blade section, feet
h/b	blade-thickness ratio
J	advance ratio $\left(\frac{V_o}{nD}\right)$
M	tunnel-datum (forward) Mach number (tunnel Mach number uncorrected for tunnel-wall constraint)
M_t	helical-tip Mach number $\left(M\sqrt{1+\left(\frac{\pi}{J}\right)^2}\right)$
n	propeller rotational speed, revolutions per second
P	power, foot-pounds per second
q	dynamic pressure $\left(\frac{\rho V^2}{2}\right)$
R	propeller-tip radius, feet
r	blade-section radius, feet

[redacted]

r_w	wake-section radius, feet
T	thrust, pounds
T_c	thrust disk-loading coefficient $\left(\frac{T}{2qD^2}\right)$
V	tunnel-datum velocity (tunnel velocity uncorrected for tunnel-wall constraint), feet per second
V_o	equivalent free-air velocity (tunnel-datum velocity corrected for tunnel-wall constraint), feet per second
x	blade-section station (r/R)
x_w	wake station (r_w/R)
ρ	air density, slugs per cubic foot
β	section blade angle, degrees
$\beta_{0.75R}$	blade angle at 0.75 radius, degrees
η_{max}	maximum efficiency
$\frac{dC_T}{dx_w}$	section thrust coefficient

APPARATUS, METHODS, AND TESTS

The tests presented herein were conducted in the Langley 8-foot high-speed tunnel with the same apparatus and methods as those previously described in reference 1. A sketch of the 800-horsepower dynamometer as installed in the tunnel is included as figure 1.

Blade-form curves are presented in figure 2 and are the same for both the NACA 4-(3)(08)-03 and NACA 4-(5)(08)-03 propellers except for design lift coefficient. A photograph of the NACA 4-(5)(08)-03 propeller is shown as figure 3. The gaps between the spinner and the blades were sealed for all operating conditions.

The total-pressure measurements were obtained by means of the rakes shown in figure 1. The rakes had a maximum thickness ratio of 10 percent perpendicular to the leading edge and were swept back at an angle of 45°. This was done in order to keep the choking tunnel Mach number at as high a level as possible. The total pressure was measured in a plane

[redacted]

17 inches downstream from the center line of the propeller. A slant-type manometer board was used to measure total pressure and was such that 3 inches of measurements were obtained for each inch of vertical height produced by the total pressure.

Thrust, torque, and rotational speed were measured throughout the operating range of the propellers. The propellers were tested with the blade angle fixed and the rotational speed was varied over a range for each tunnel Mach number. The range of blade angles presented for each forward Mach number is given in the following table:

Forward Mach number M	Blade angle at 0.75 radius, $\beta_{0.75R}$, (deg) (a)					
0.175	40	45				
.23		45				
.35	40		50		60	
.43	40	45		55	[b]60	65
.53	40	45	50			[c]65
.60	40	45	50	55		65
.65		45	50	55	60	[b]65
.70		45	50	55	60	65
.75		45	50	55	60	65
.80			50	55	60	65
.85				55	60	65
.90				55	60	65
.925				55	60	65

[a]Only blade angles of 55°, 60°, and 65° were tested for the the NACA 4-(3)(08)-03 propeller.

[b]For NACA 4-(3)(08)-03 propeller only.

[c]For NACA 4-(5)(08)-03 propeller only.

[redacted]

REDUCTION OF DATA

Section thrust coefficient was computed from the measurements of static-pressure and total-pressure changes in the wake of the propeller. A detailed explanation of the method used can be found in reference 3. The total pressure was measured by the rakes previously described. The static-pressure gradient without the propeller operating was measured and found to be constant radially outward from the dynamometer barrel. With the propeller operating, the static pressure was assumed to be constant radially outward from the dynamometer barrel and was measured by an orifice located on the barrel in the plane in which the total-pressure measurements were taken. The advance ratio was corrected for the effect of tunnel-wall constraint by use of the ratio of free-air velocity to the tunnel-datum velocity as a function of thrust disk-loading coefficient and tunnel-datum Mach number presented in figure 4.

ACCURACY OF RESULTS

The section-thrust-coefficient curves are derived from total-pressure and static-pressure measurements in the wake of the propellers. The method of obtaining these measurements has been previously described. For maximum efficiency at relatively high speeds, it was found that the pressures measured could be read within 1 percent of the total deflection of their readings on the manometer board.

The integrated values of the section-thrust-coefficient curves are generally higher than the force-test results by approximately 3 percent. (See fig. 5.) This variation can be explained as follows: The rotational component of the slipstream is not removed from the incremental-thrust values because there would be little difference in the distribution with or without the rotational component included, and these data are primarily used to show the load distributions of the propeller qualitatively and not quantitatively. This rotational component of the slipstream was calculated to have a maximum value of 5 percent of the incremental thrust in some instances of the present results; however, the over-all corrections are, in general, of the same magnitude as the differences shown between force and wake results. The method used in calculating the rotational component of the slipstream may be found in reference 4. This method does not account for compressibility effects, but these effects even at the highest Mach numbers tested would be small.

Incremental-thrust-coefficient values are not presented in the curves for radial stations inboard of the $x = 0.40$ station. These points are not presented because of the scatter of the data measured by the survey equipment. This scatter was present both with and without

the propeller installed in the setup and, therefore, was caused by the erratic nature of the basic flow and not by the propeller. The section-thrust-coefficient curves were faired to the spinner location, however, basing the fairing of the inboard sections of the curves on the scattered test data for these inboard stations.

RESULTS AND DISCUSSION

The basic section-thrust-coefficient curves for the NACA 4-(3)(08)-03 propeller are shown in figure 6 for $\beta_{0.75R} = 55^\circ$ to 65° through the Mach number and advance-ratio range tested. A range of section Mach numbers for these curves is also included. Similar curves for the NACA 4-(5)(08)-03 propeller for $\beta_{0.75R} = 40^\circ$ to 65° are presented in figure 7. The force-test basic-characteristic curves corresponding to these section-thrust-coefficient curves have already been presented in references 1 and 2.

Effect of compressibility.- The effects of compressibility on maximum efficiency for the NACA 4-(3)(08)-03 and NACA 4-(5)(08)-03 propellers are practically the same; therefore, only the NACA 4-(5)(08)-03 propeller will be considered in this part of the discussion.

Figure 8 shows the effect of forward Mach number on the section-thrust-coefficient curves at maximum efficiency for constant blade angle. The advance ratio for each curve of this figure is also included. The figure shows that at relatively low speeds for all blade angles, that is, all blade stations operating below their critical speeds, the section-thrust-coefficient curves approximate a Betz load distribution. With the advent of supercritical section speeds (beginning at the tip and moving inboard as forward Mach number is increased), there is a loss in section thrust coefficient at these sections due to flow separation around the blade. The curves also show that with further increases in Mach number, the tip sections begin assuming load which had previously been lost due to adverse compressibility effects. This effect was reported in reference 5.

The effect of forward Mach number on maximum efficiency (fig. 9) has already been reported in reference 1. A comparison of the trends shown in figures 8 and 9 shows good correlation between wake-survey and force-test measurements; for example, as long as the section-thrust-coefficient curves show low-speed distribution, the maximum efficiencies from force tests do not show any appreciable reduction; however, when these curves show compressibility effects, the force-test curves show definite reductions in efficiency. It may also be noted that when the loads at the tip sections begin increasing, the force-test curves show

[redacted]

a lower rate of loss in efficiency. This lower rate of loss in efficiency does not begin until the increase in thrust coefficient at the tip sections of the propeller become greater than the loss in thrust coefficient at the shank sections. As previously mentioned in reference 1, large gains in propeller maximum efficiency are possible through operation at low advance ratios. These gains in maximum efficiency are largely due to the more favorable geometry of the force vectors. The data for this propeller indicate that the beneficial effect of low-advance-ratio operation at high speeds (shown in fig. 9) is most effective after the tip sections of this propeller have started assuming load again. (See fig. 8.)

The effect of blade angle on the section-thrust-coefficient curves at an advance ratio for maximum efficiency at a given Mach number is presented in figure 10. These curves are the same as those presented in figure 8. The curves show that the adverse effects of compressibility are experienced first by the lowest blade angles. With increase in forward Mach number, these effects are experienced at progressively high blade angles.

The section-thrust-coefficient curves presented in figures 8 and 10 for maximum efficiency show that, for supercritical propeller operation in the speed range of these tests, the greater portion of the load is carried by the outer blade sections. The outer blade sections operate at the highest Mach numbers and, if they are the thinnest of the sections as designed at this time, their lift-to-drag ratios are higher than those for the inboard sections at and above supercritical speeds. Since the tip portions are then the most efficient, the distribution of load along the blade for maximum-efficiency conditions would be expected to be one in which increased loading at the tip occurs. Analysis shows that the induced losses are small compared with pressure drag for the lift-to-drag ratios at these speeds and, therefore, from an aerodynamic consideration the design should lean towards loading up the tip sections of the propeller rather than attempting to maintain minimum induced losses all along the blade. It should be recognized that this type of design may be difficult to obtain from a structural standpoint.

The effect of tip Mach number on maximum efficiency is presented in figure 11. The data presented show that as blade angle decreases, the critical tip Mach number increases. This is obvious since, for a given tip Mach number, as the blade angle and advance ratio decrease the gradient of section Mach number becomes steeper and therefore less of the blade is in the Mach number range in which adverse compressibility effects are experienced. Because of the favorable effect of low-advance-ratio operation at high supercritical speeds, the rate of loss of maximum efficiency in the supercritical tip Mach number range also becomes less as blade angle is decreased, at least to a blade angle of 40°, and some data, unpresented, indicate that this trend extends to still lower blade angles.

[redacted]

Effect of design section camber.- The effect of design section camber is shown in figure 12 by comparing section-thrust-coefficient curves at the same advance ratio near maximum efficiency for the NACA 4-(3)(08)-03 and NACA 4-(5)(08)-03 propellers. For a low-speed condition, exemplified by Mach numbers of 0.60 and 0.65, the section-thrust-coefficient curves for these two propellers have similar distributions; however, the higher-cambered propeller produces more thrust than the lower-cambered propeller. For high-speed operating conditions (forward Mach numbers of 0.75 and 0.90), these curves are of the same shape and magnitude. Figure 13, which is typical of all blade angles tested, shows little difference in maximum efficiency throughout the Mach number range tested for these two propellers. Consequently, it is obvious that at low speeds the higher-cambered propeller absorbs more power; however, at high speeds, the effect of this difference in camber on propeller characteristics is overshadowed by compressibility effects. It may be noted in some instances that there are large differences in incremental thrust coefficients for the two blades at their inner blade stations, but, as previously mentioned, because of the wake-measuring system and tunnel conditions, these values are only estimates and should not be used quantitatively. Force-test results, which encompass the above wake-survey results, are presented in figure 14. In this figure, the effect of Mach number on thrust coefficient is shown for several constant advance-ratio conditions. The results show good correlation with the wake results presented in figure 12. Curves of power coefficient plotted against Mach number for several constant advance-ratio conditions are presented in figure 15. Since the maximum efficiencies for the two propellers are the same throughout the Mach number range, it would be expected that the power-coefficient curves would be similar to the thrust-coefficient curves. Comparison of figures 14 and 15 shows the same trends for thrust and power coefficients plotted against Mach number.

In summation, it may therefore be stated that when take-off and climb conditions as well as the high-speed condition are important, the NACA 4-(5)(08)-03 propeller would be a more logical propeller to use than the NACA 4-(3)(08)-03 propeller because at subcritical speeds it absorbs more power and produces more thrust with the same maximum efficiency and at supercritical speeds the propeller characteristics are essentially the same.

CONCLUSIONS

Tests of the NACA 4-(3)(08)-03 and NACA 4-(5)(08)-03 two-blade propellers in the Langley 8-foot high-speed tunnel for blade angles between 40° and 65° and through a forward Mach number range up to 0.925 indicate the following results:

[redacted]

1. If the outboard sections of a propeller are the thinnest, the design of propellers in the supercritical Mach number range should incorporate loading distribution which is concentrated at the tip sections.

2. The characteristics of the NACA 4-(5)(08)-03 propeller at maximum efficiency are superior to those for the NACA 4-(3)(08)-03 propeller for take-off and climb operation; they are about the same for high-speed operation.

3. The trends of the force-test results are accurately reflected in the wake results presented in this paper.

Langley Aeronautical Laboratory
National Advisory Committee for Aeronautics
Langley Air Force Base, Va.

REFERENCES

1. Delano, James B., and Carmel, Melvin M.: Investigation of the NACA 4-(5)(08)-03 Two-Blade Propeller at Forward Mach Numbers to 0.925. NACA RM L9G06a, 1949.

2. Delano, James B., and Morgan, Francis G., Jr.: Investigation of the NACA 4-(3)(08)-03 Two-Blade Propeller at Forward Mach Numbers to 0.925. NACA RM L9I06, 1949.

3. Baals, Donald D., and Mourhess, Mary J.: Numerical Evaluation of the Wake-Survey Equations for Subsonic Flow Including the Effect of Energy Addition. NACA ARR L5H27, 1945.

4. Pankhurst, R. C.: Airscrew Thrust Grading by Pitot Traverse: Allowance for Rotation of Slipstream at High Rates of Advance. R. & M. No. 2049, British A.R.C., 1945.

5. Carmel, Melvin M., and Robinson, Harold L.: Further Investigation of NACA 4-(5)(08)-03 Two-Blade Propeller at High Forward Speeds. NACA RM L7E12, 1947.

[redacted]

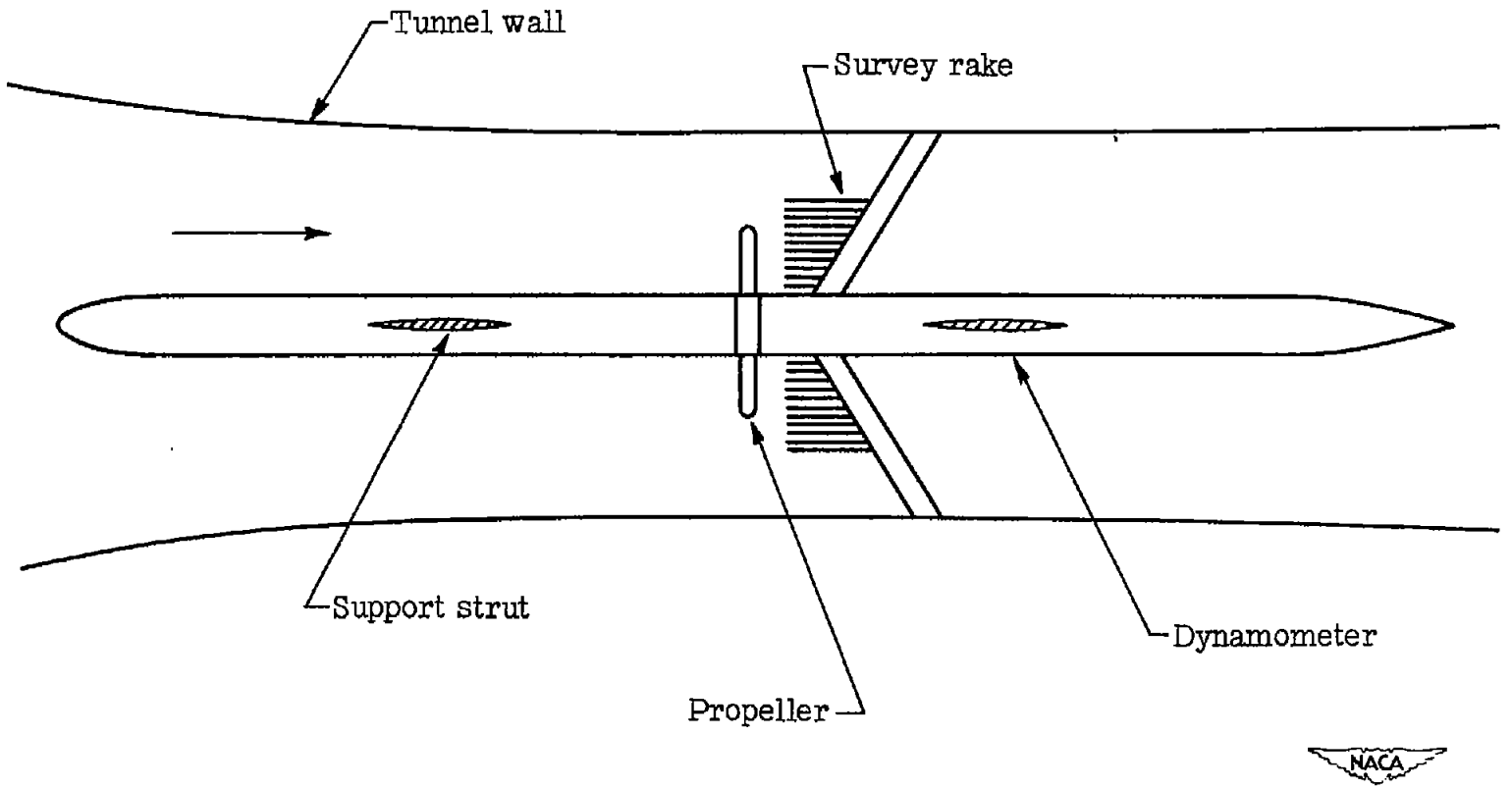

Figure 1.- Test apparatus.

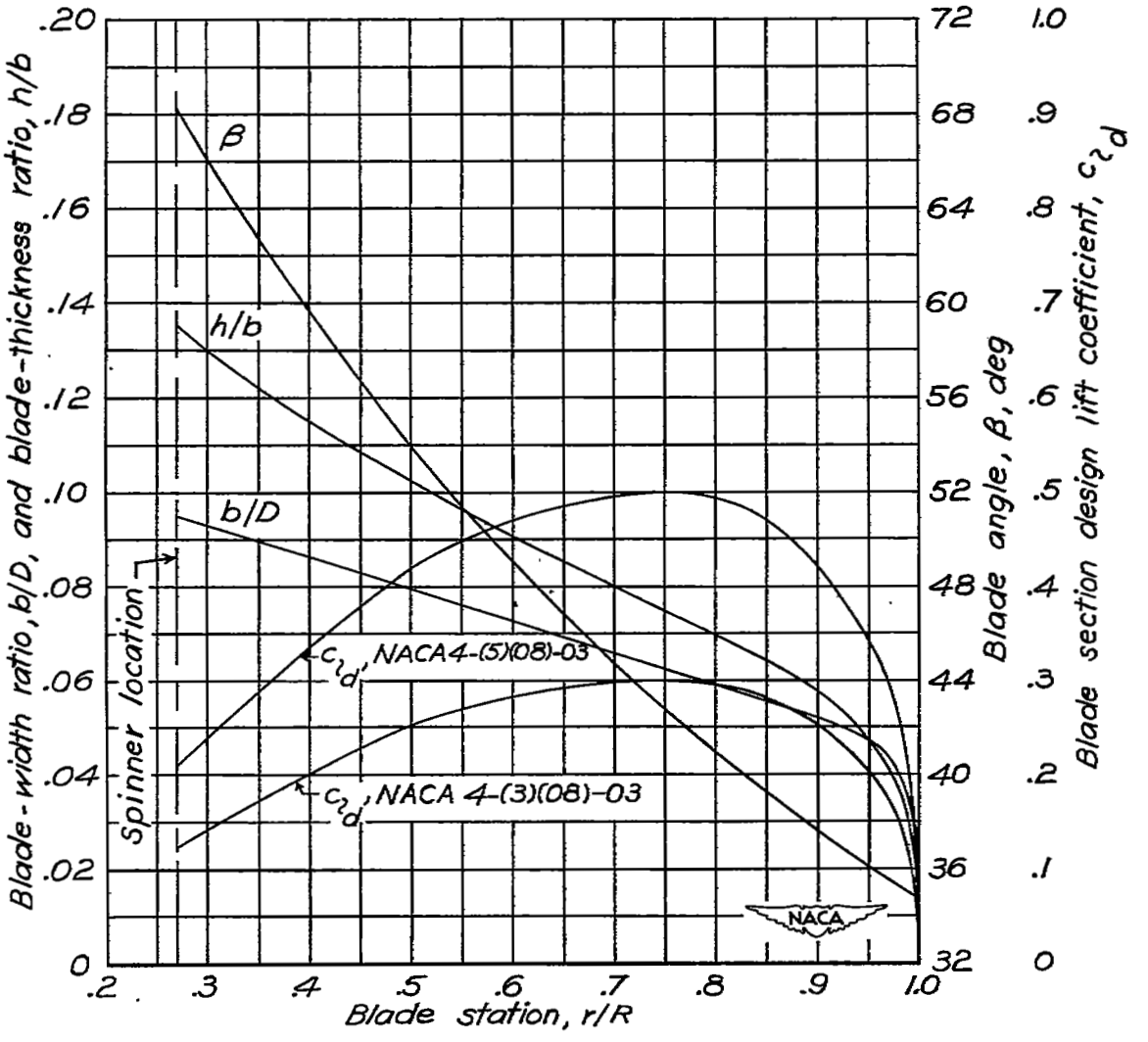

Figure 2.- NACA 4-(3)(08)-03 and NACA 4-(5)(08)-03 propeller blade-form curves.

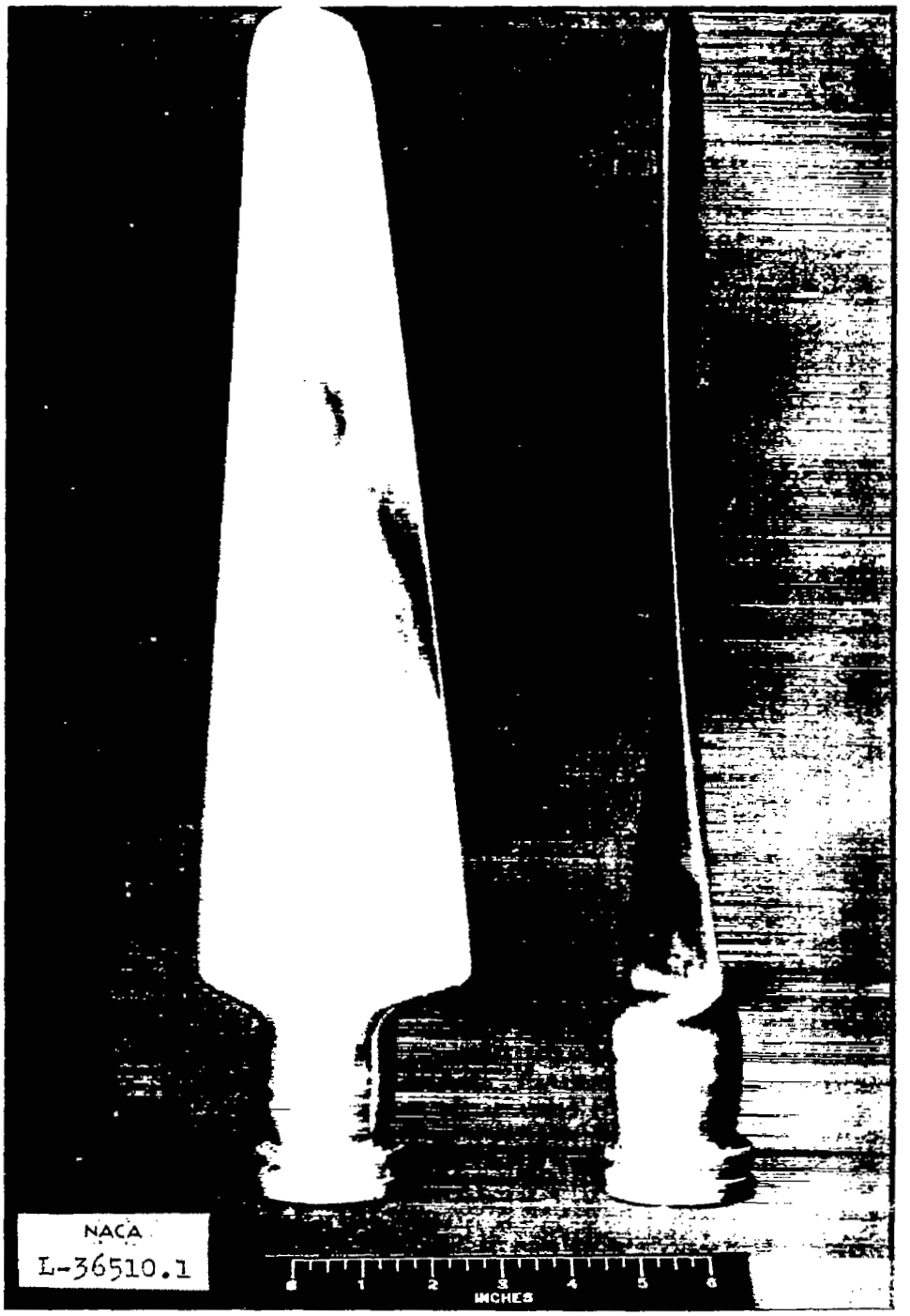

Figure 3.- NACA 4-(5)(08)-03 two-blade propeller.

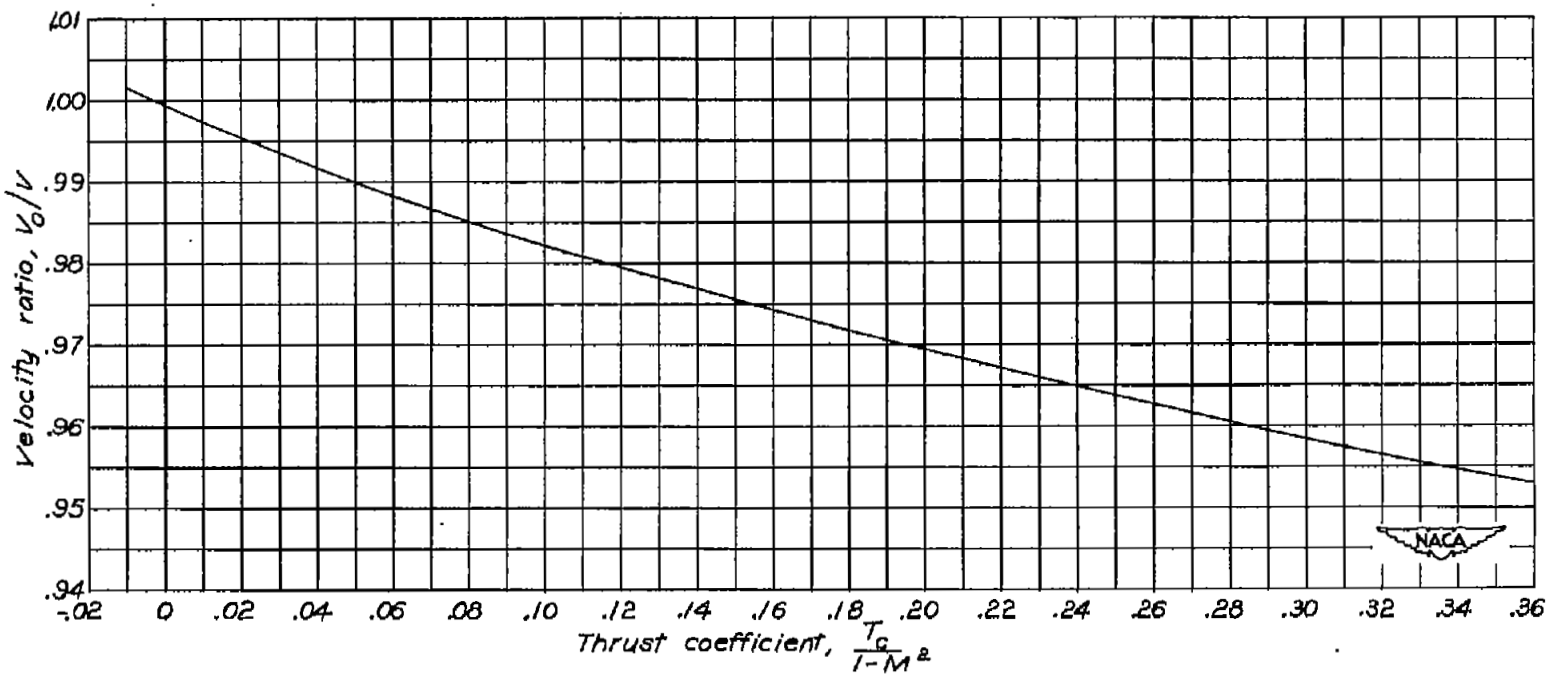

Figure 4.- Tunnel-wall-interference correction for 4-foot-diameter propellers in Langley 8-foot high-speed tunnel.

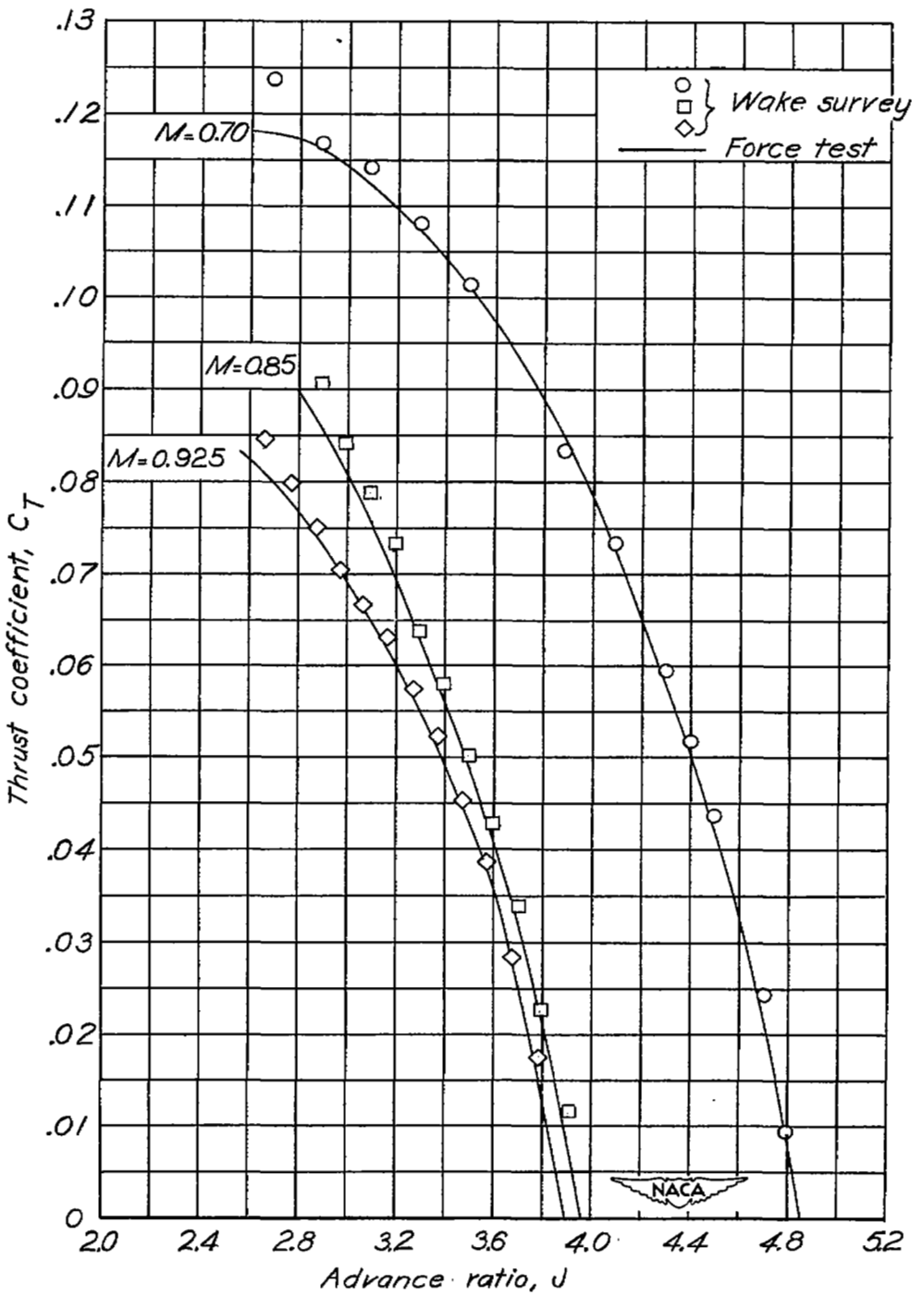

Figure 5.- Comparison of force-test and wake-survey data. NACA 4-(5)(08)-03 propeller. $\beta_{0.75R} = 60°$.

[redacted]

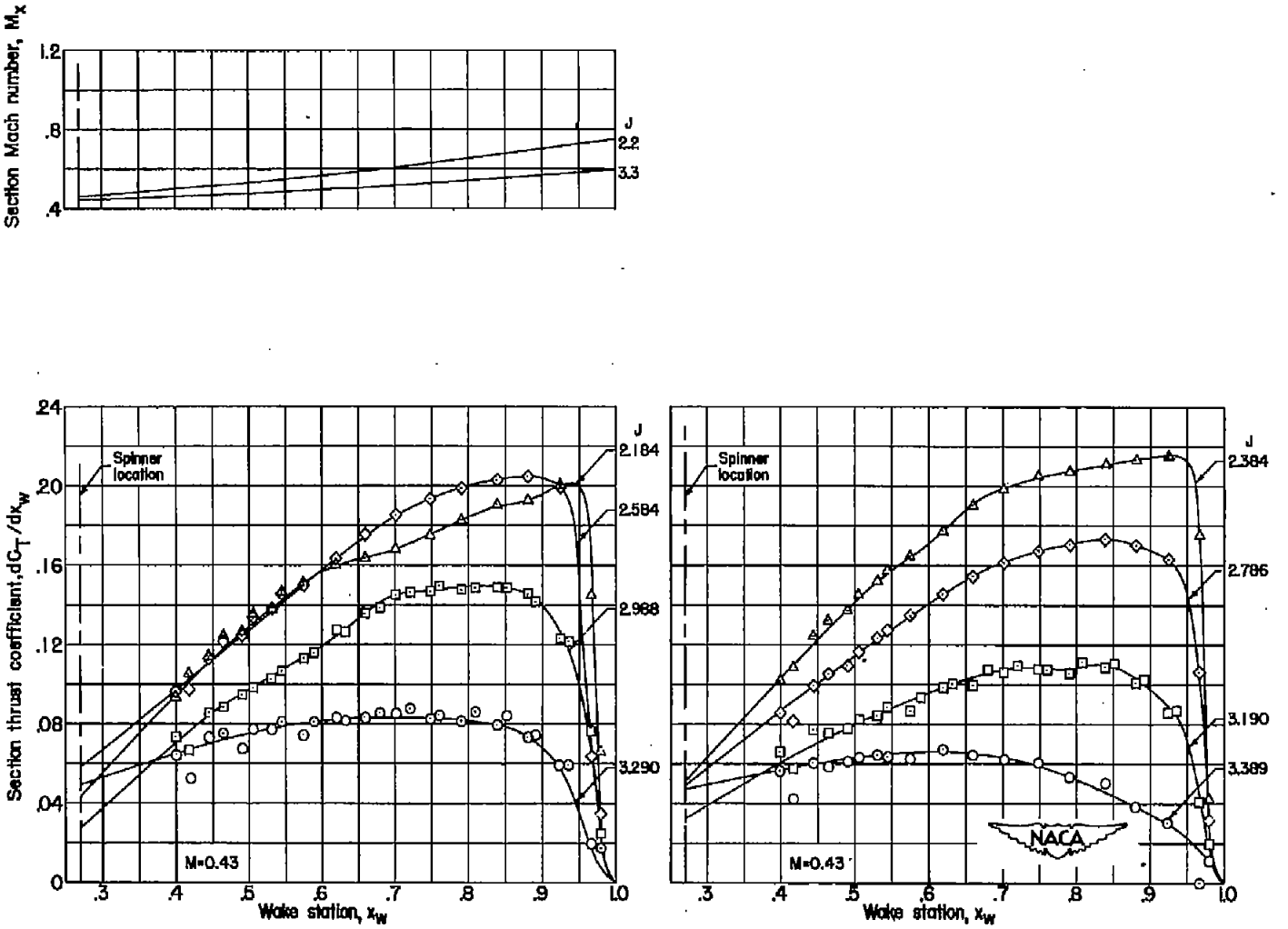

(a) $\beta_{0.75R} = 55^{\circ}$.

Figure 6.- Basic section-thrust-coefficient curves for NACA 4-(3)(08)-03 propeller.

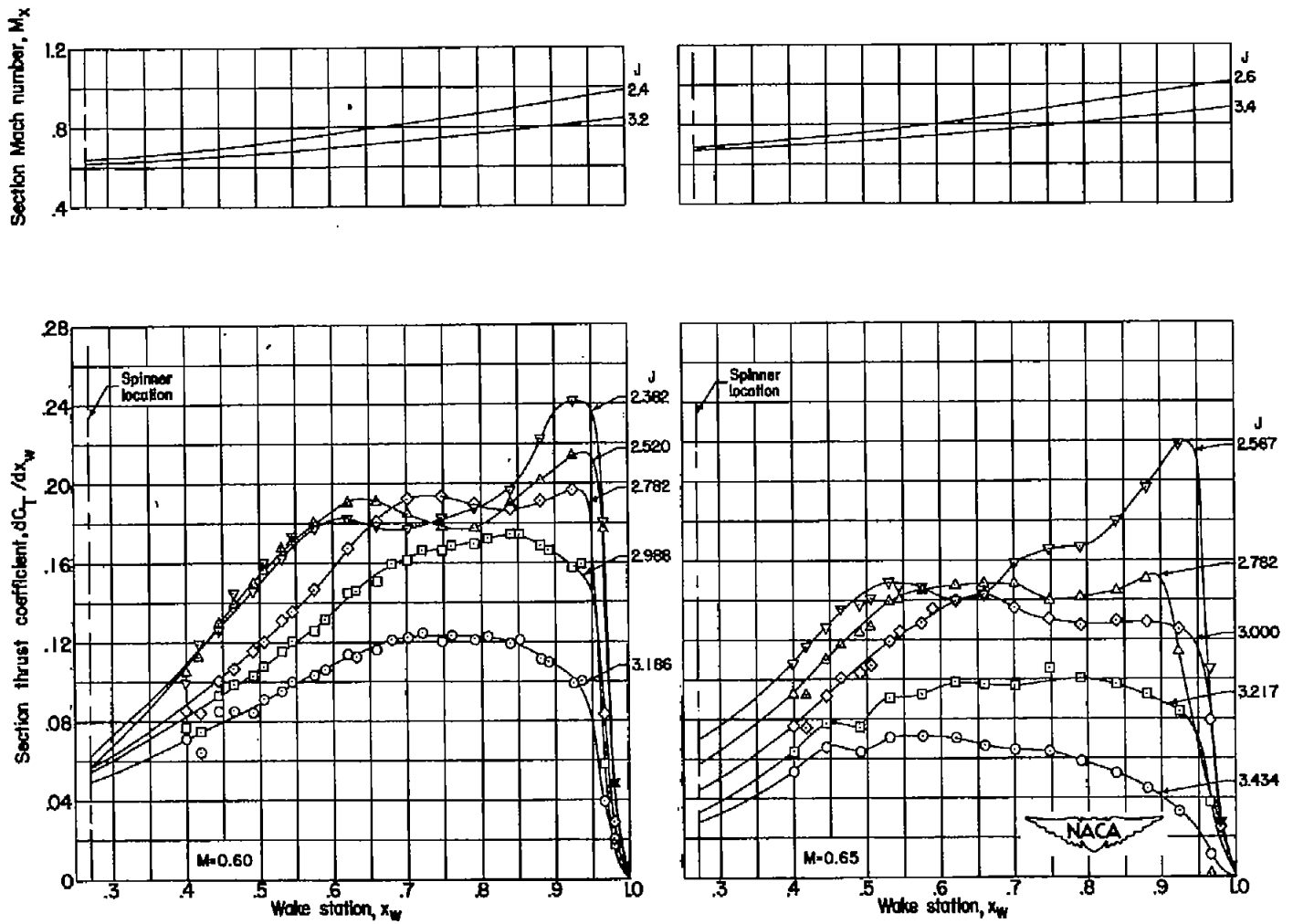

(a) Continued. $\beta_{0.75R} = 55^\circ$.

Figure 6.- Continued.

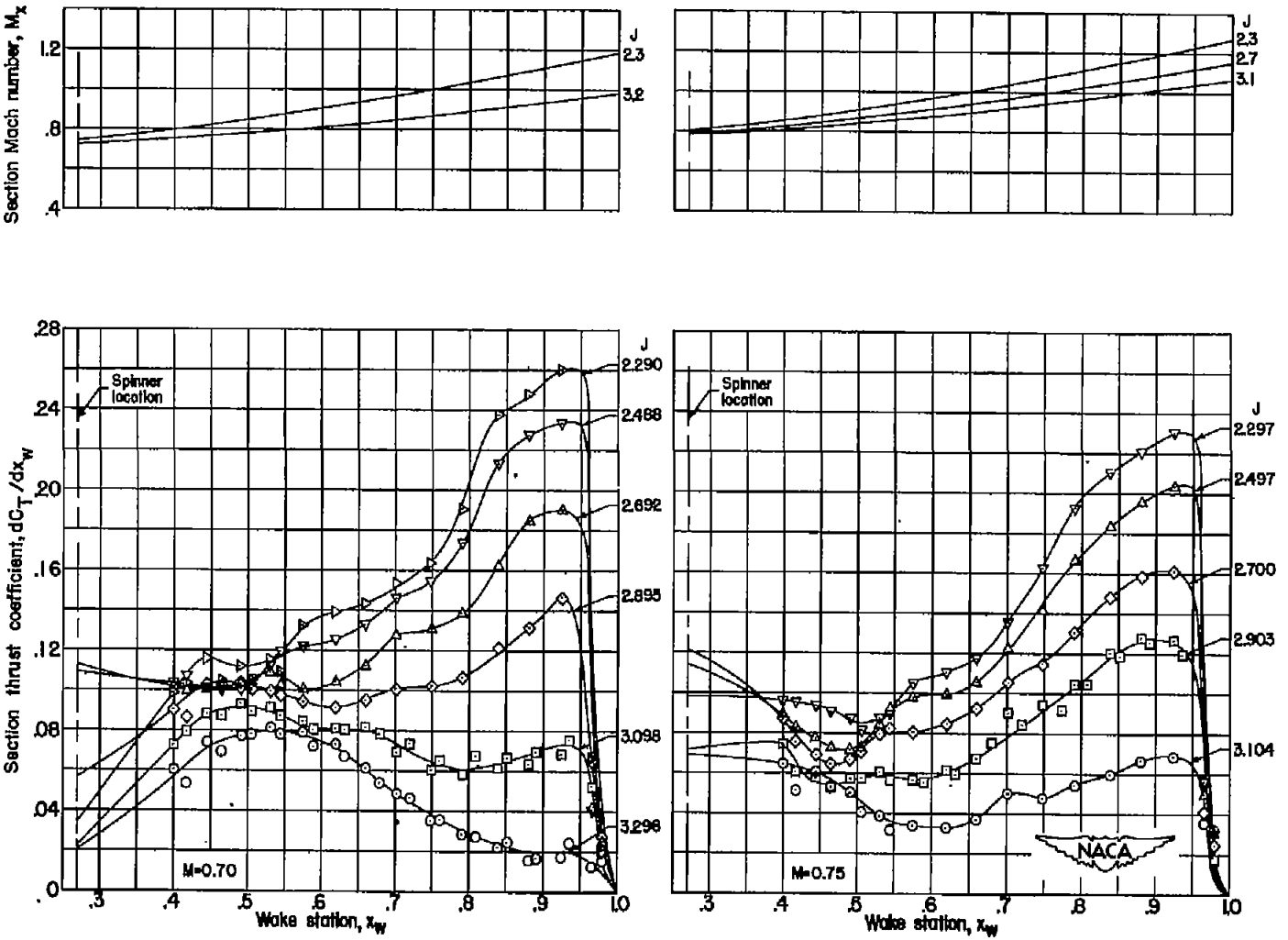

(a) Continued. $\beta_{0.75R} = 55^\circ$.

Figure 6.- Continued.

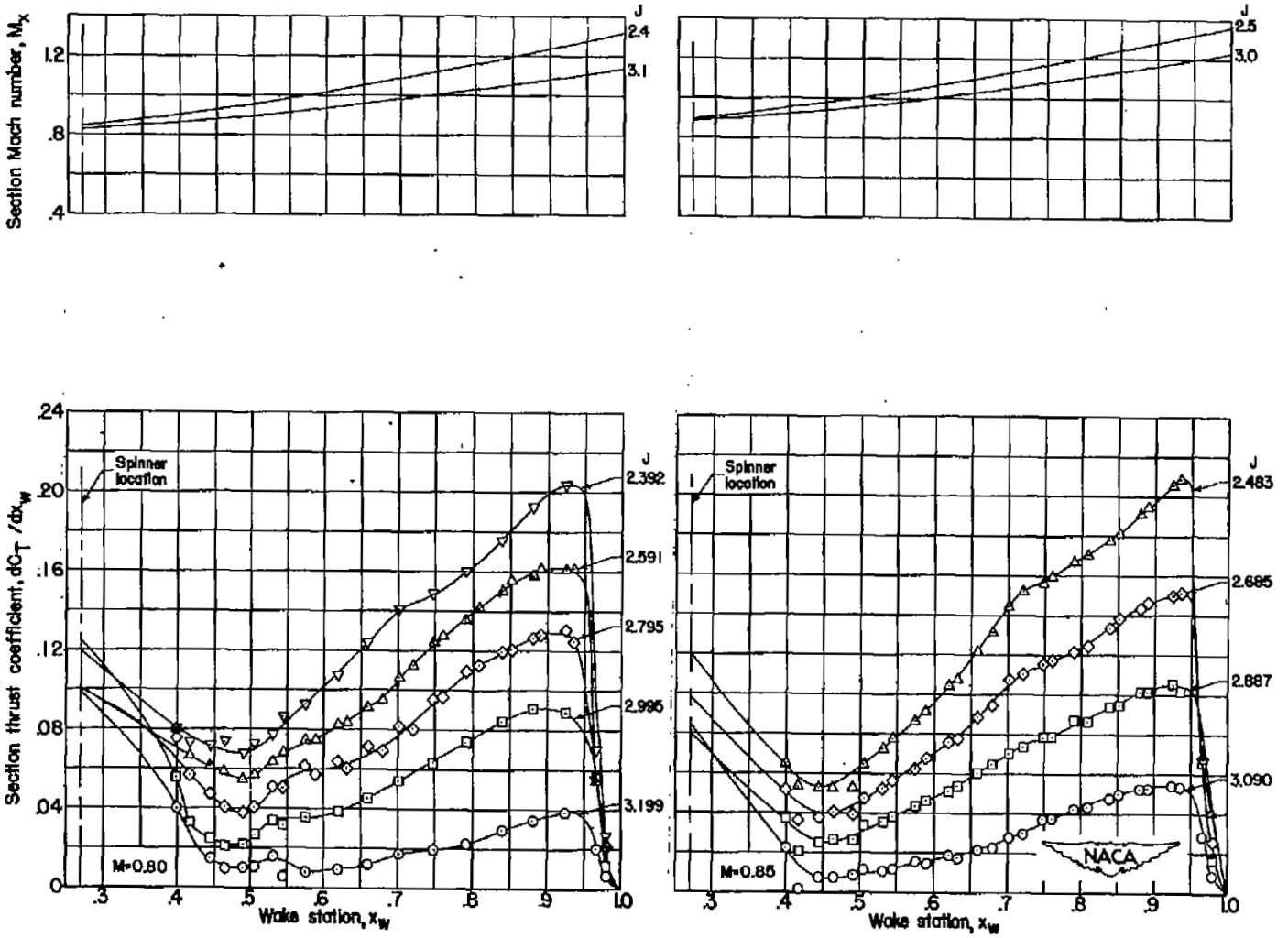

(a) Continued. $\beta_{0.75R} = 55°$.

Figure 6.- Continued.

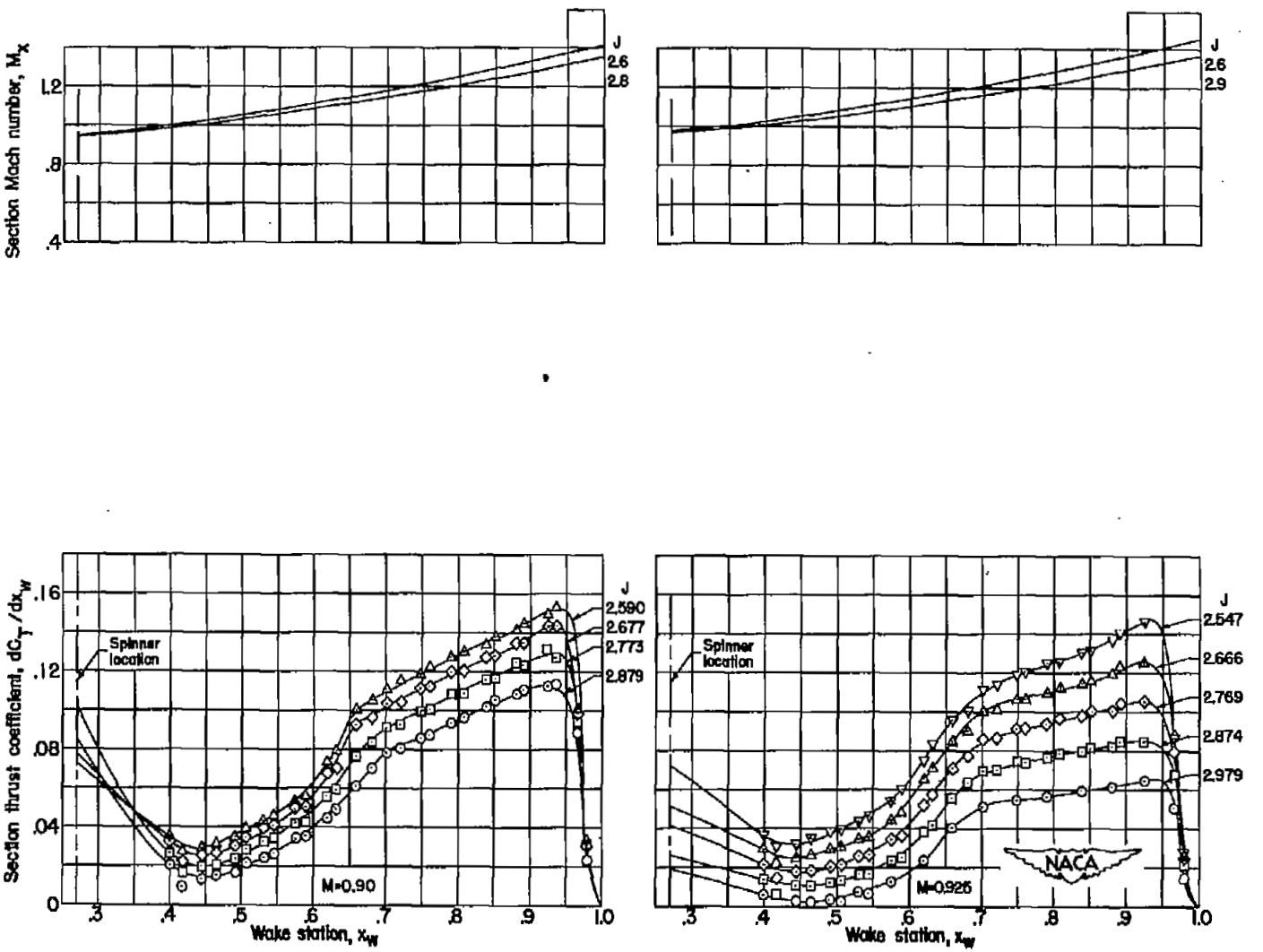

(a) Concluded. $\beta_{0.75R} = 55^{\circ}$.

Figure 6.- Continued.

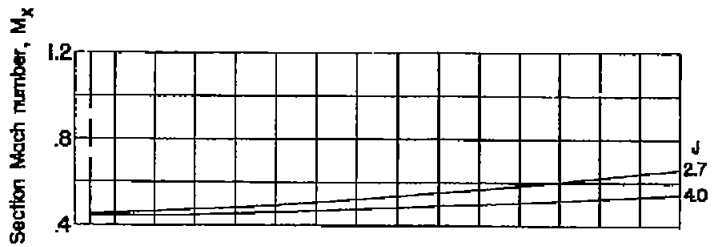

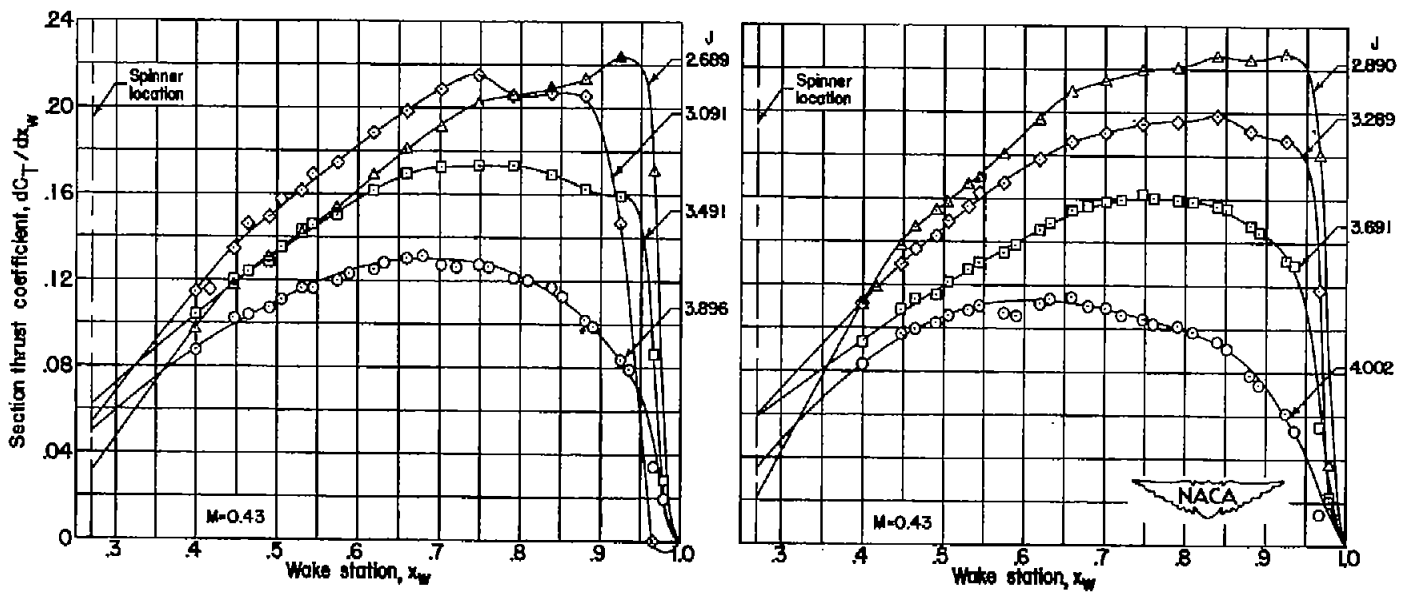

(b) $\beta_{0.75R} = 60^\circ$.

Figure 6.- Continued.

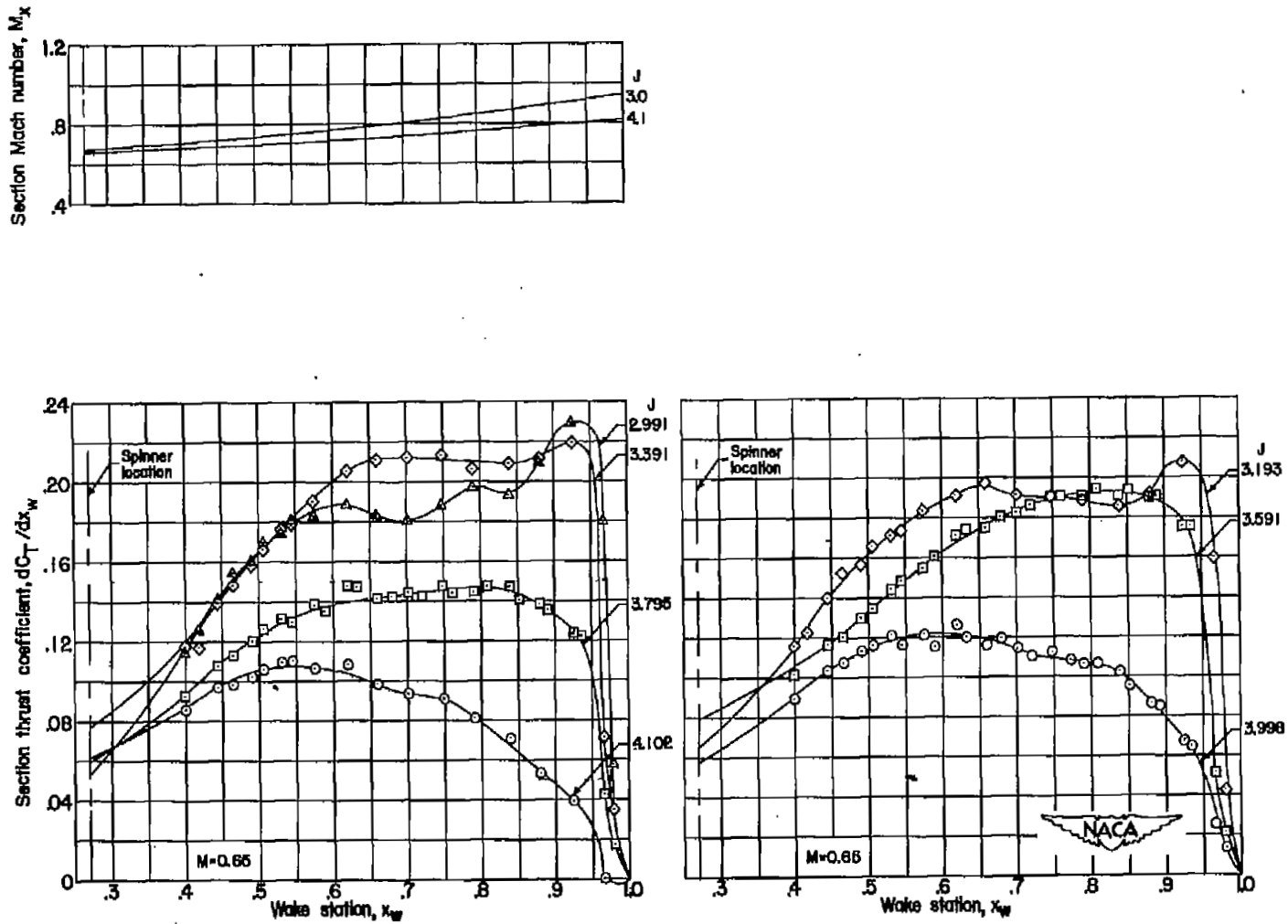

(b) Continued. $\beta_{0.75R} = 60°$.

Figure 6.- Continued.

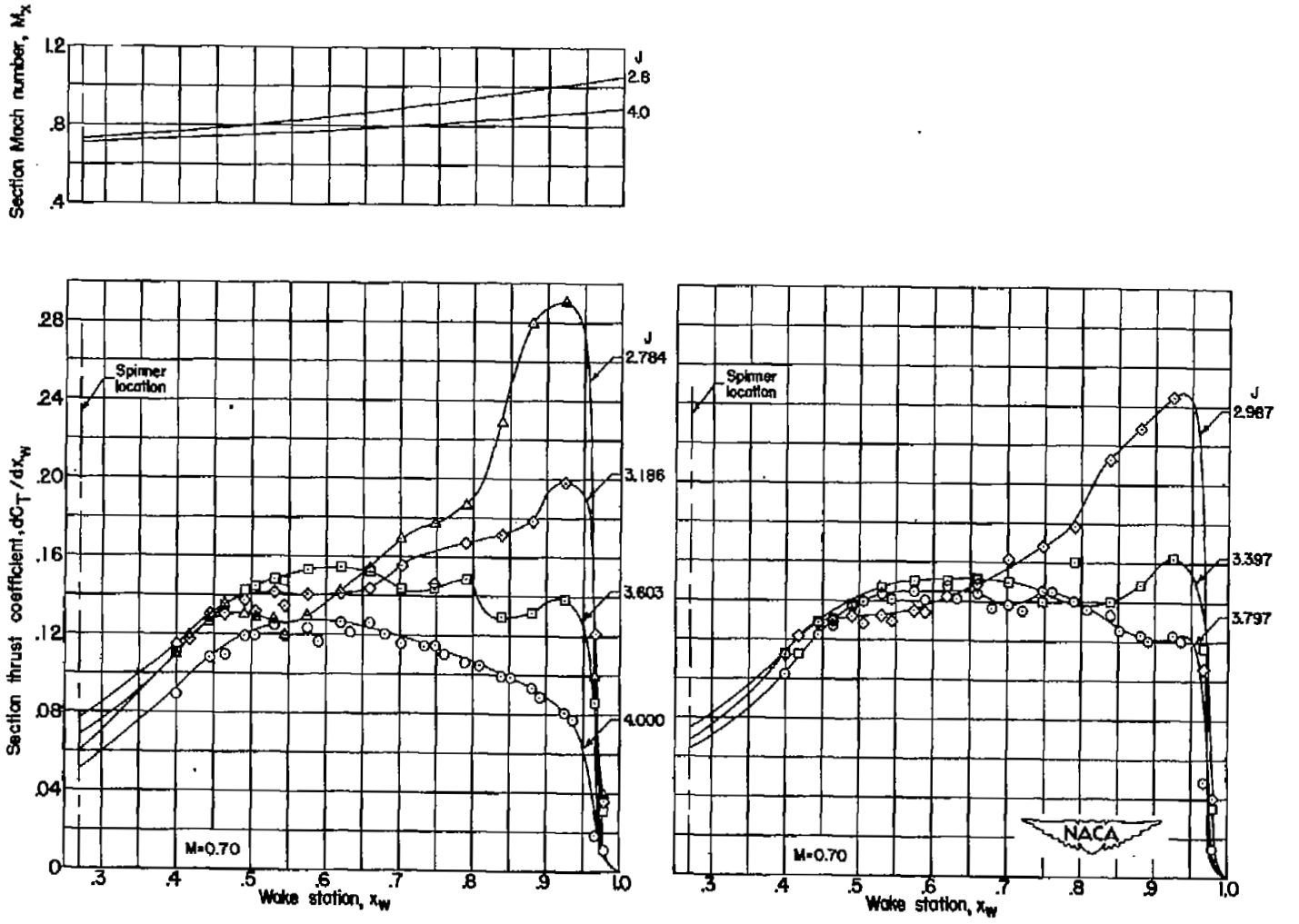

(b) Continued. $\beta_{0.75R} = 60°$.

Figure 6.- Continued.

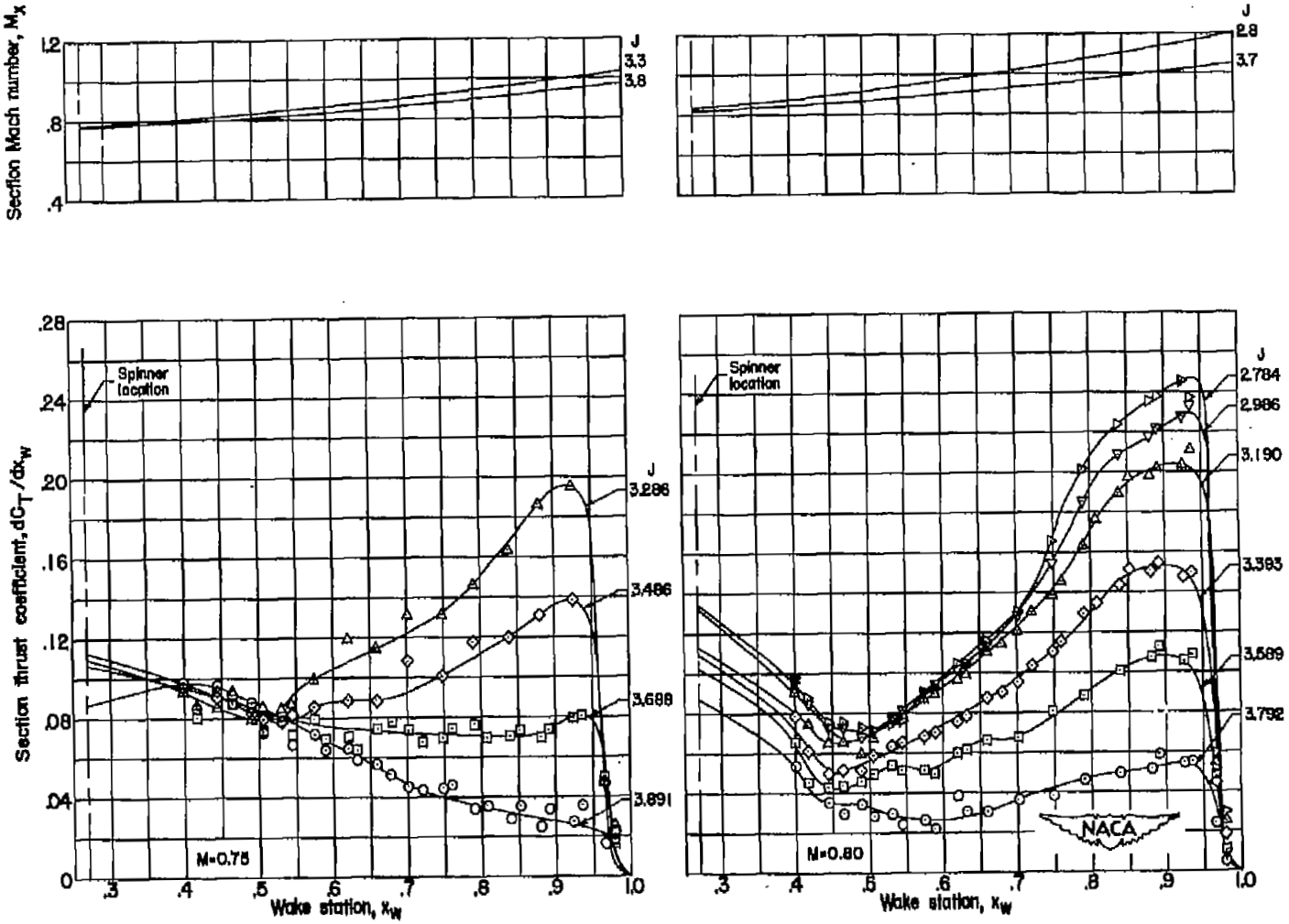

(b) Continued. $\beta_{0.75R} = 60^\circ$.

Figure 6.- Continued.

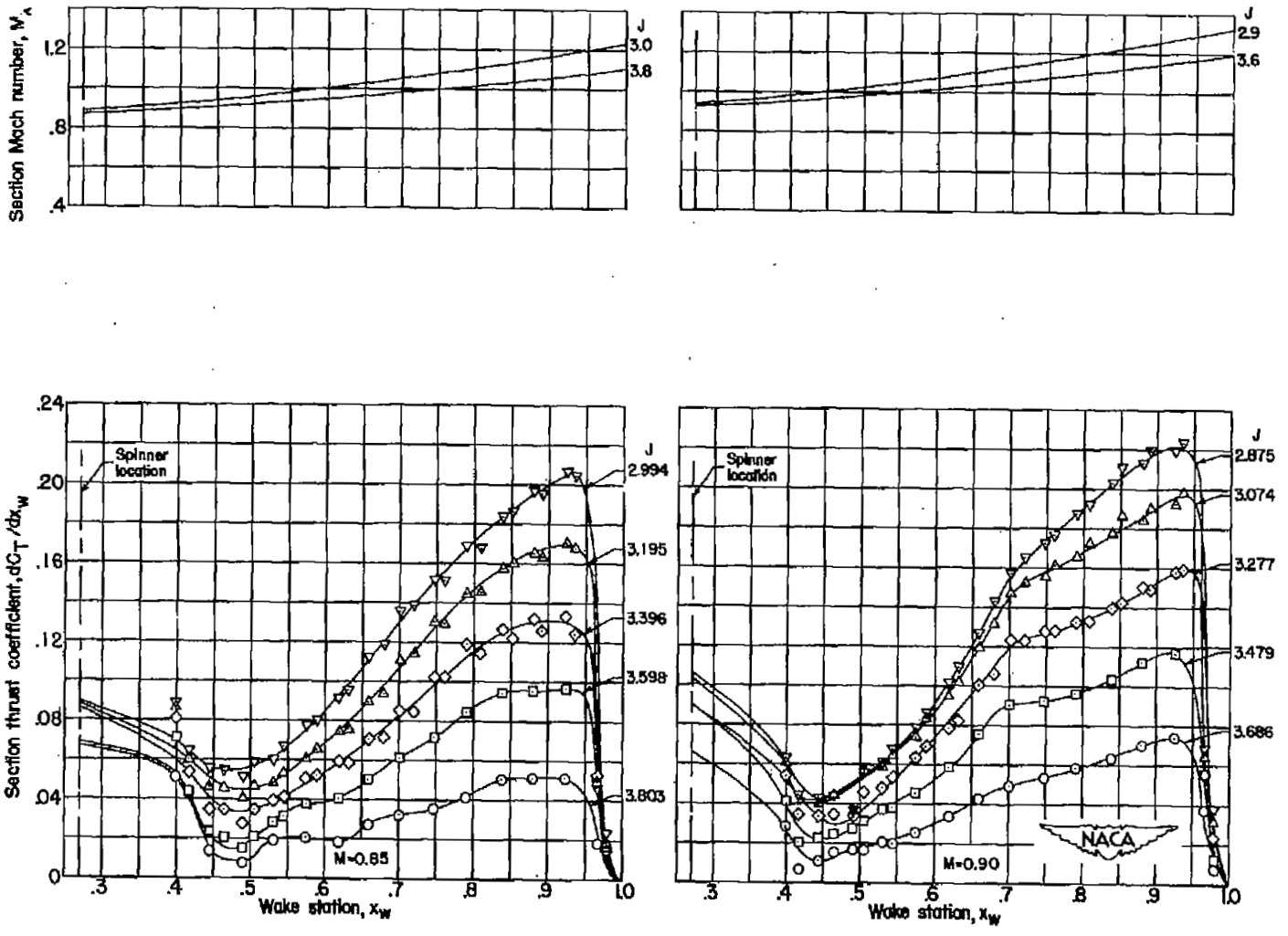

(b) Continued. $\beta_{0.75R} = 60°$.

Figure 6.- Continued.

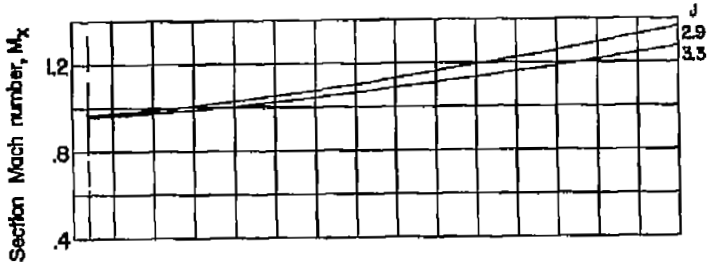

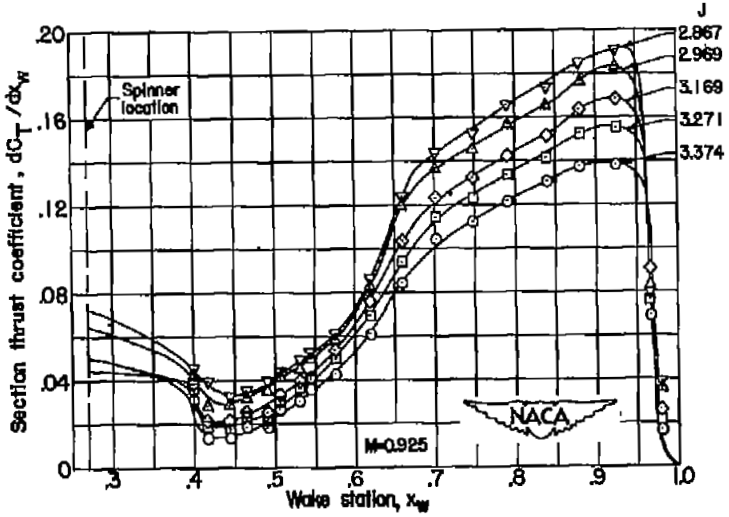

(b) Concluded. $\beta_{0.75R} = 60°$.

Figure 6.- Continued.

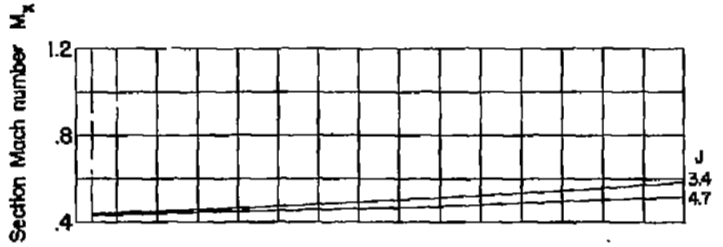

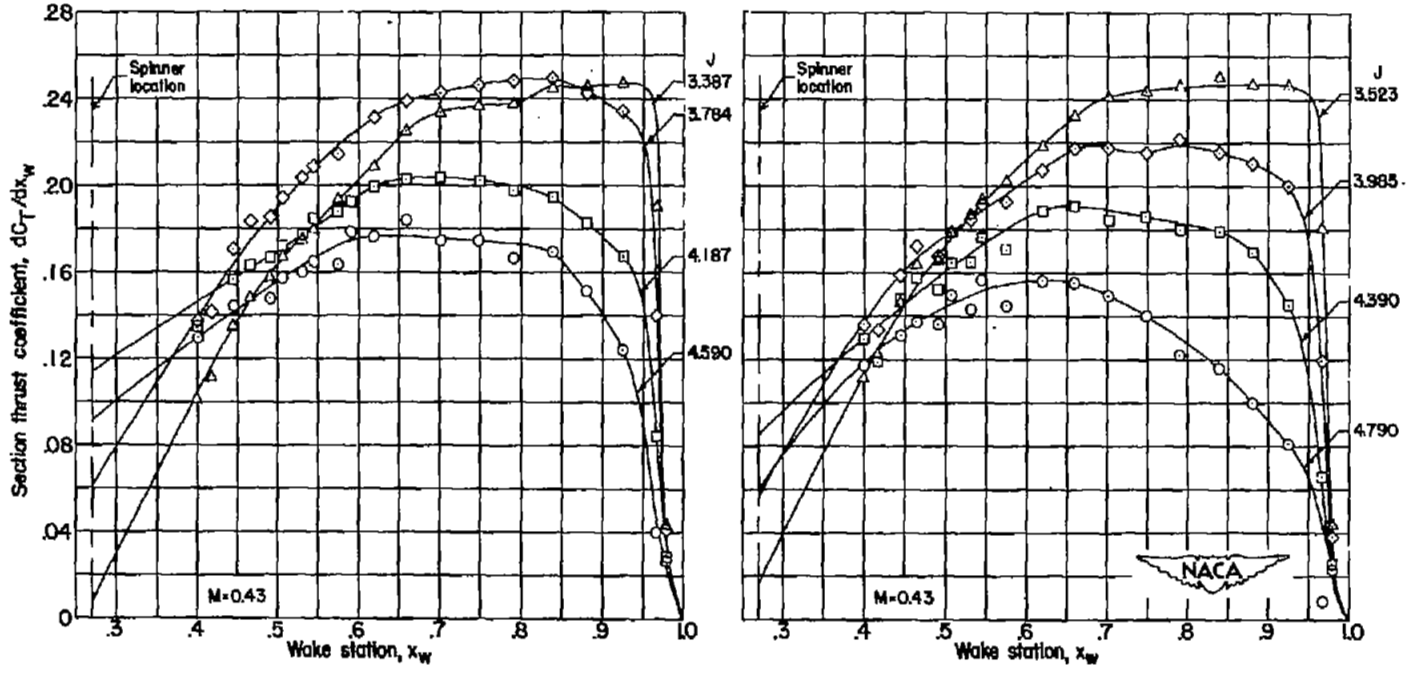

(c) $\beta_{0.75R} = 65°$.

Figure 6.- Continued.

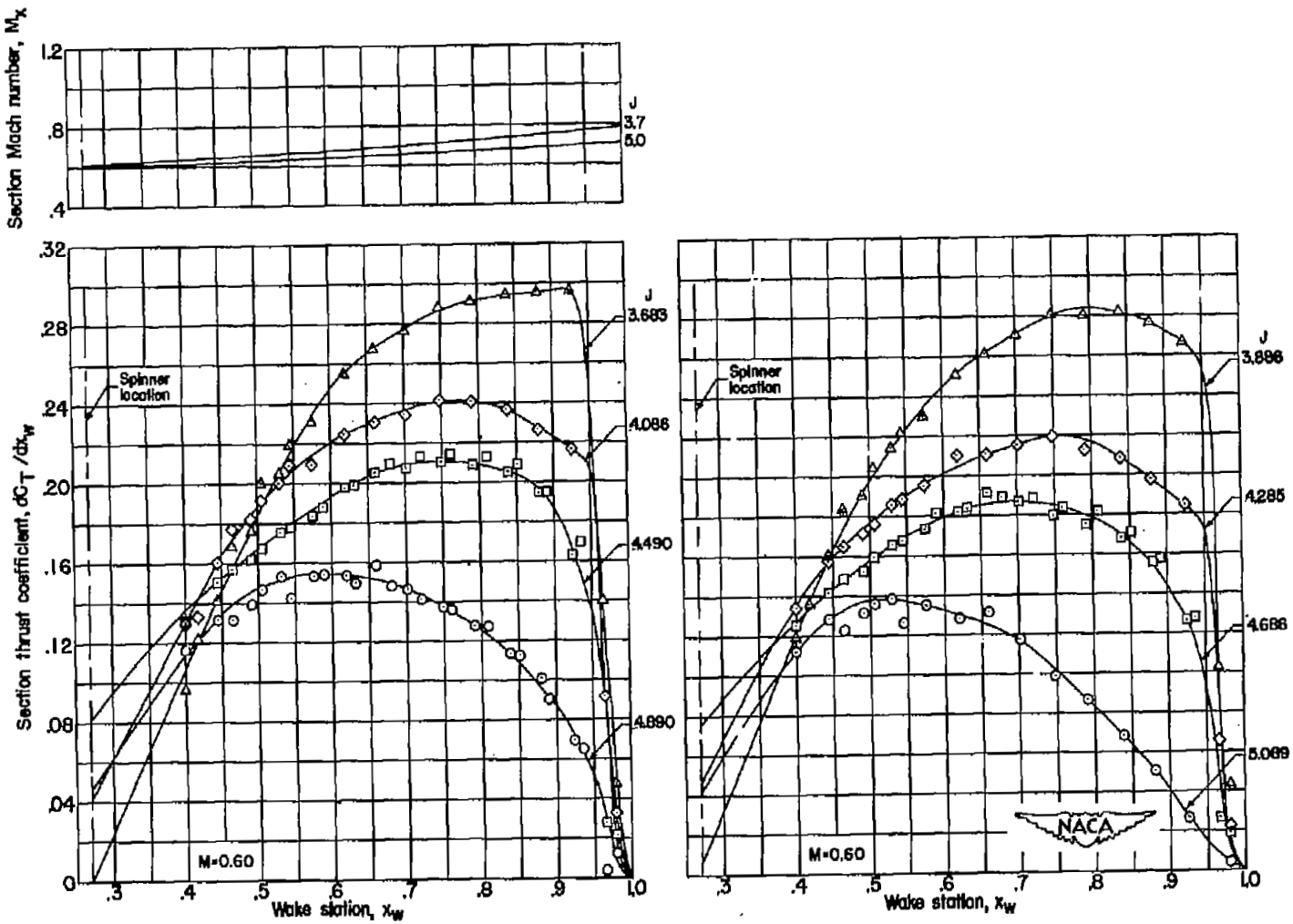

(c) Continued. $\beta_{0.75R} = 65^\circ$.

Figure 6.- Continued.

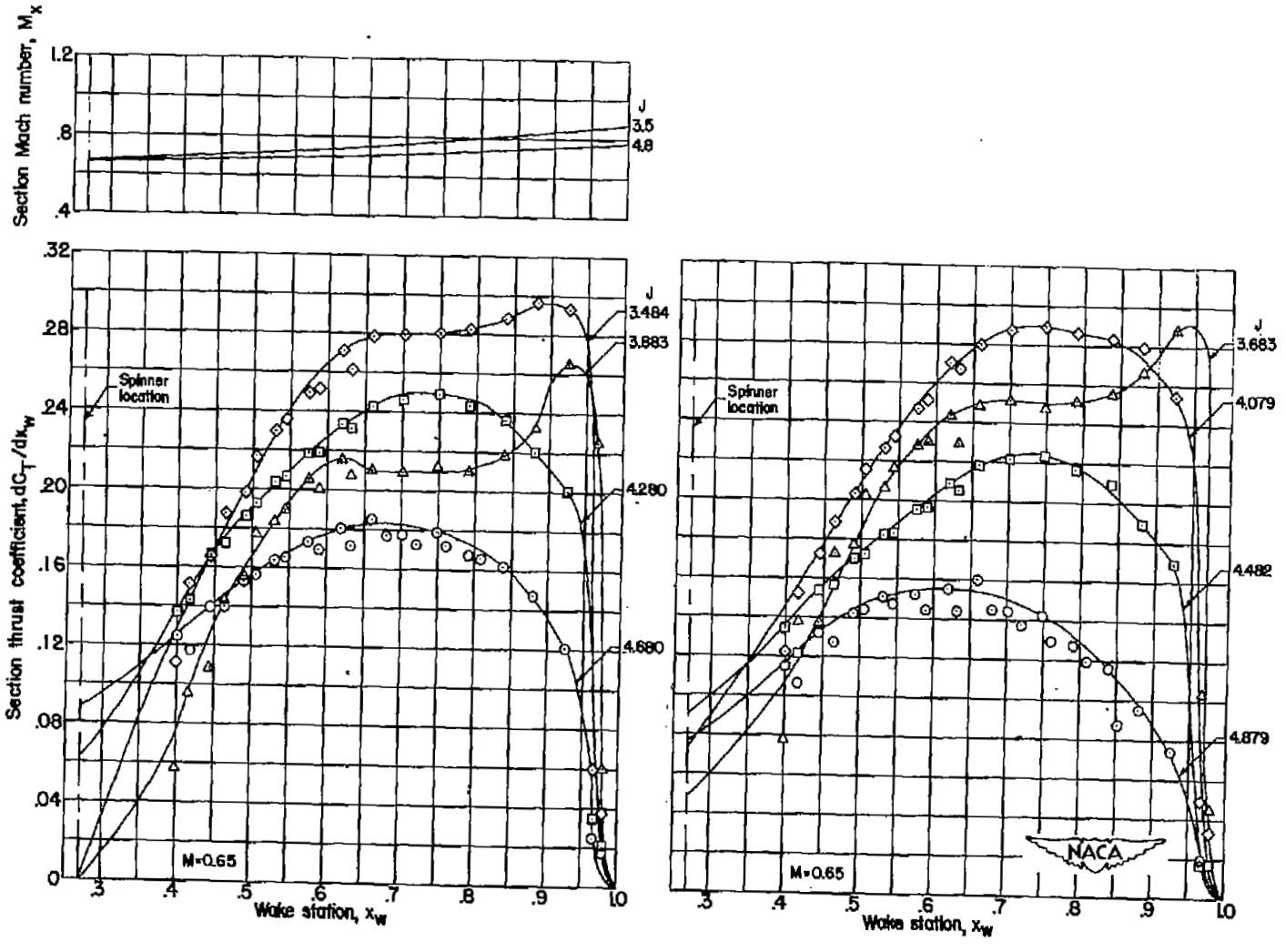

(c) Continued. $\beta_{0.75R} = 65°$.

Figure 6.- Continued.

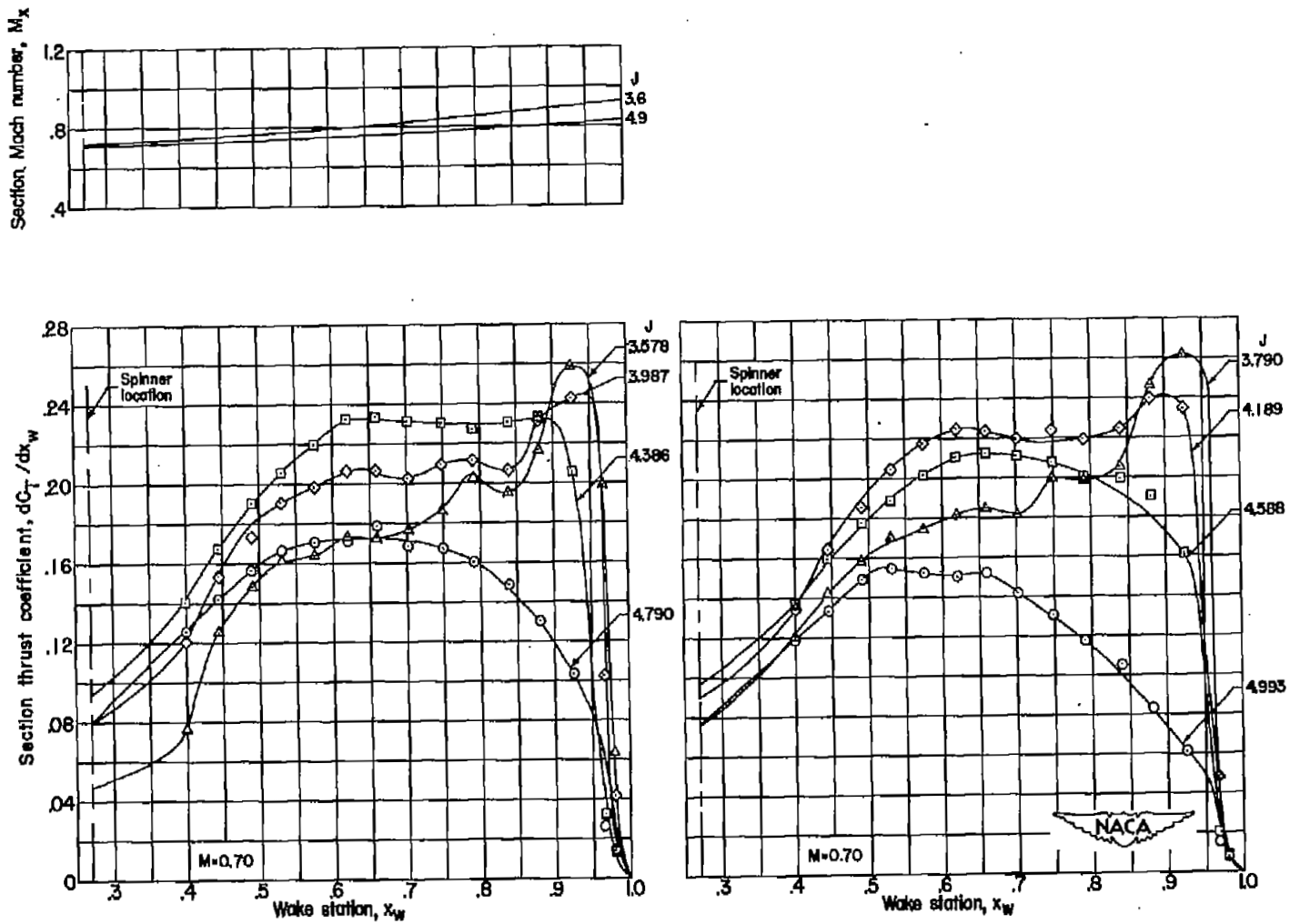

(c) Continued. $\beta_{0.75R} = 65°$.

Figure 6.- Continued.

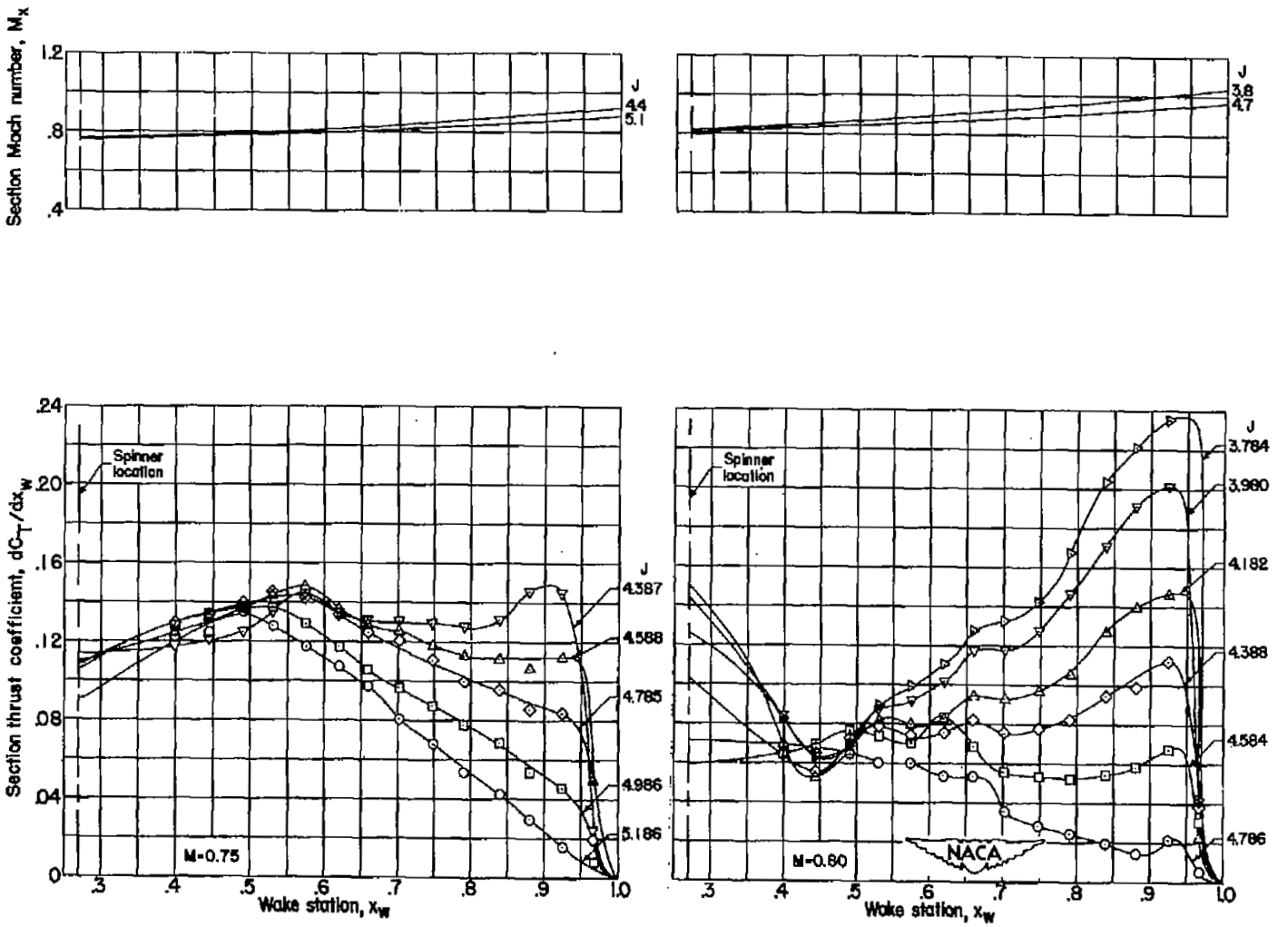

(c) Continued. $\beta_{0.75R} = 65^\circ$.

Figure 6.- Continued.

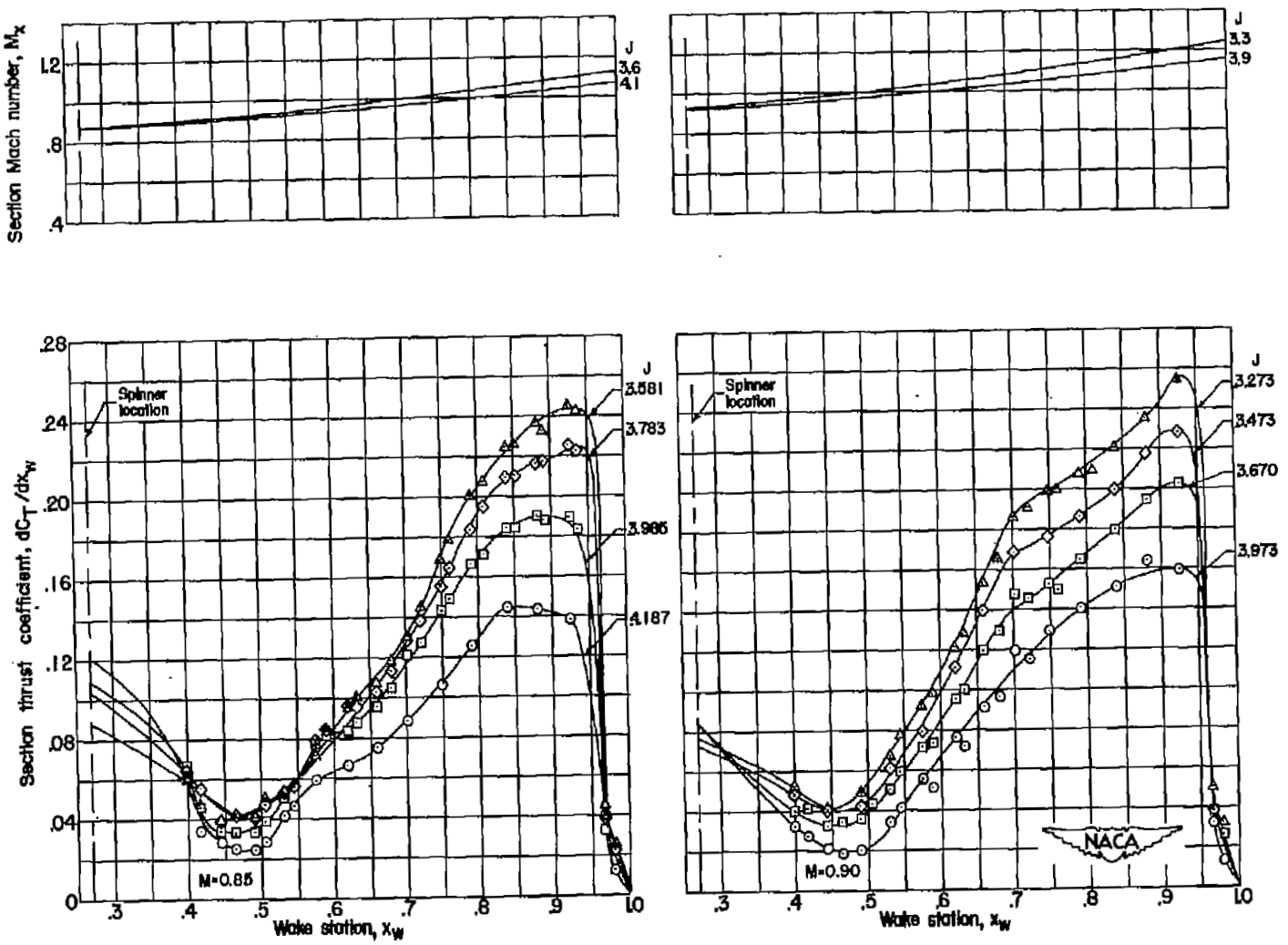

(c) Continued. $\beta_{0.75R} = 65^\circ$.

Figure 6.- Continued.

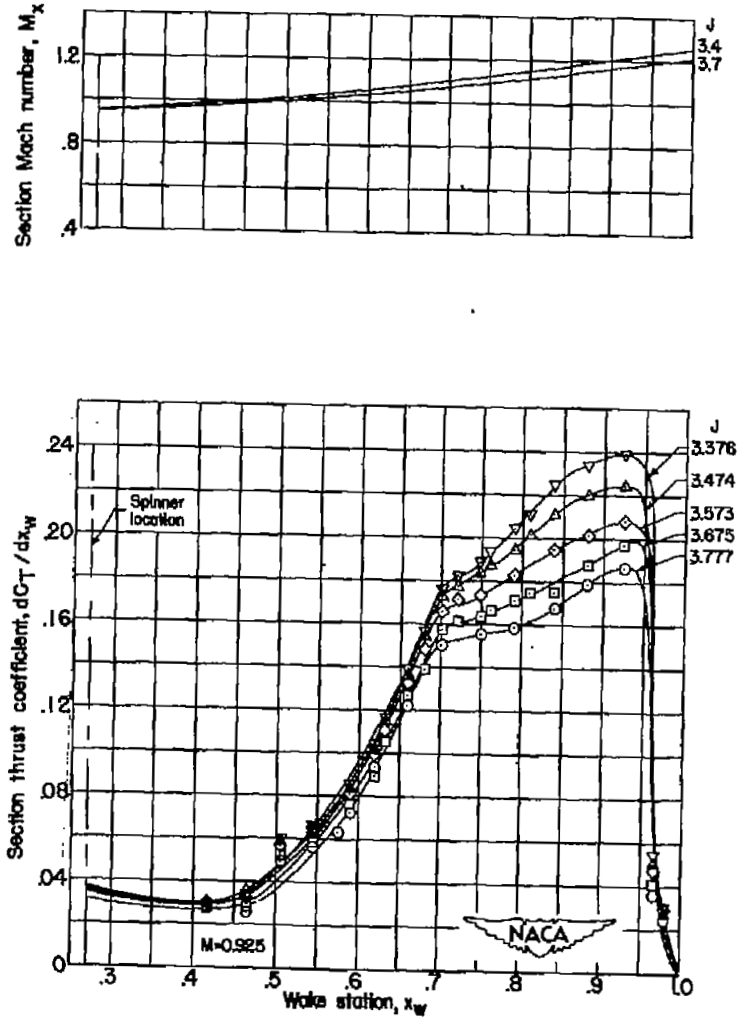

(c) Concluded. $\beta_{0.75R} = 65^\circ$.

Figure 6.- Concluded.

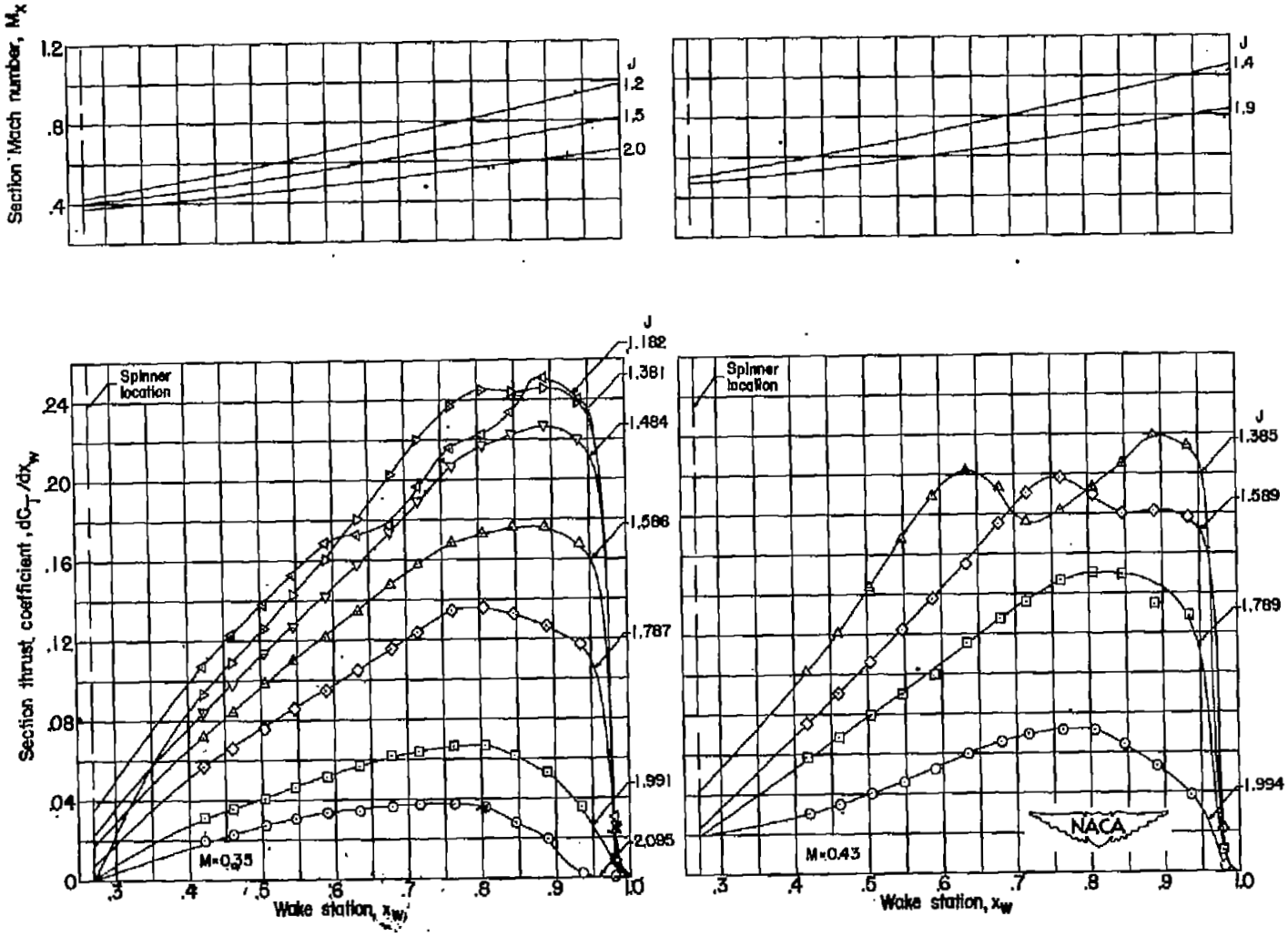

(a) $\beta_{0.75R} = 40^{\circ}$.

Figure 7.- Basic section-thrust-coefficient curves for NACA 4-(5)(08)-03 propeller.

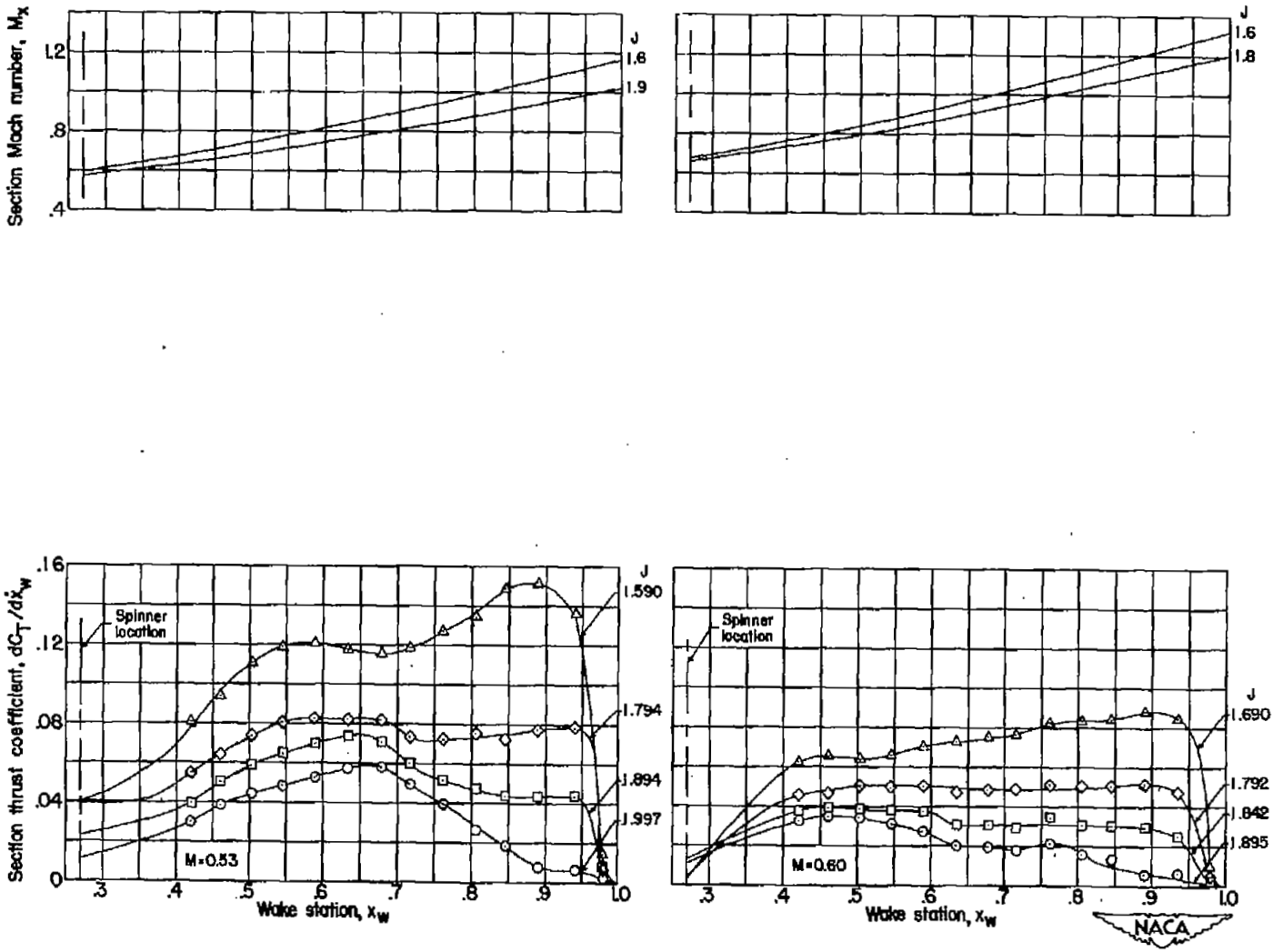

(a) Concluded. $\beta_{0.75R} = 40^\circ$.

Figure 7.- Continued.

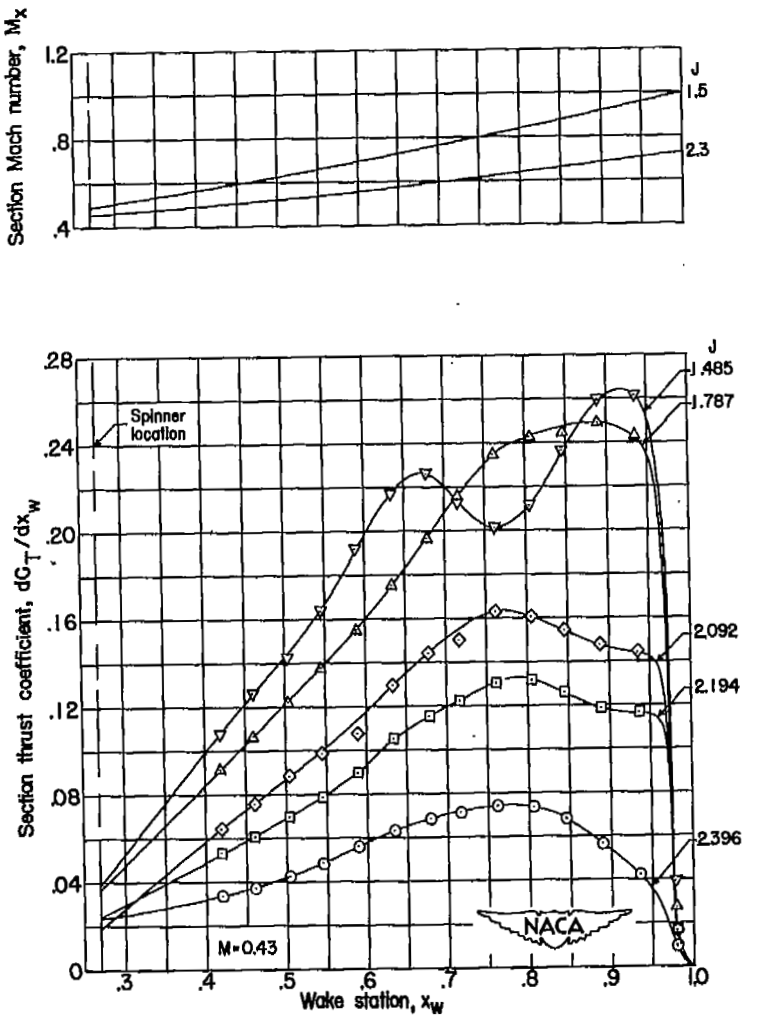

(b) $\beta_{0.75R} = 45^\circ$.

Figure 7.- Continued.

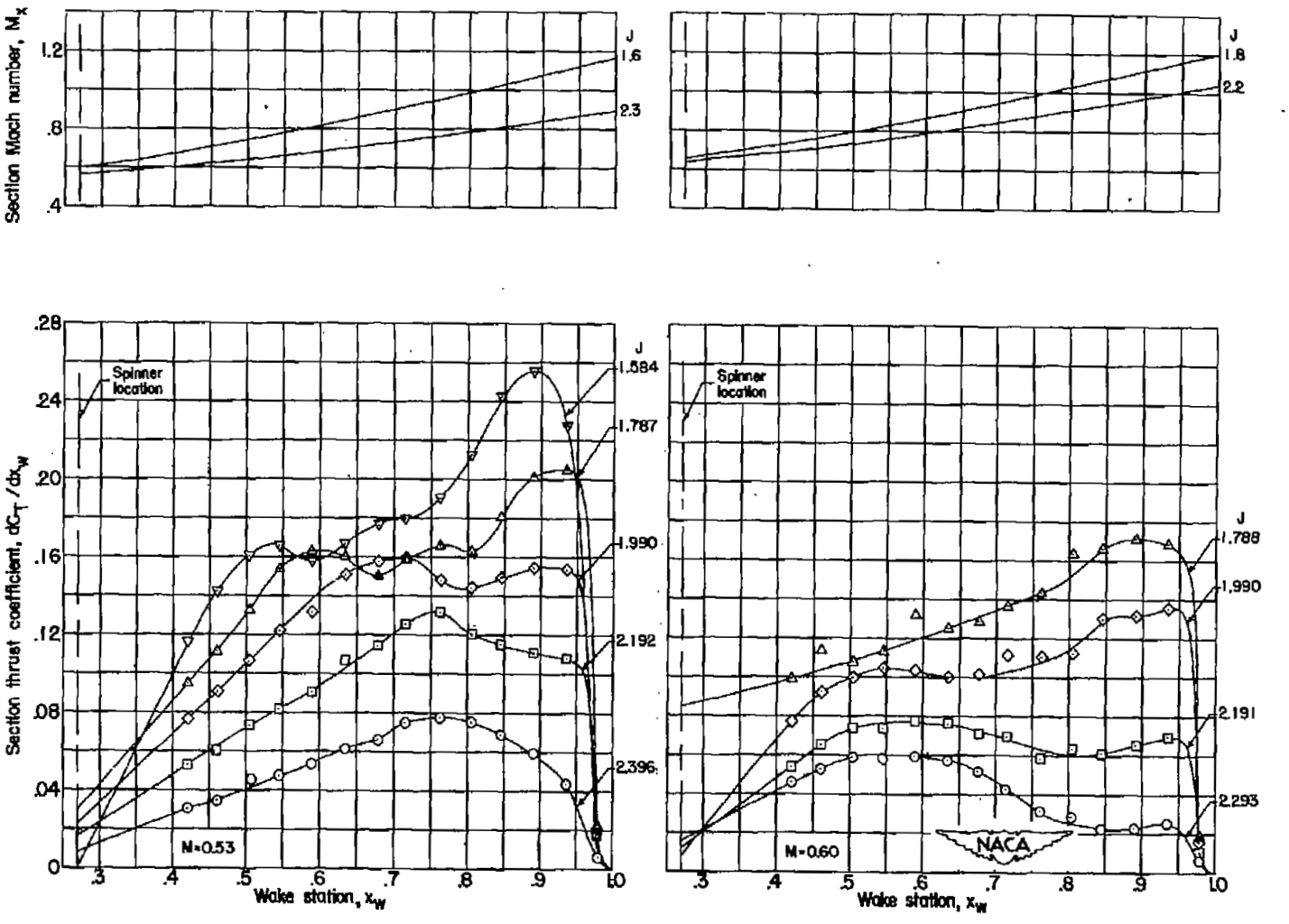

(b) Continued. $\beta_{0.75R} = 45°$.

Figure 7.- Continued.

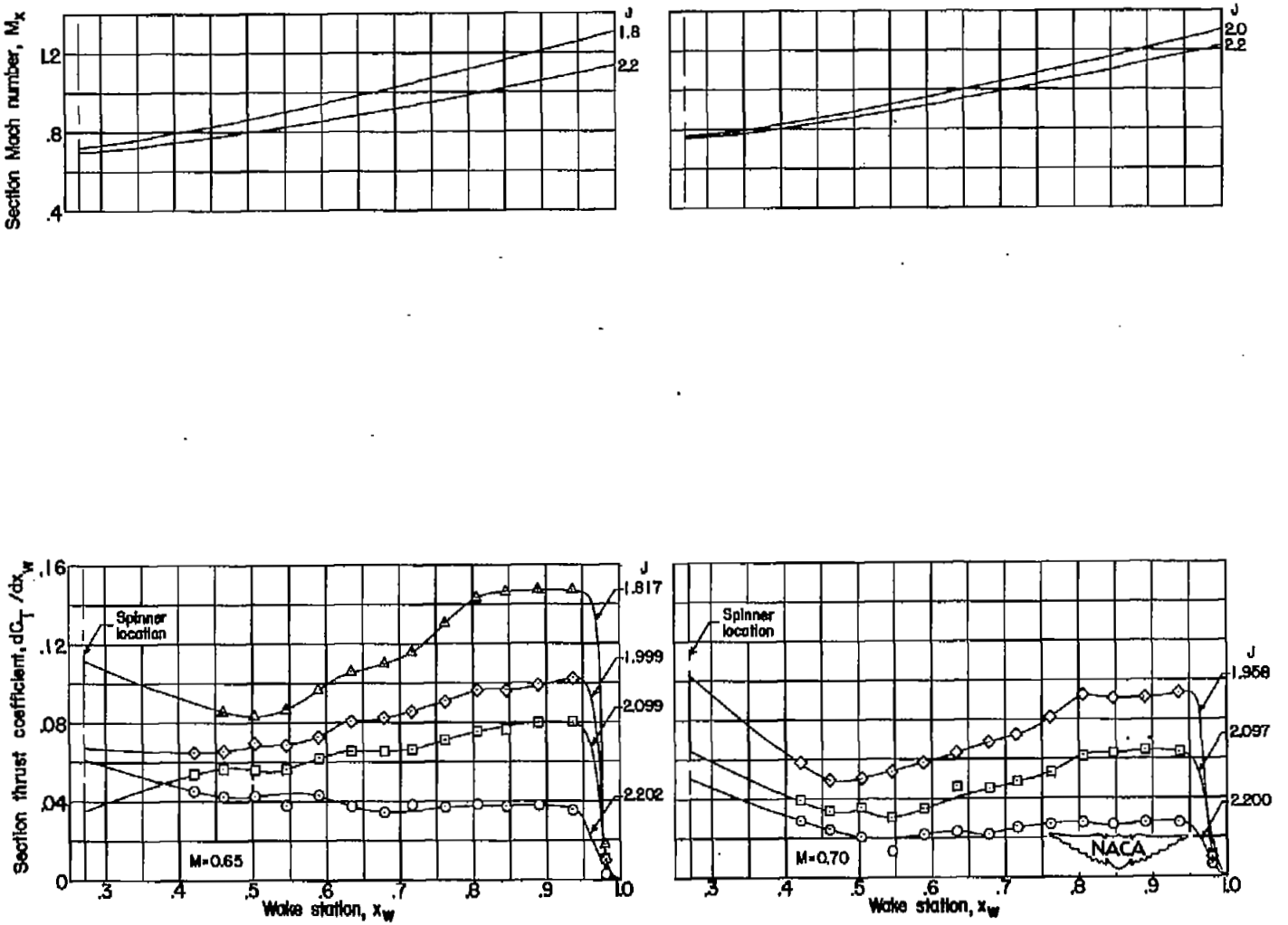

(b) Concluded. $\beta_{0.75R} = 45°$.

Figure 7.- Continued.

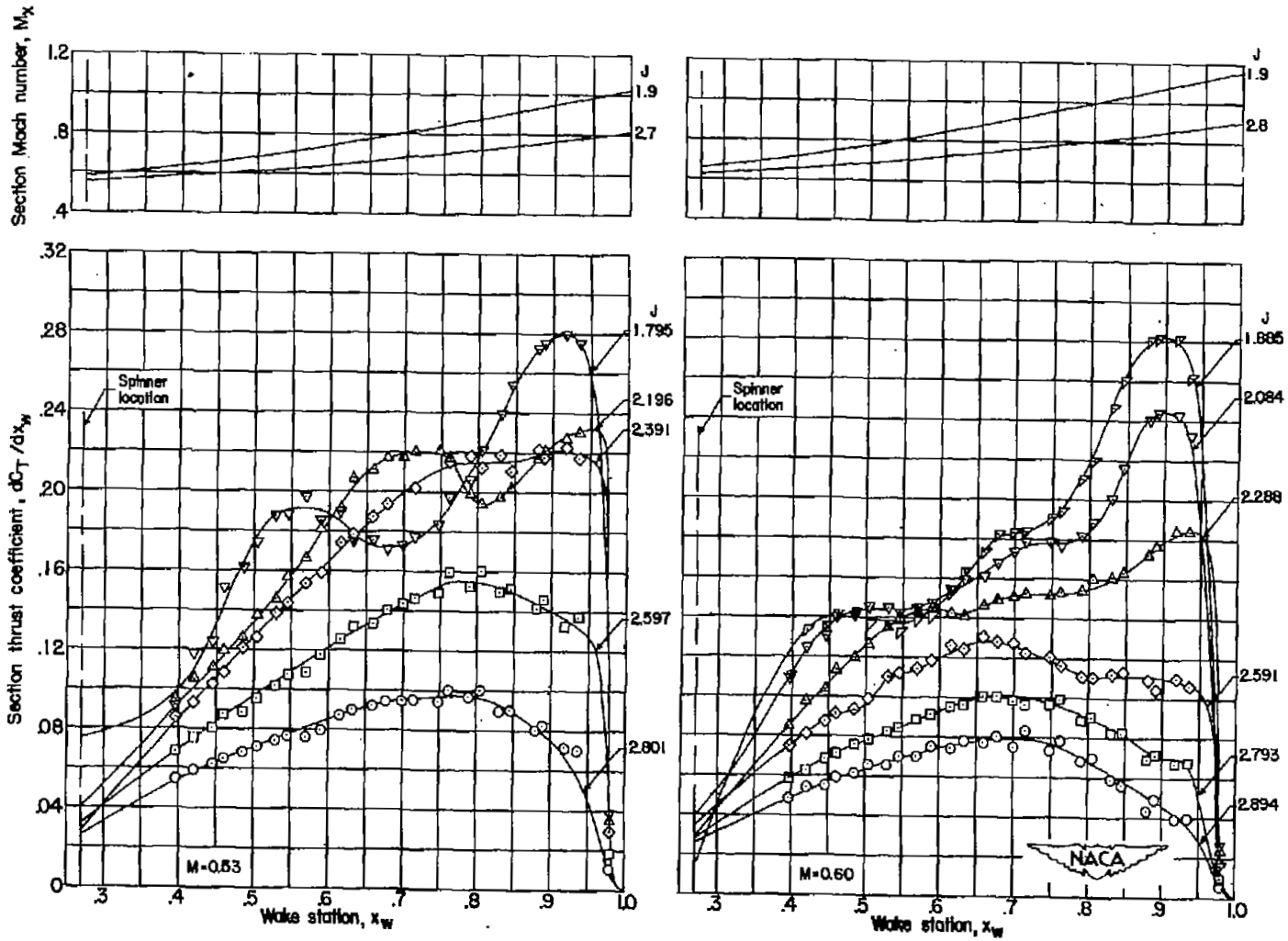

(c) $\beta_{0.75R} = 50^{\circ}$.

Figure 7.- Continued.

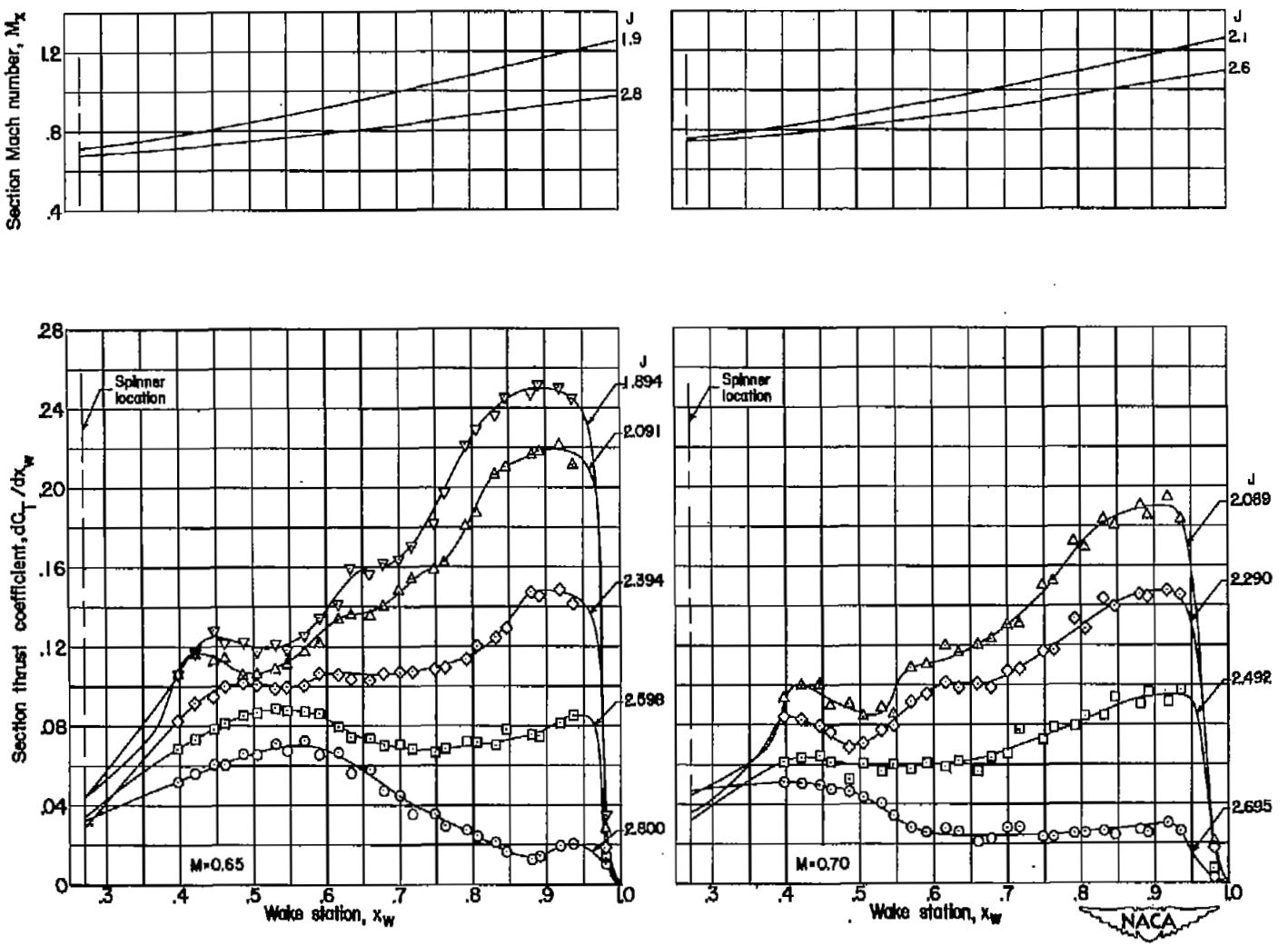

(c) Continued. $\beta_{0.75R} = 50^\circ$.

Figure 7.- Continued.

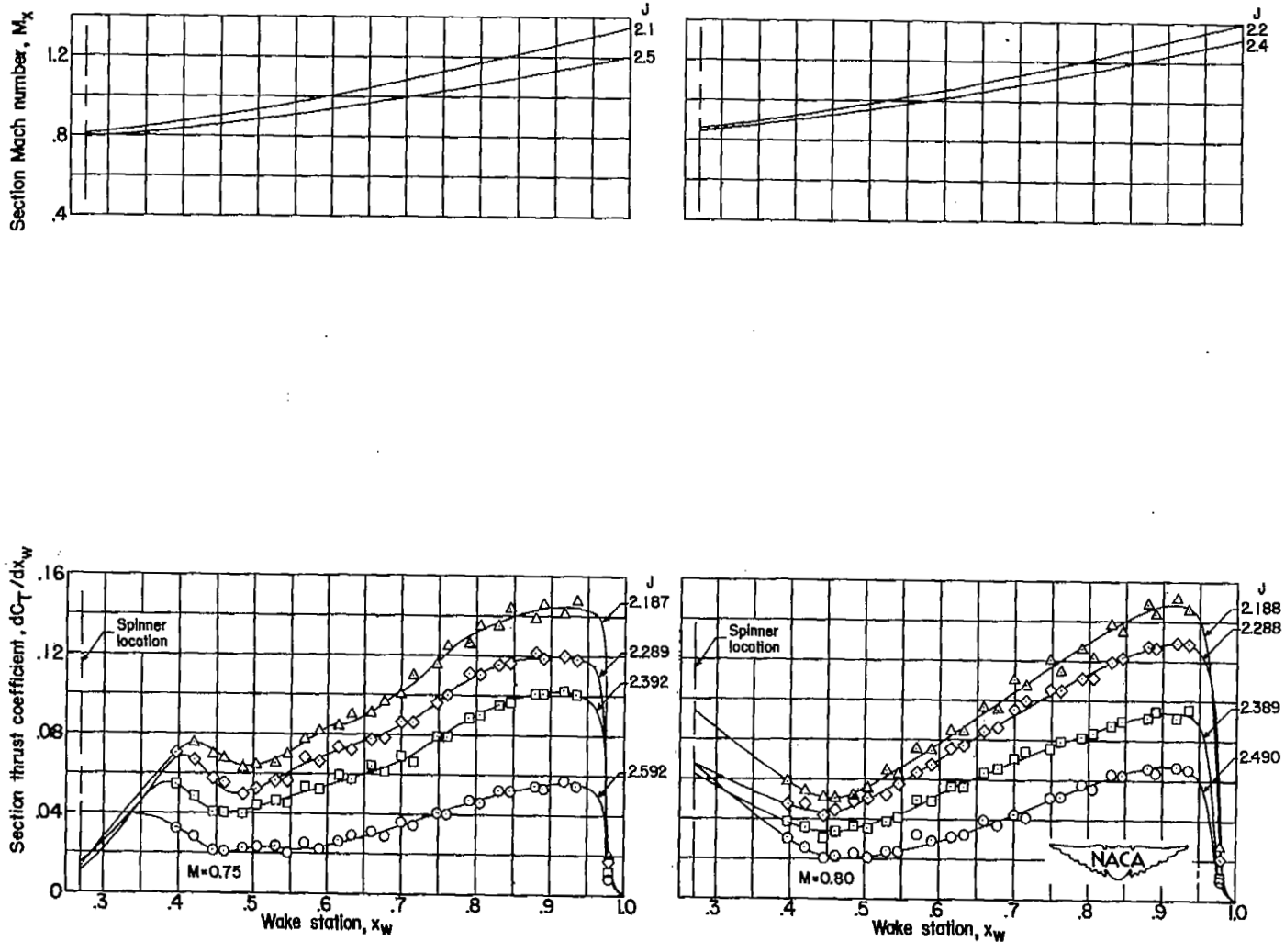

(c) Concluded. $\beta_{0.75R} = 50^{\circ}$.

Figure 7.- Continued.

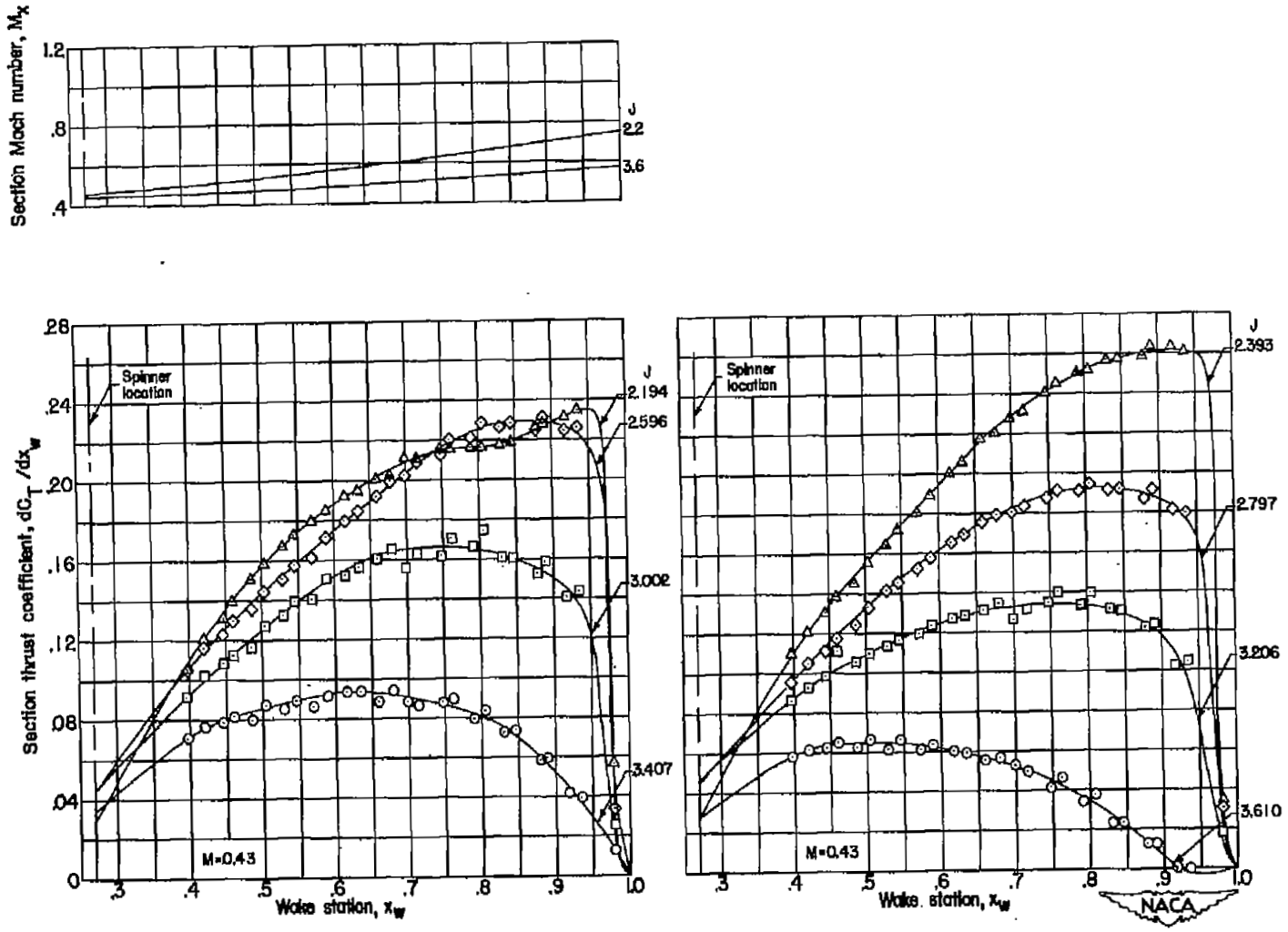

(d) $\beta_{0.75R} = 55^{\circ}$.

Figure 7.- Continued.

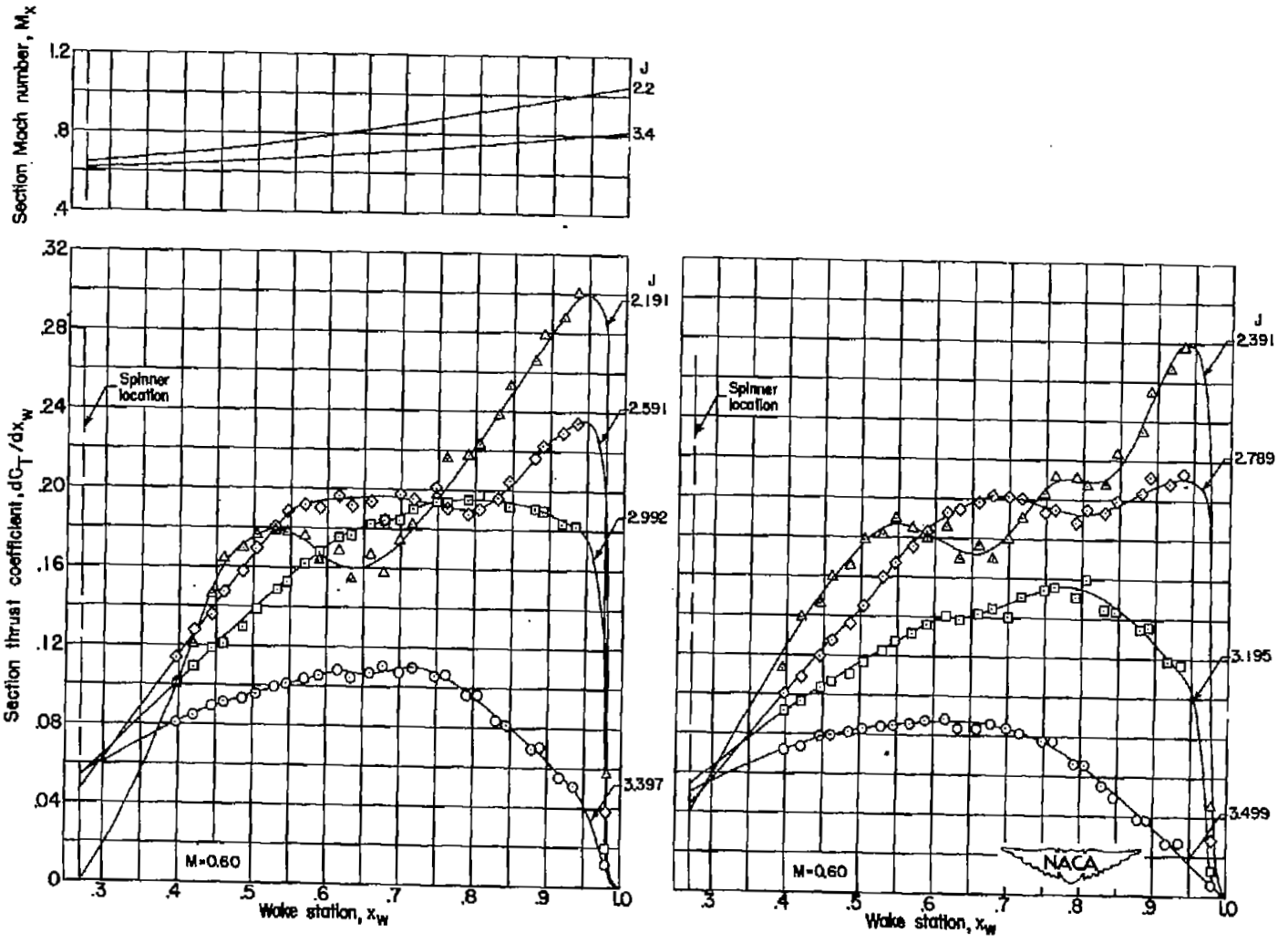

(d) Continued. $\beta_{0.75R} = 55^\circ$.

Figure 7.- Continued.

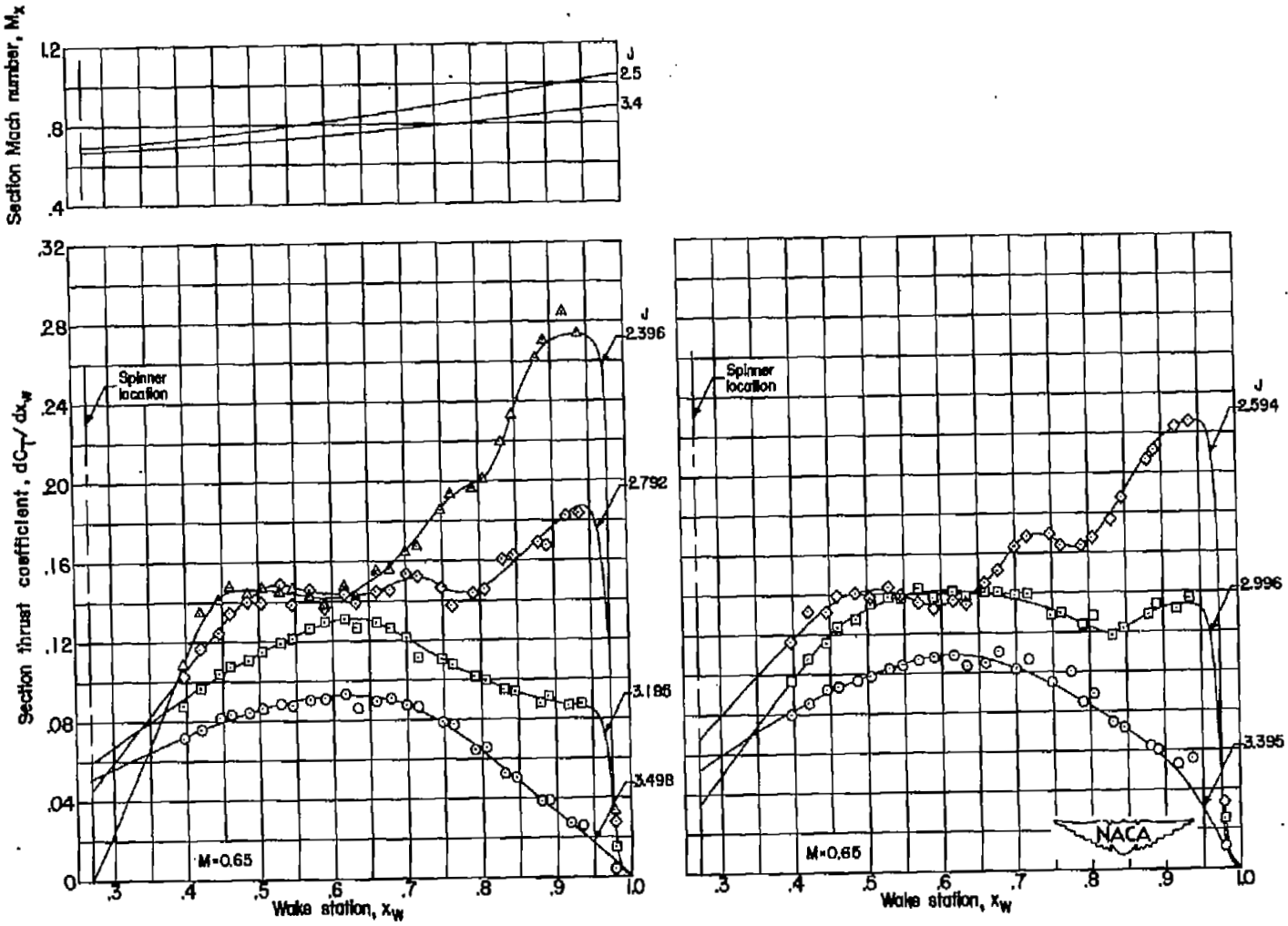

(d) Continued. $\beta_{0.75R} = 55°$.

Figure 7.- Continued.

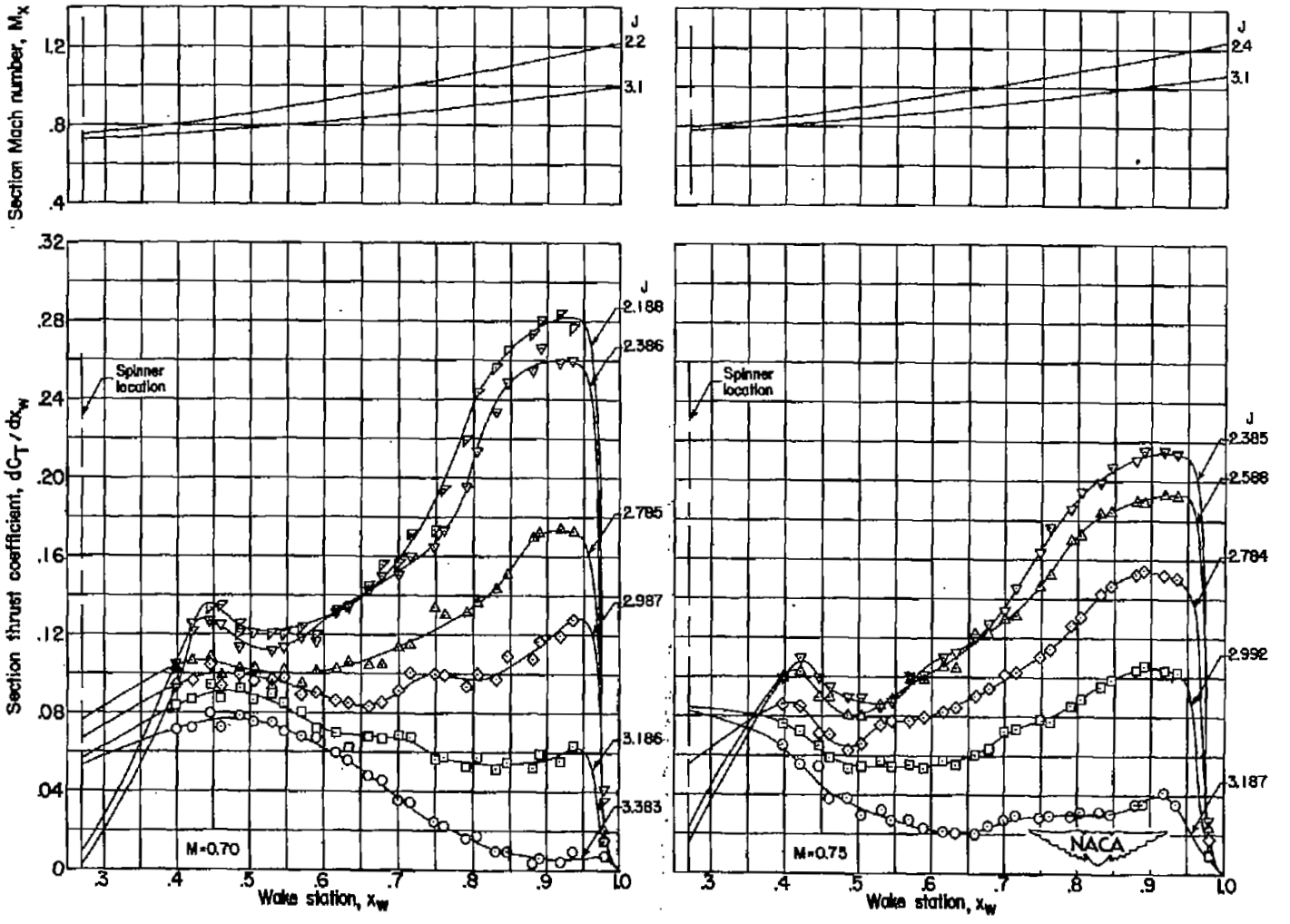

(d) Continued. $\beta_{0.75R} = 55^\circ$.

Figure 7.- Continued.

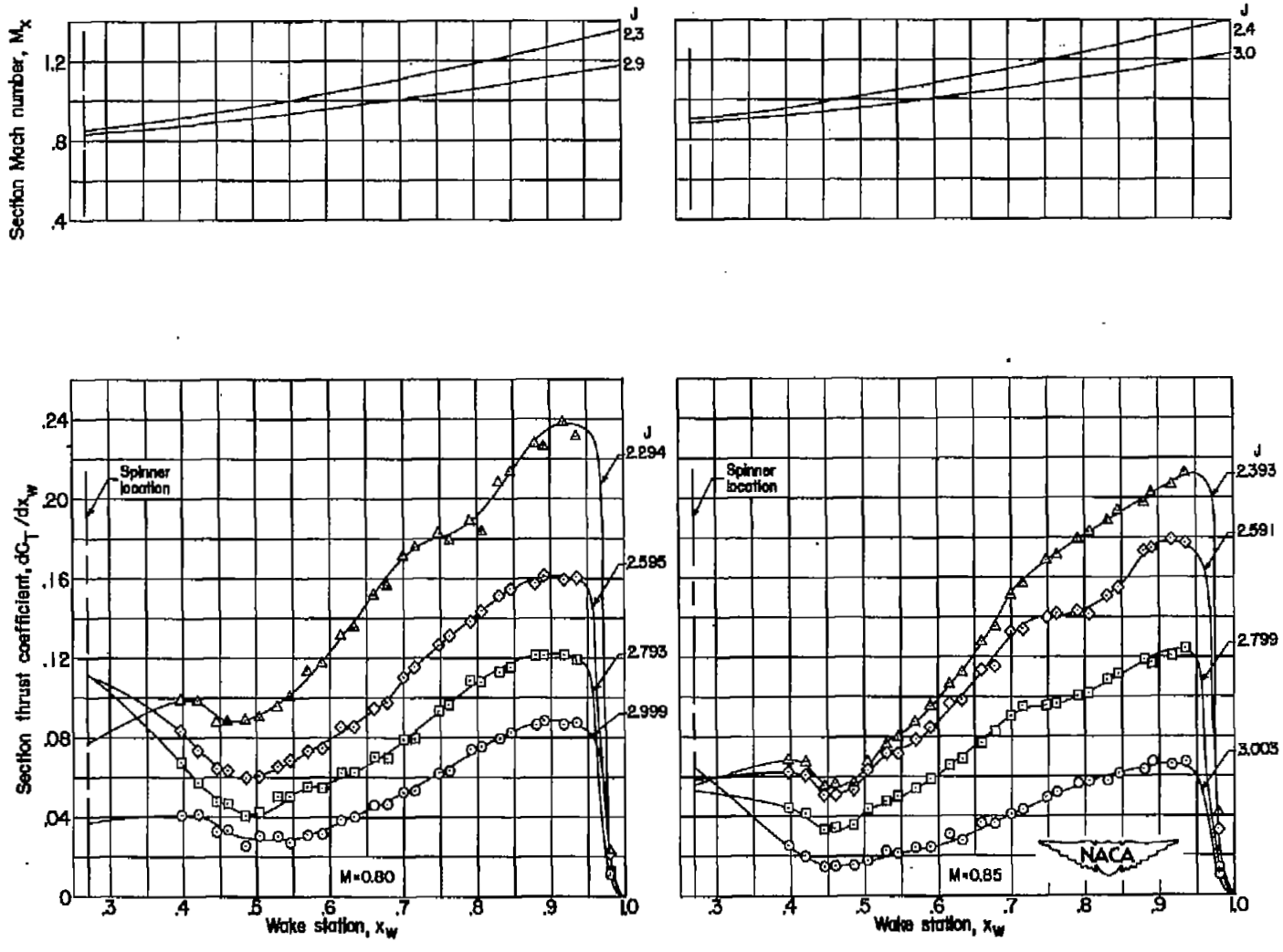

(d) Continued. $\beta_{0.75R} = 55^\circ$.

Figure 7.- Continued.

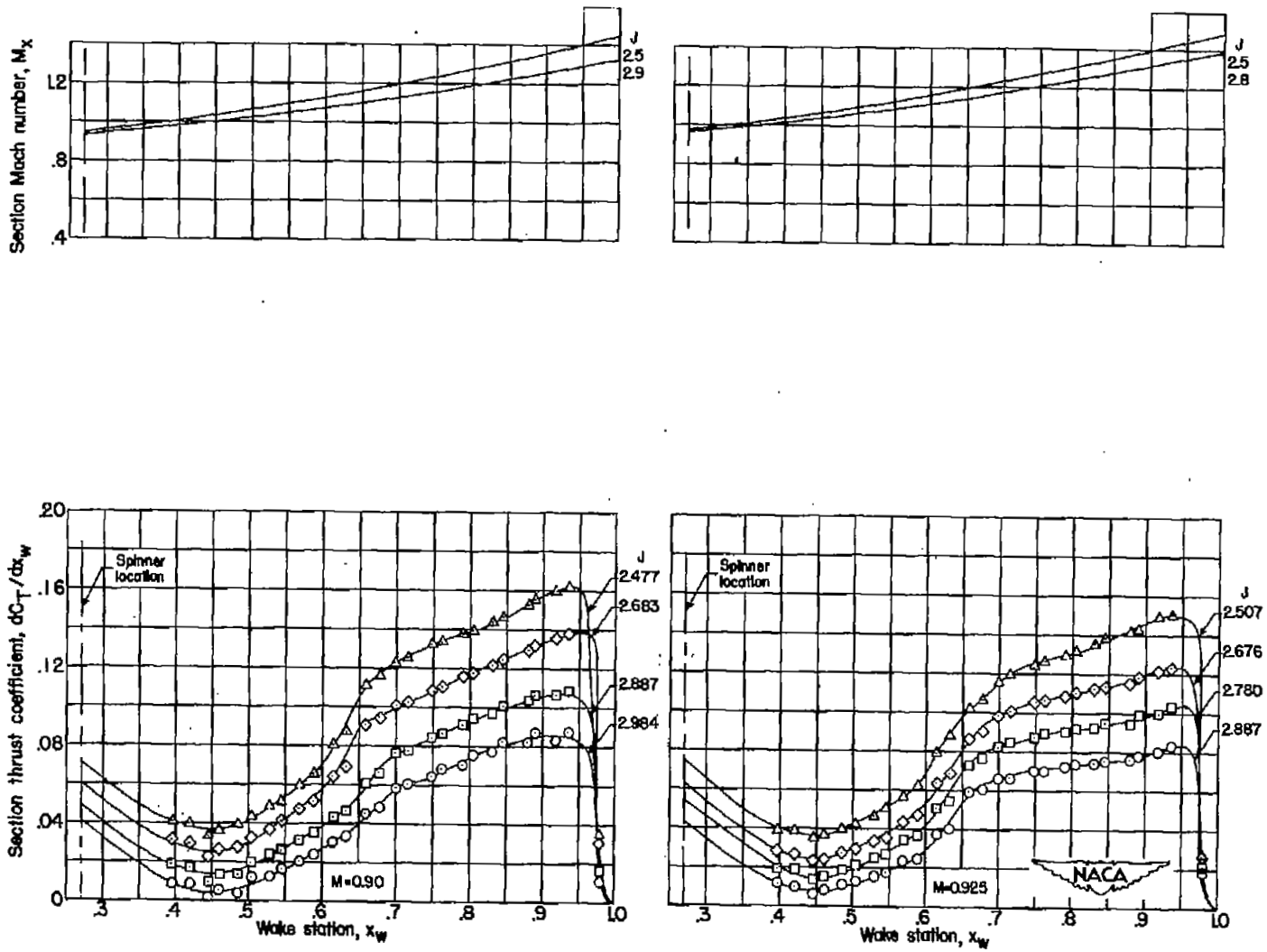

(d) Concluded. $\beta_{0.75R} = 55^\circ$.

Figure 7.- Continued.

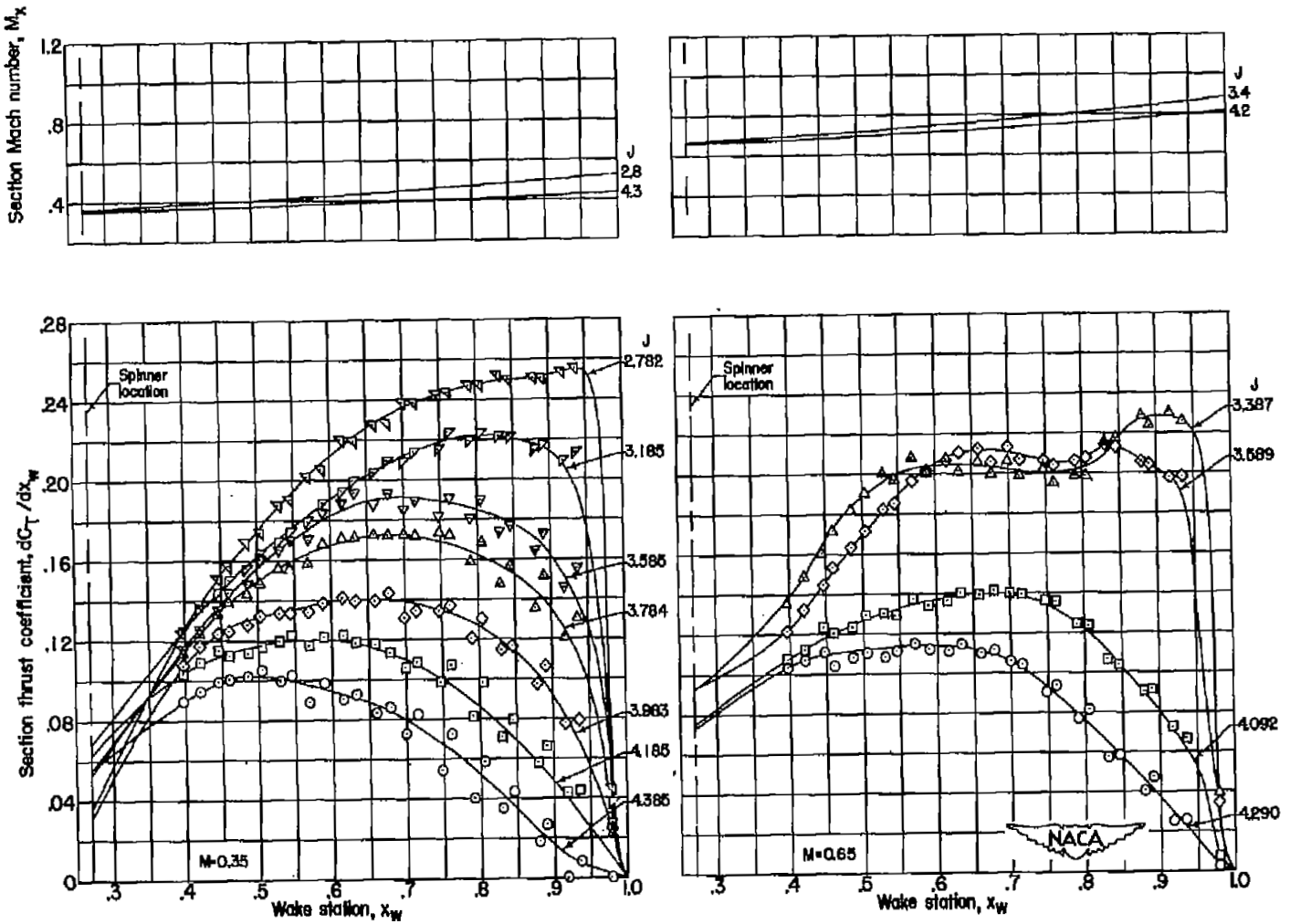

(e) $\beta_{0.75R} = 60°$.

Figure 7.- Continued.

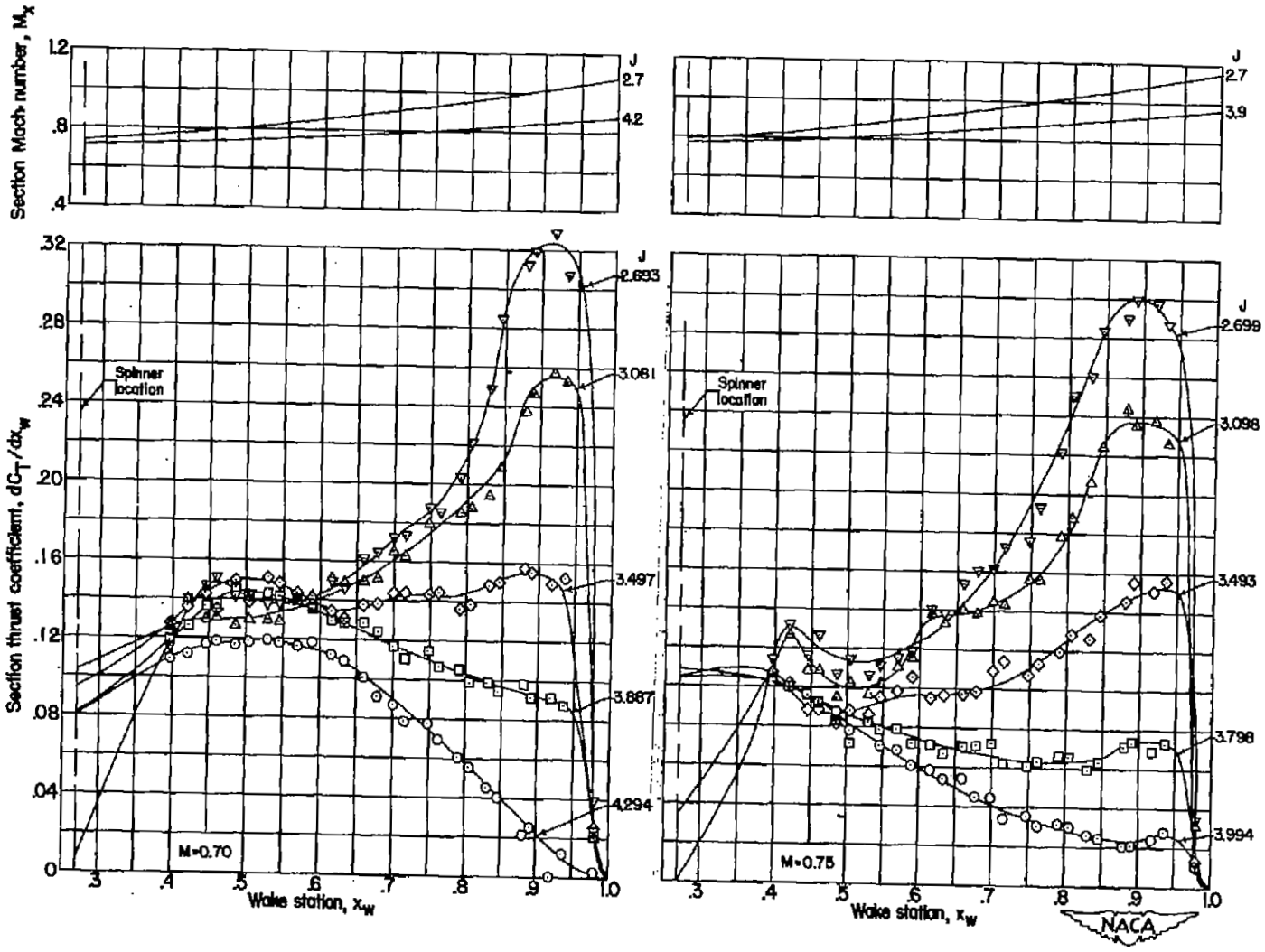

(e) Continued. $\beta_{0.75R} = 60^{\circ}$.

Figure 7.- Continued.

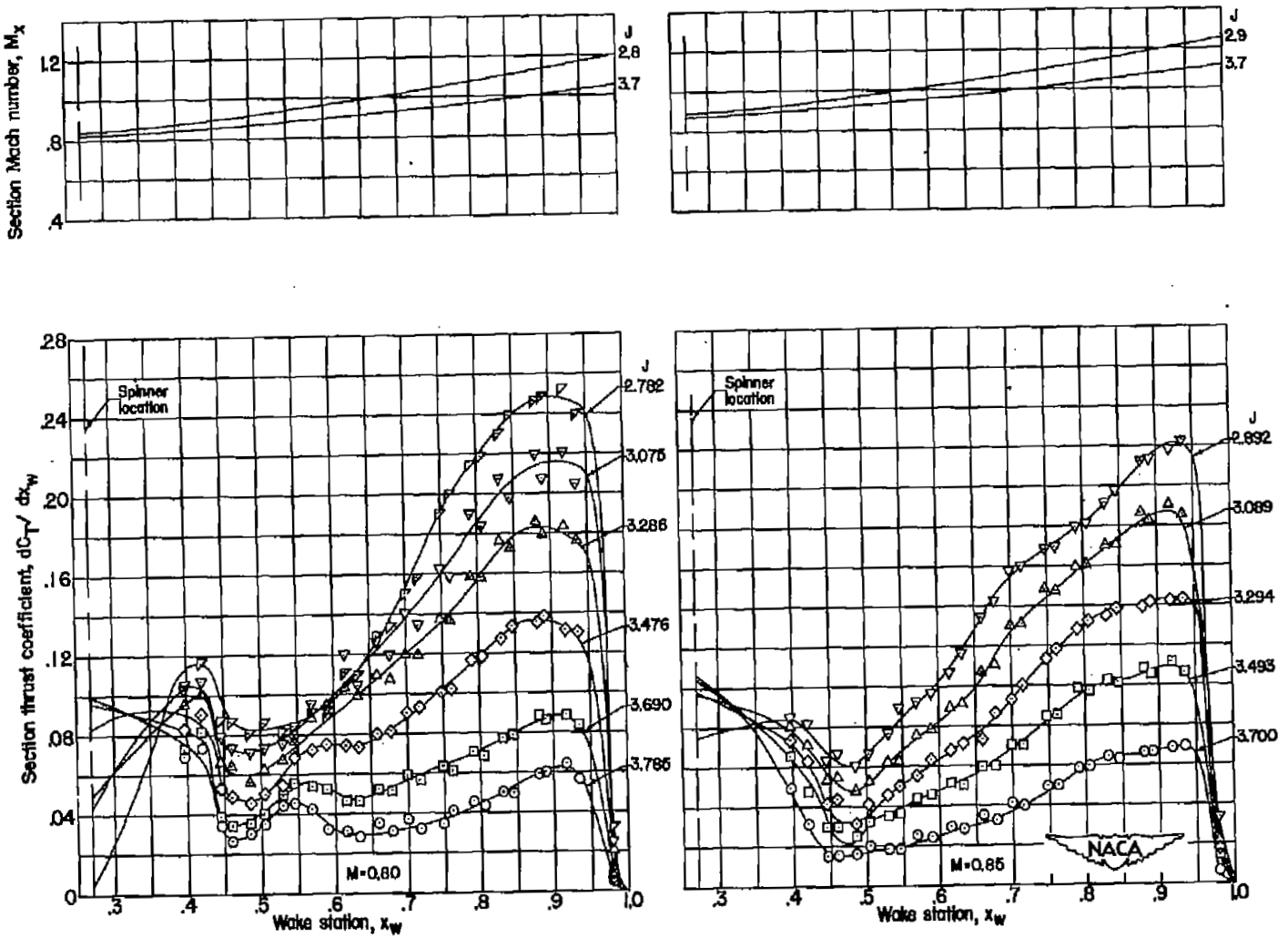

(e) Continued. $\beta_{0.75R} = 60^\circ$.

Figure 7.- Continued.

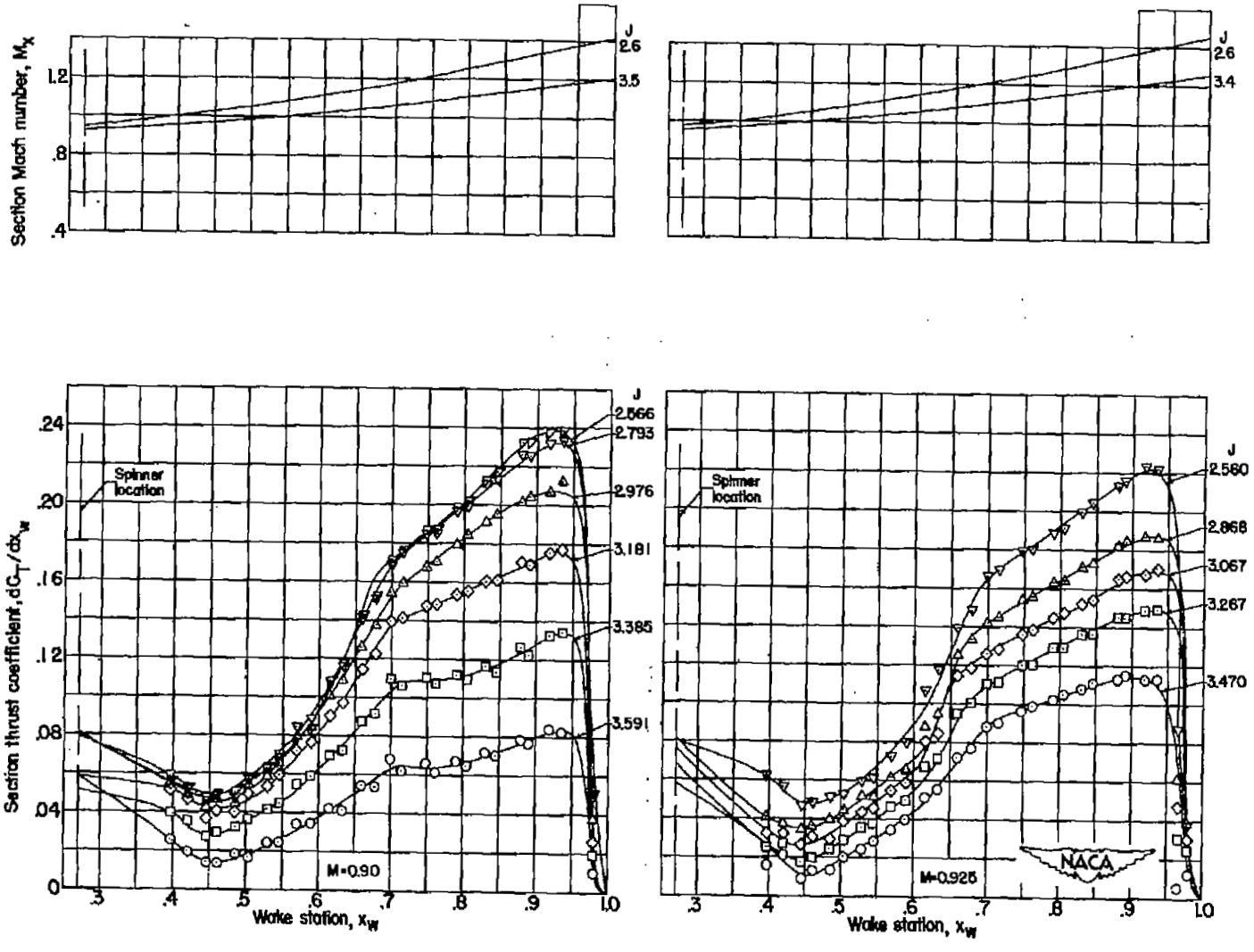

(e) Concluded. $\beta_{0.75R} = 60^\circ$.

Figure 7.- Continued.

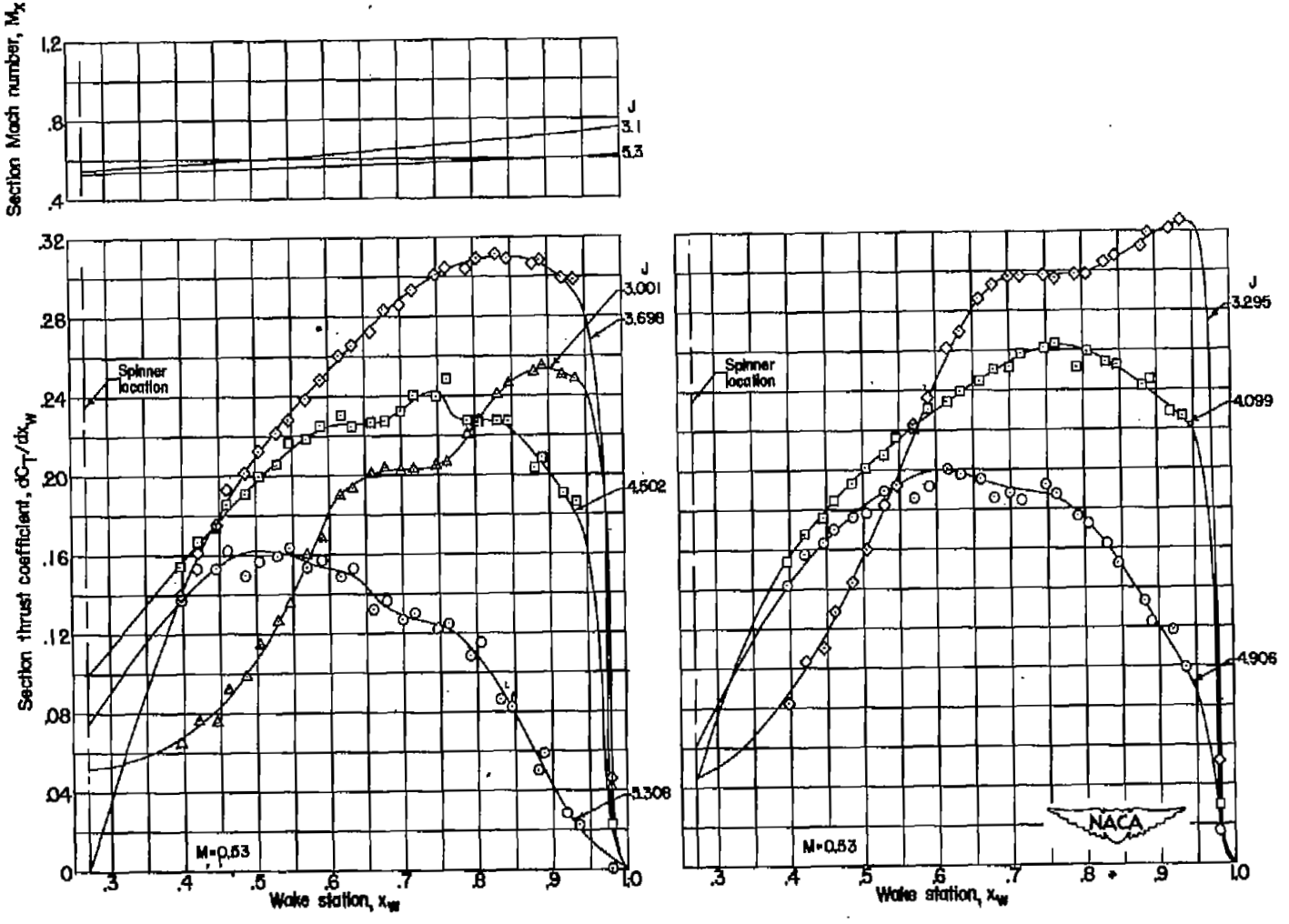

(f) $\beta_{0.75R} = 65°$.

Figure 7.- Continued.

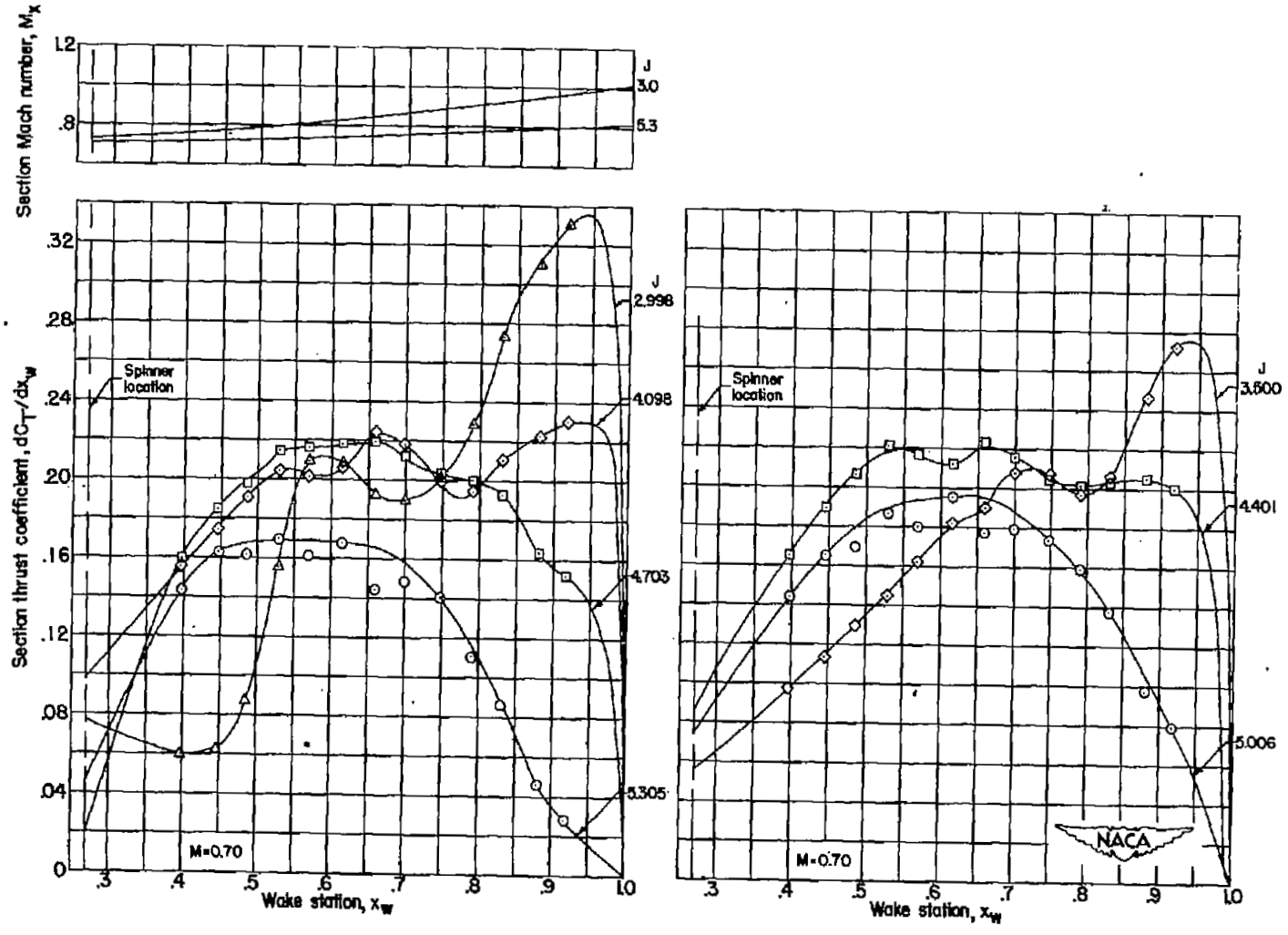

(f) Continued. $\beta_{0.75R} = 65°$.

Figure 7.- Continued.

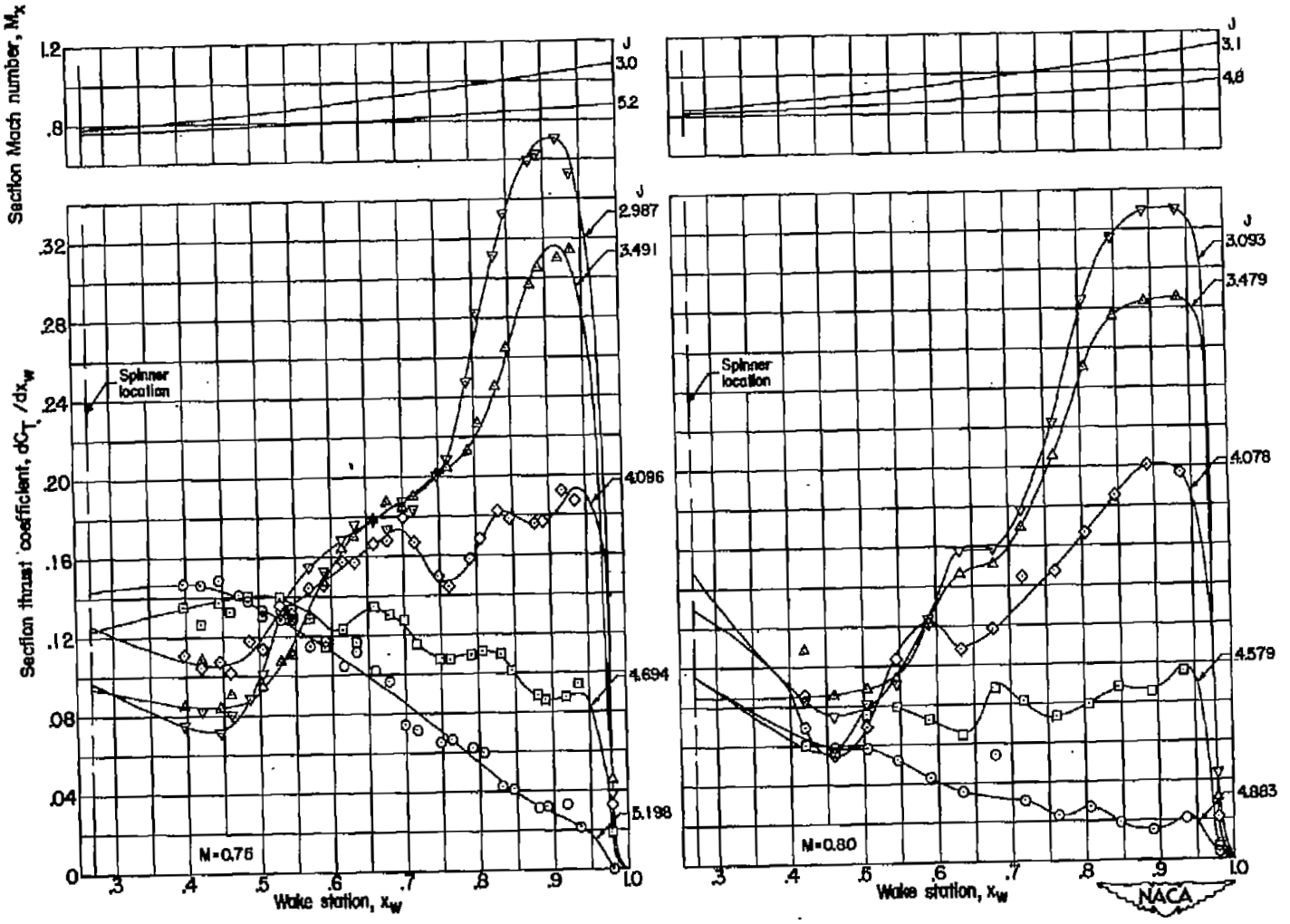

(f) Continued. $\beta_{0.75R} = 65^\circ$.

Figure 7.- Continued.

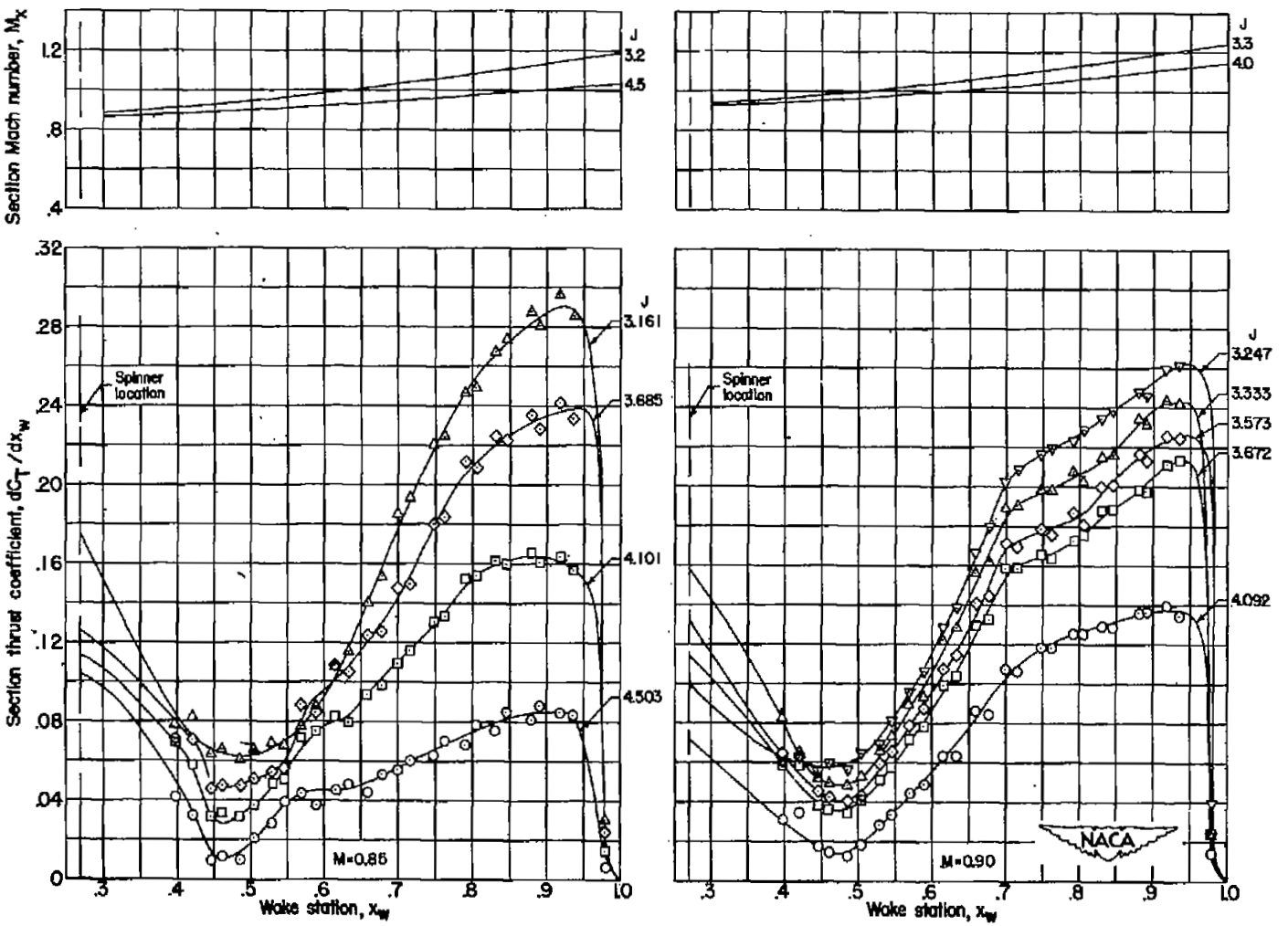

(f) Continued. $\beta_{0.75R} = 65^\circ$.

Figure 7.- Continued.

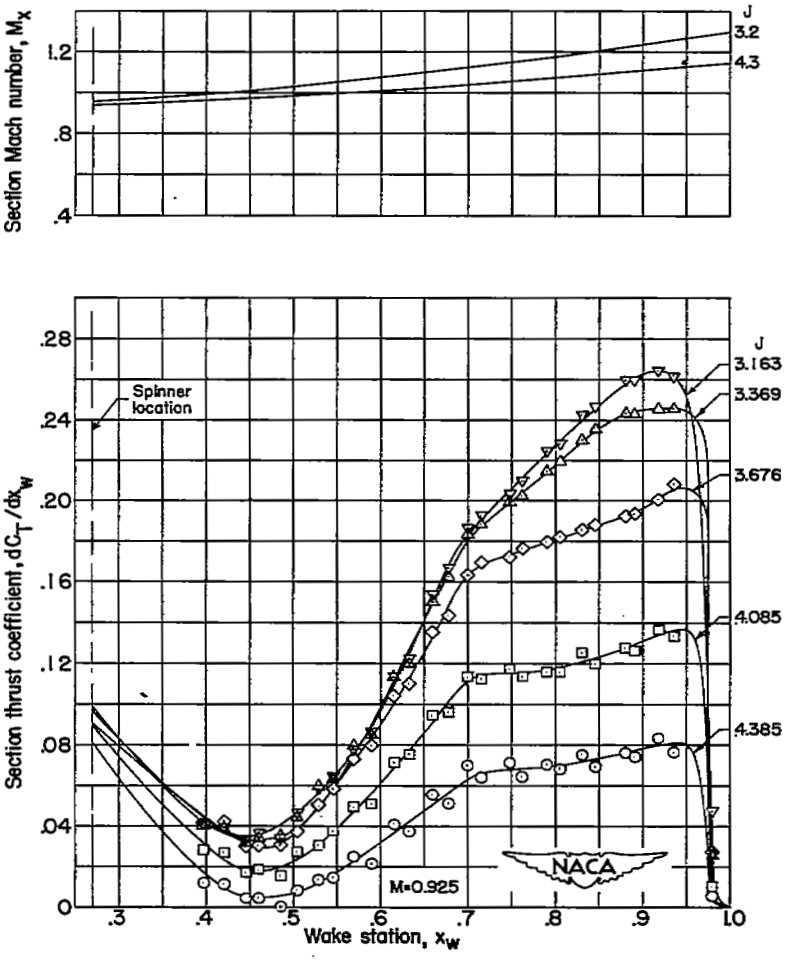

(f) Concluded. $\beta_{0.75R} = 65°$.

Figure 7.- Concluded.

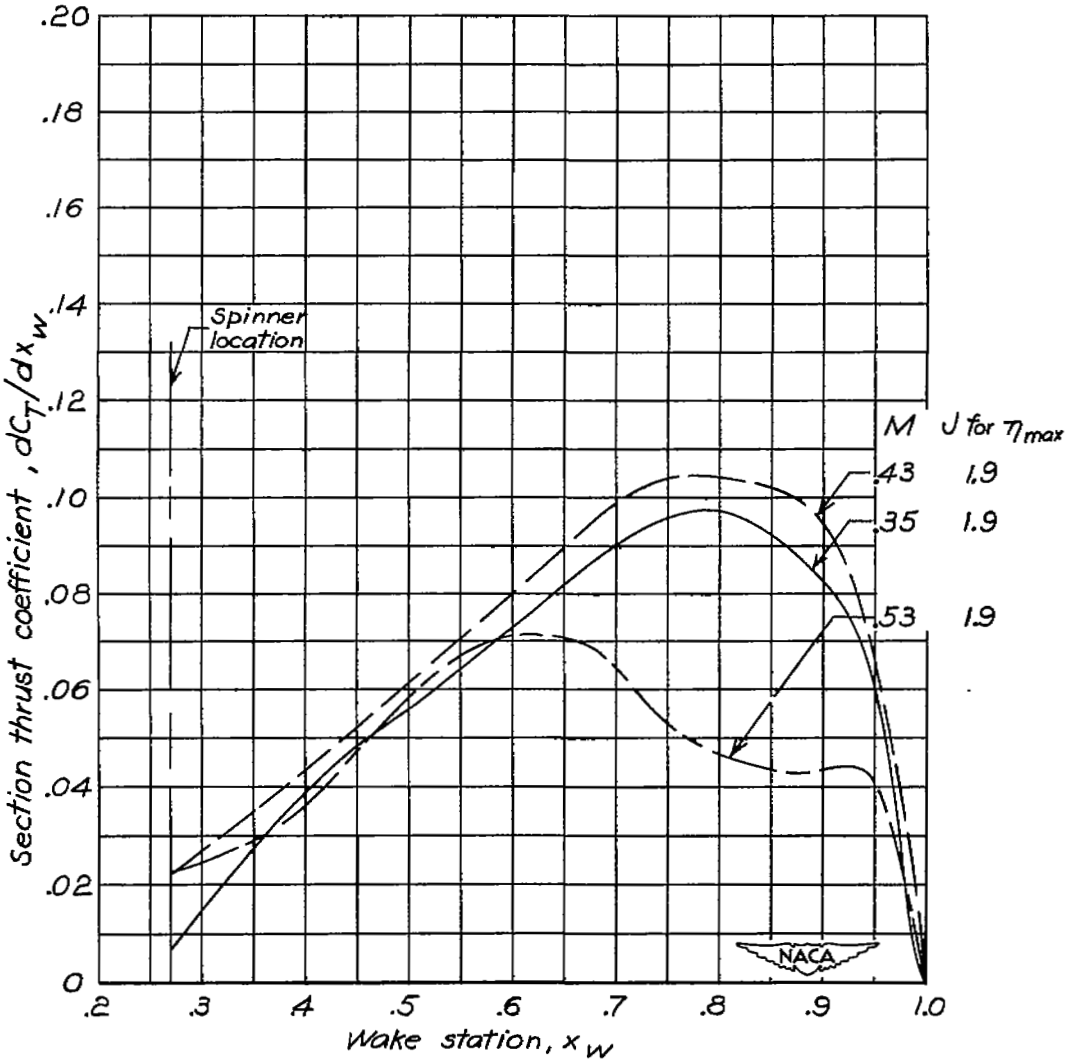

(a) $\beta_{0.75R} = 40°$.

Figure 8.- Effect of Mach number on section-thrust-coefficient curves for maximum efficiency. NACA 4-(5)(08)-03 propeller.

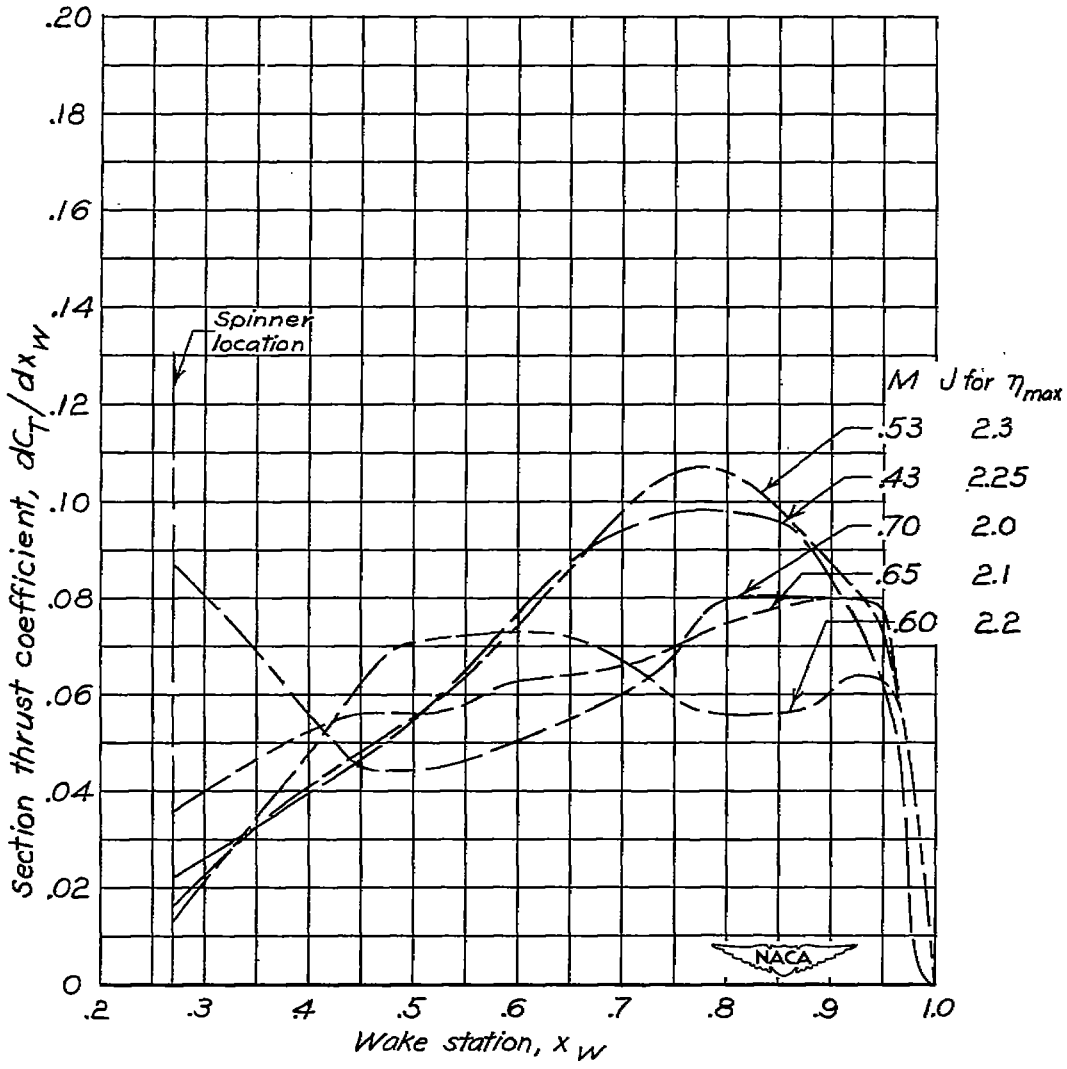

(b) $\beta_{0.75R} = 45°$.

Figure 8.- Continued.

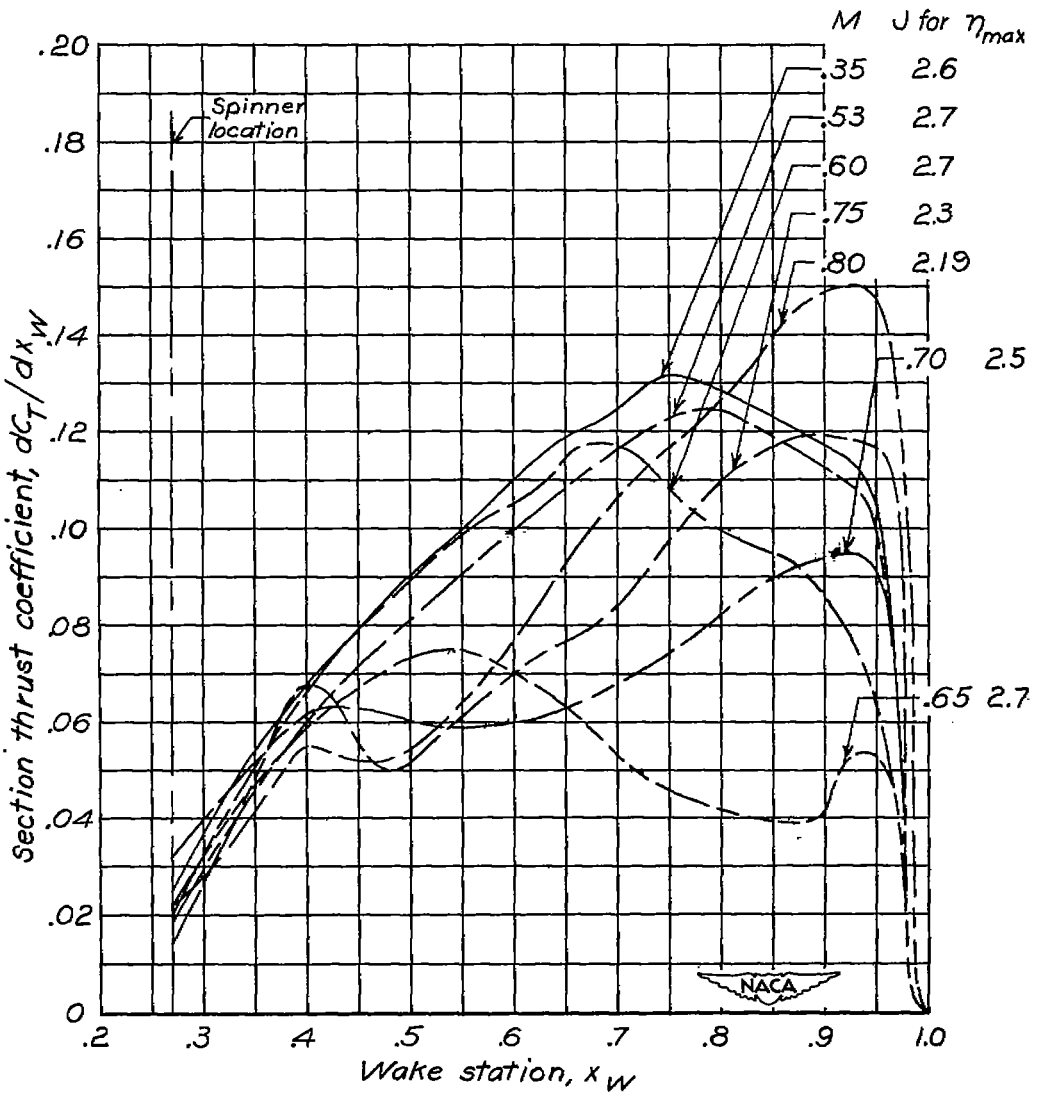

(c) $\beta_{0.75R} = 50°$.

Figure 8.- Continued.

[redacted]

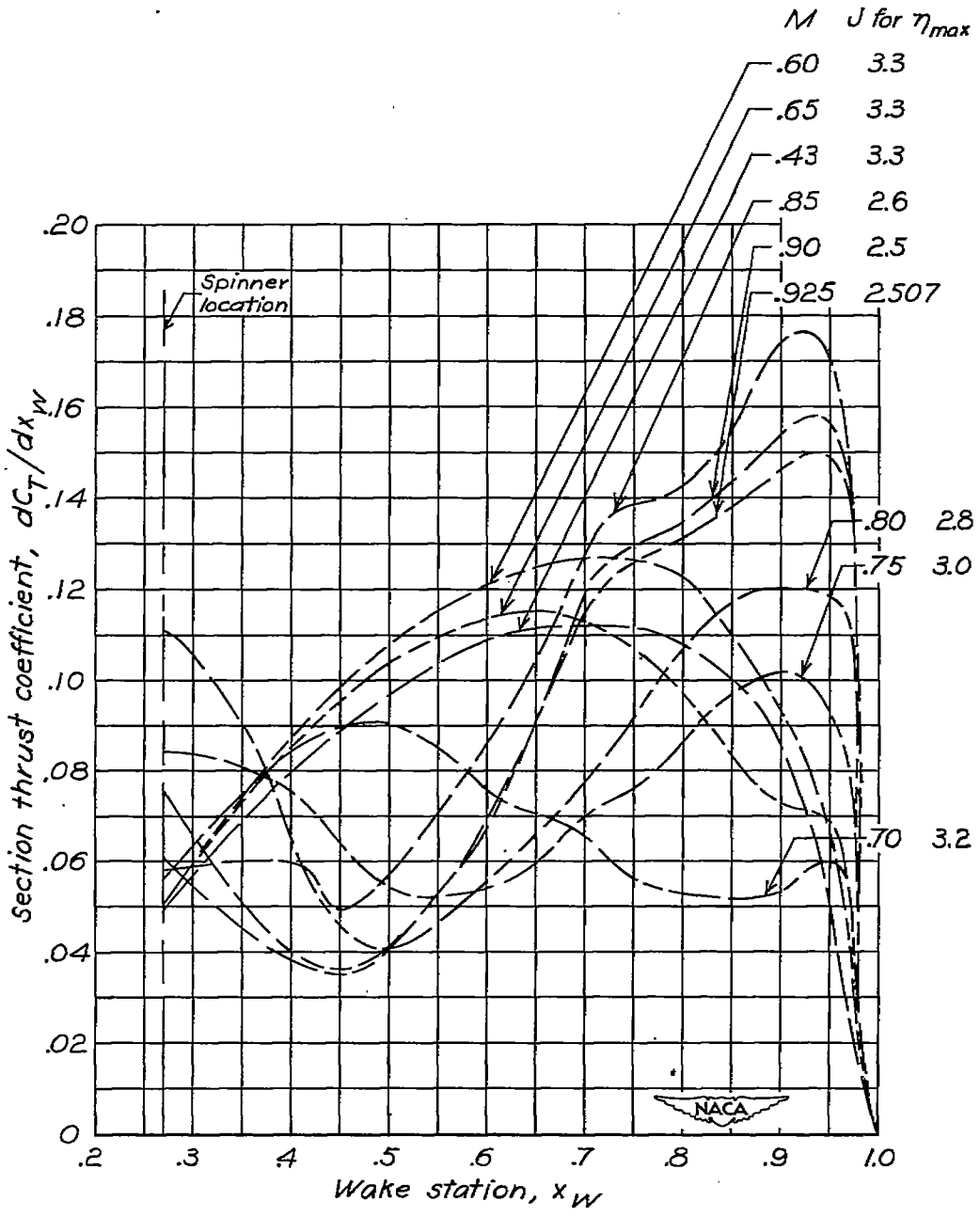

(d) $\beta_{0.75R} = 55^\circ$.

Figure 8.- Continued.

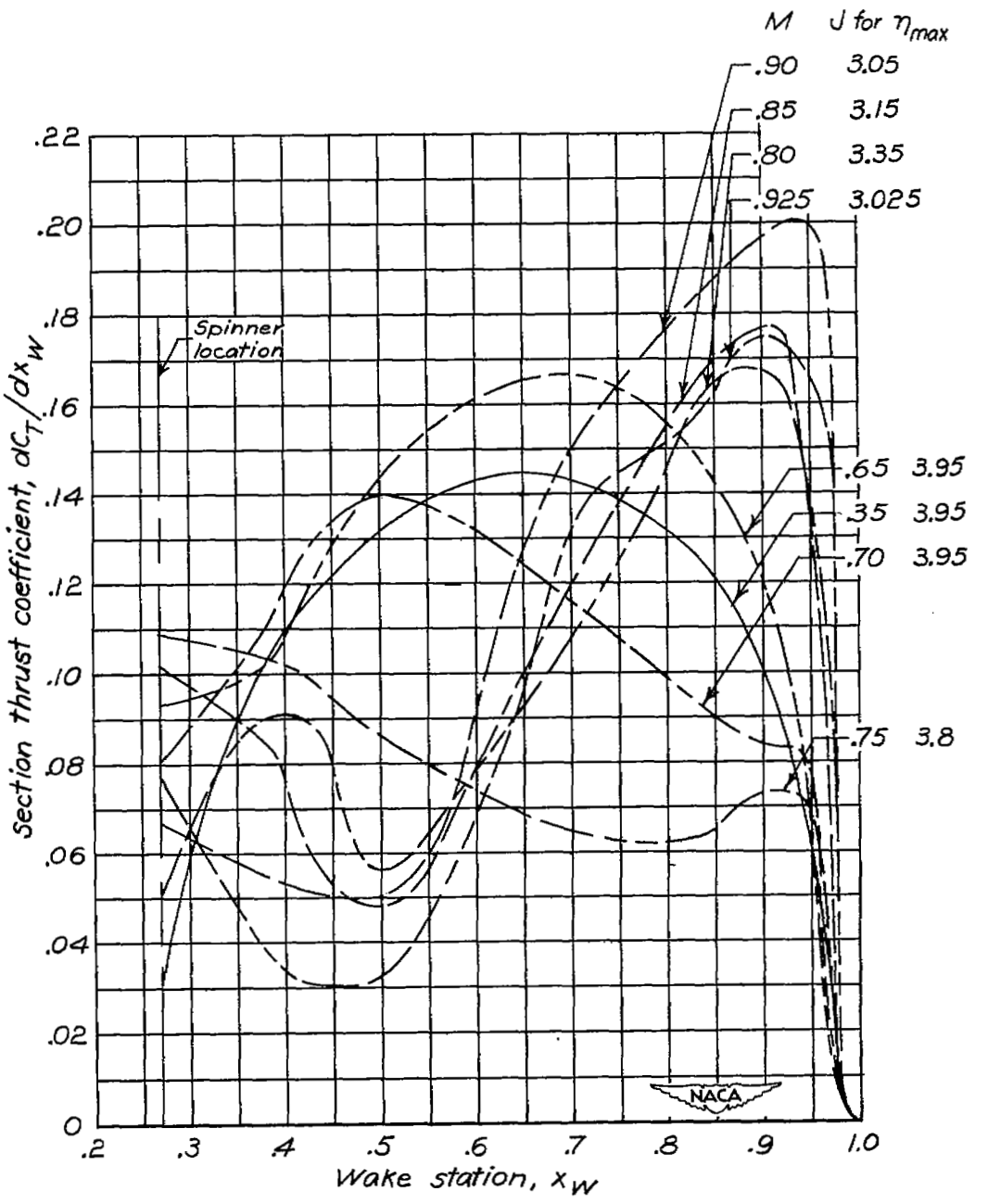

(e) $\beta_{0.75R} = 60°$.

Figure 8.- Continued.

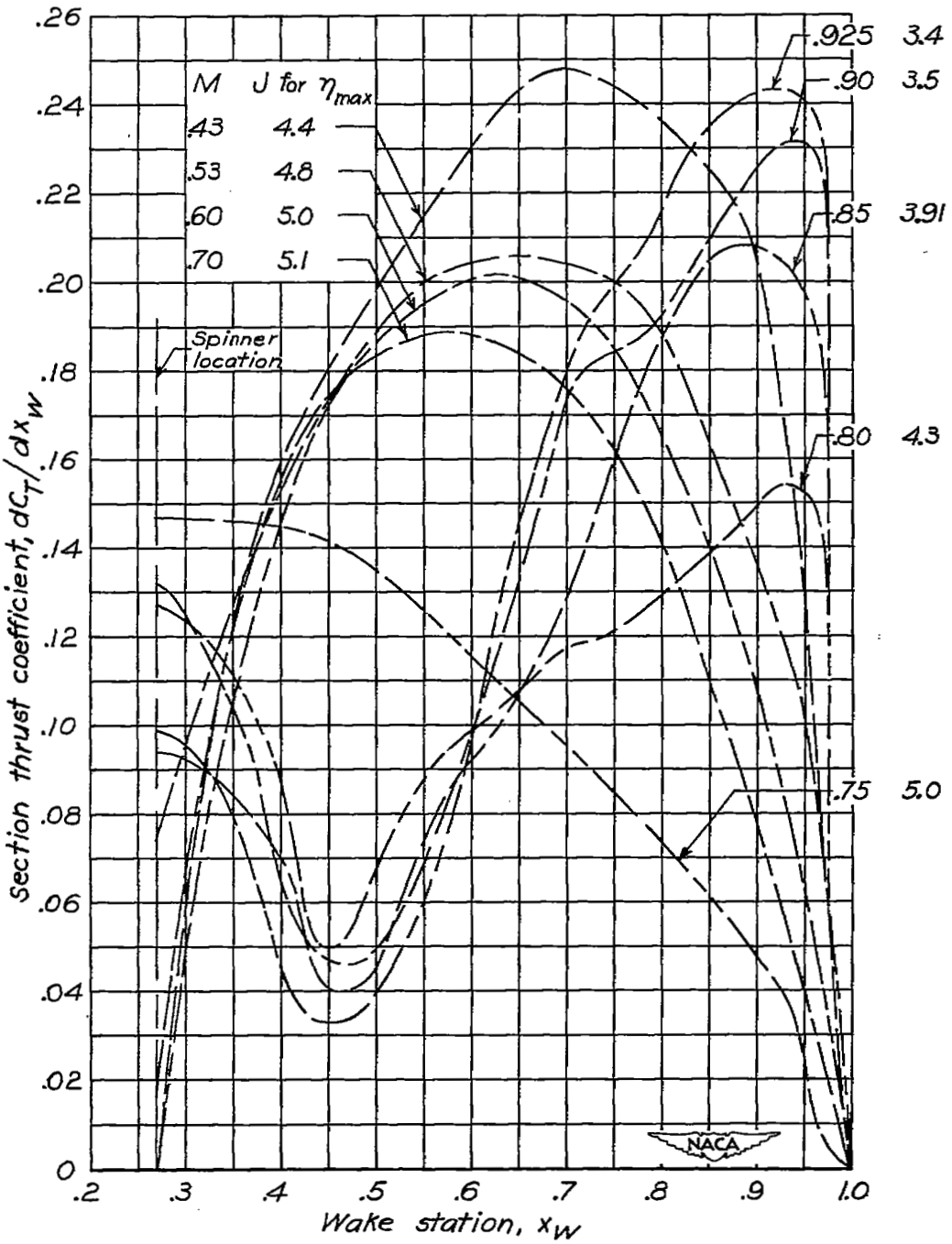

(f) $\beta_{0.75R} = 65°$.

Figure 8.- Concluded.

[redacted]

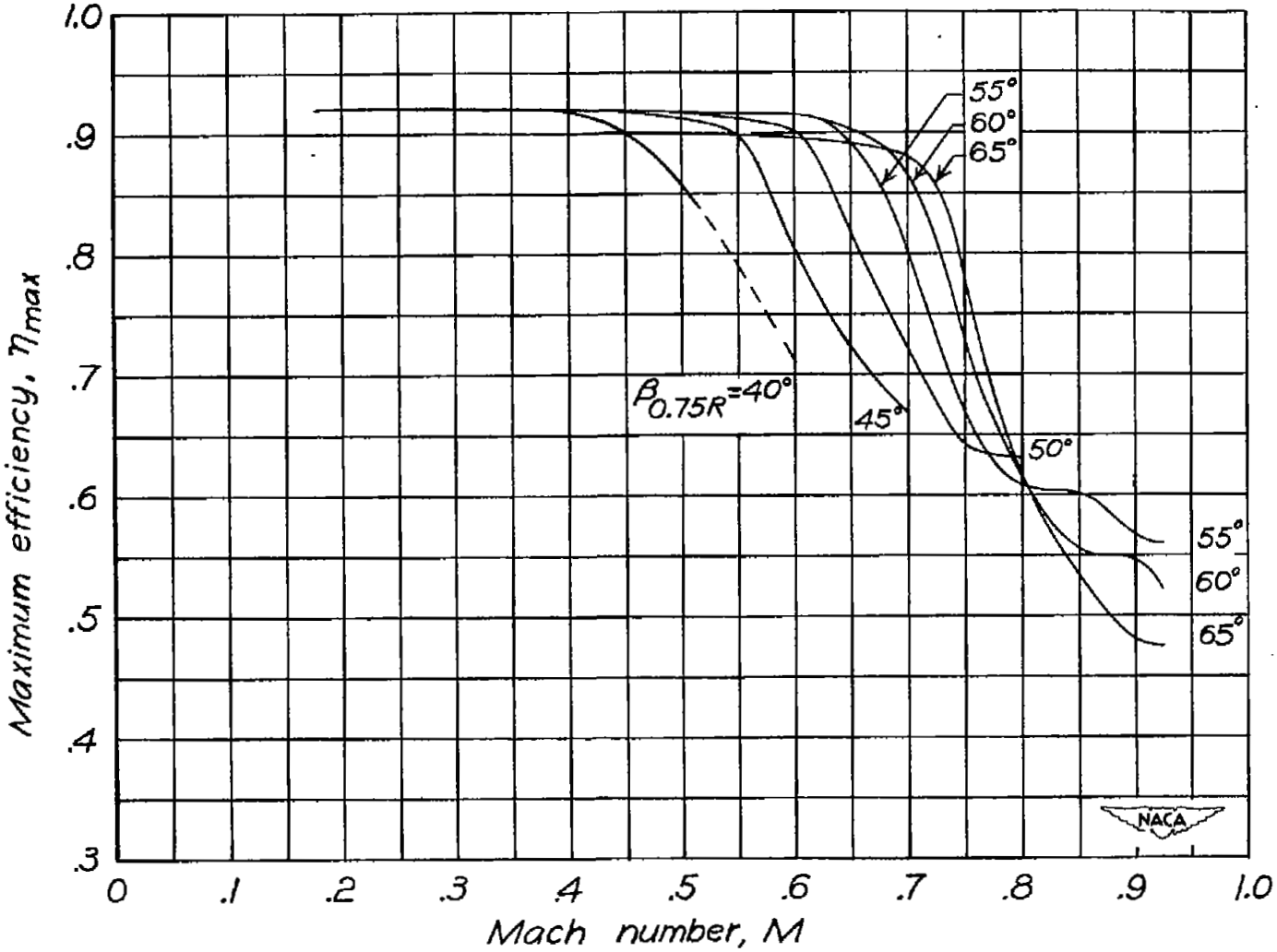

Figure 9.- Effect of forward Mach number on maximum efficiency. NACA 4-(5)(08)-03 propeller. (Dashed line indicates maximum efficiency was not attained.)

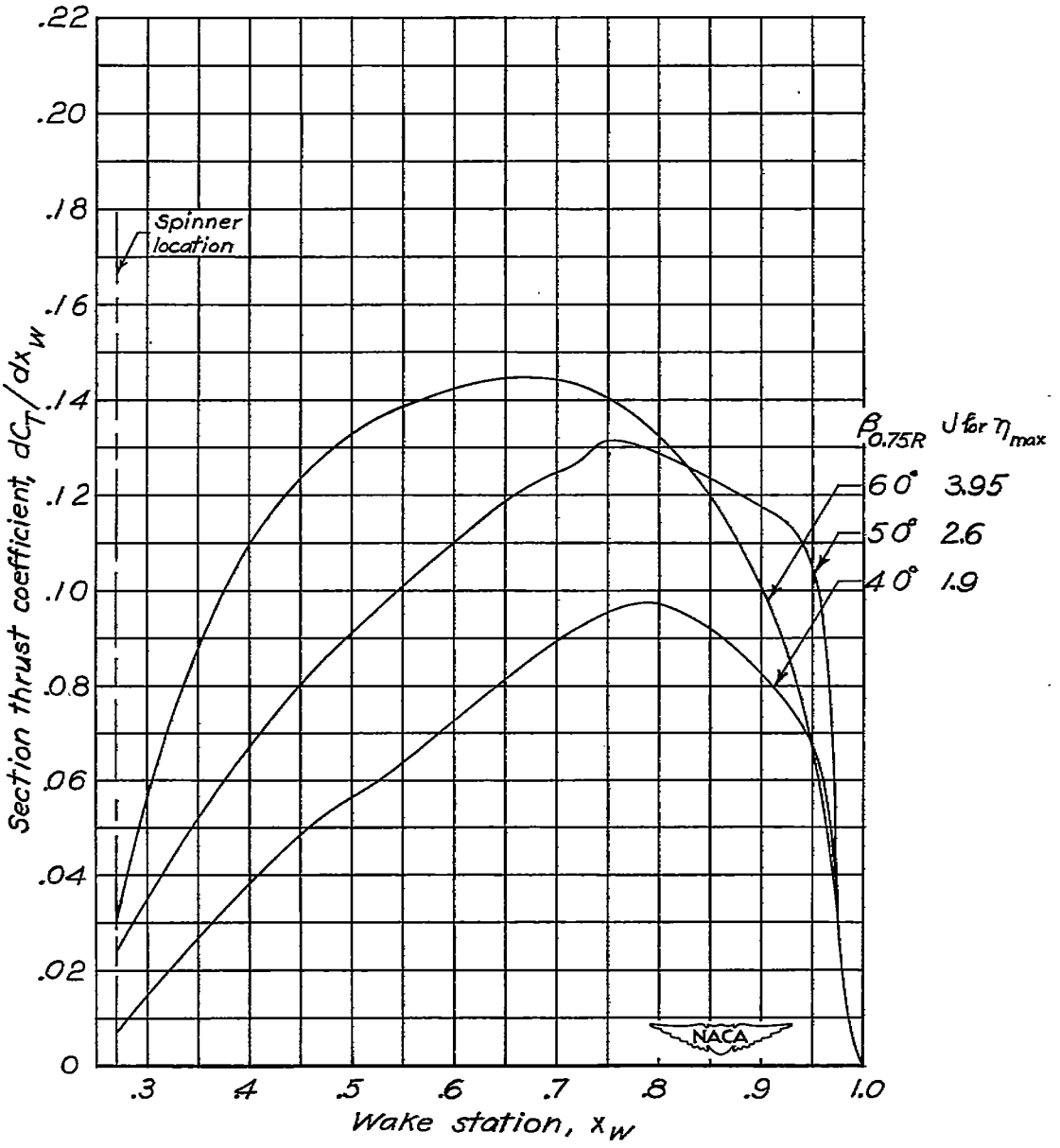

(a) M = 0.35.

Figure 10.- Effect of blade angle on section-thrust-coefficient curves for maximum efficiency. NACA 4-(5)(08)-03 propeller.

[redacted]

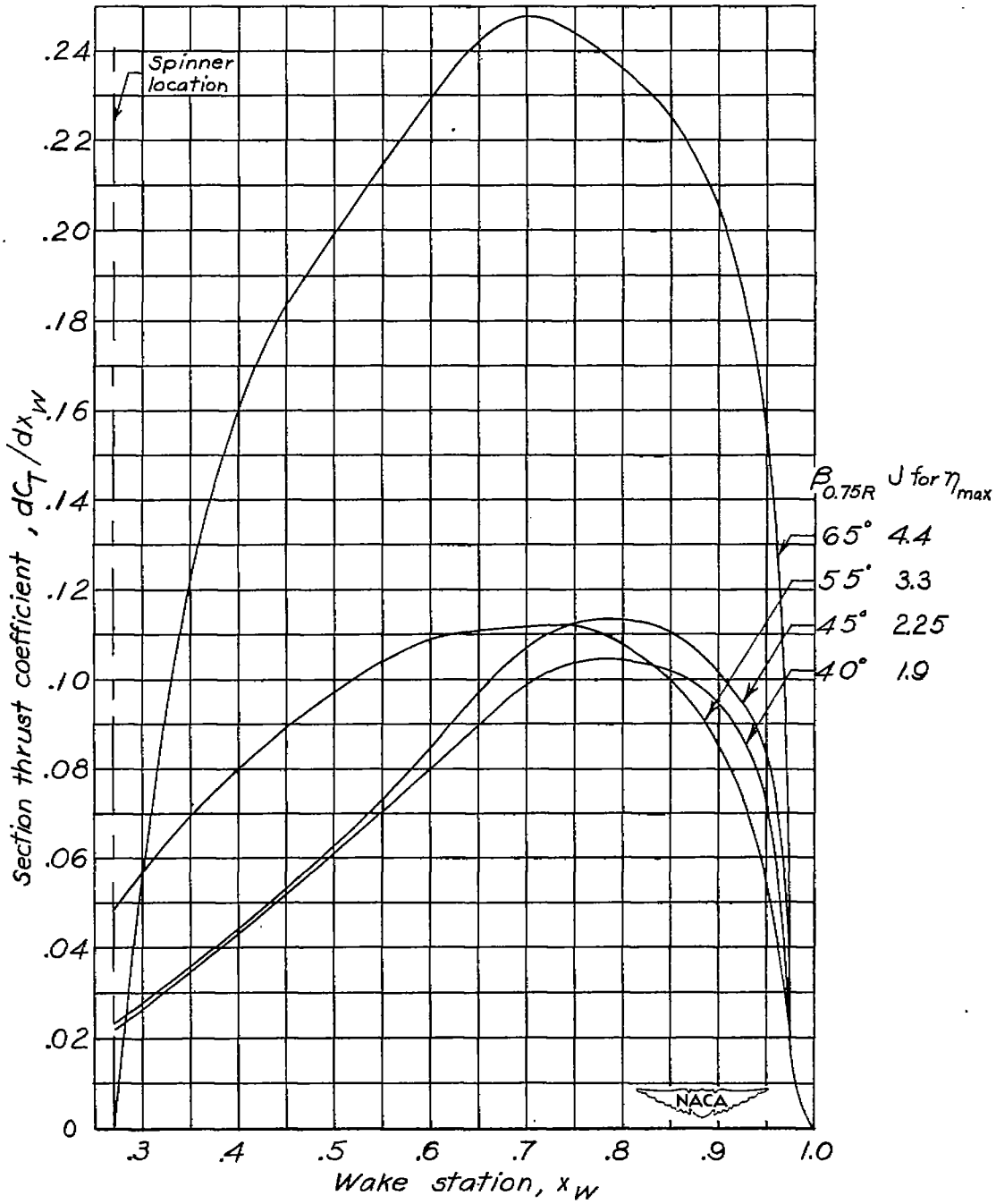

(b) M = 0.43.

Figure 10.- Continued.

[redacted]

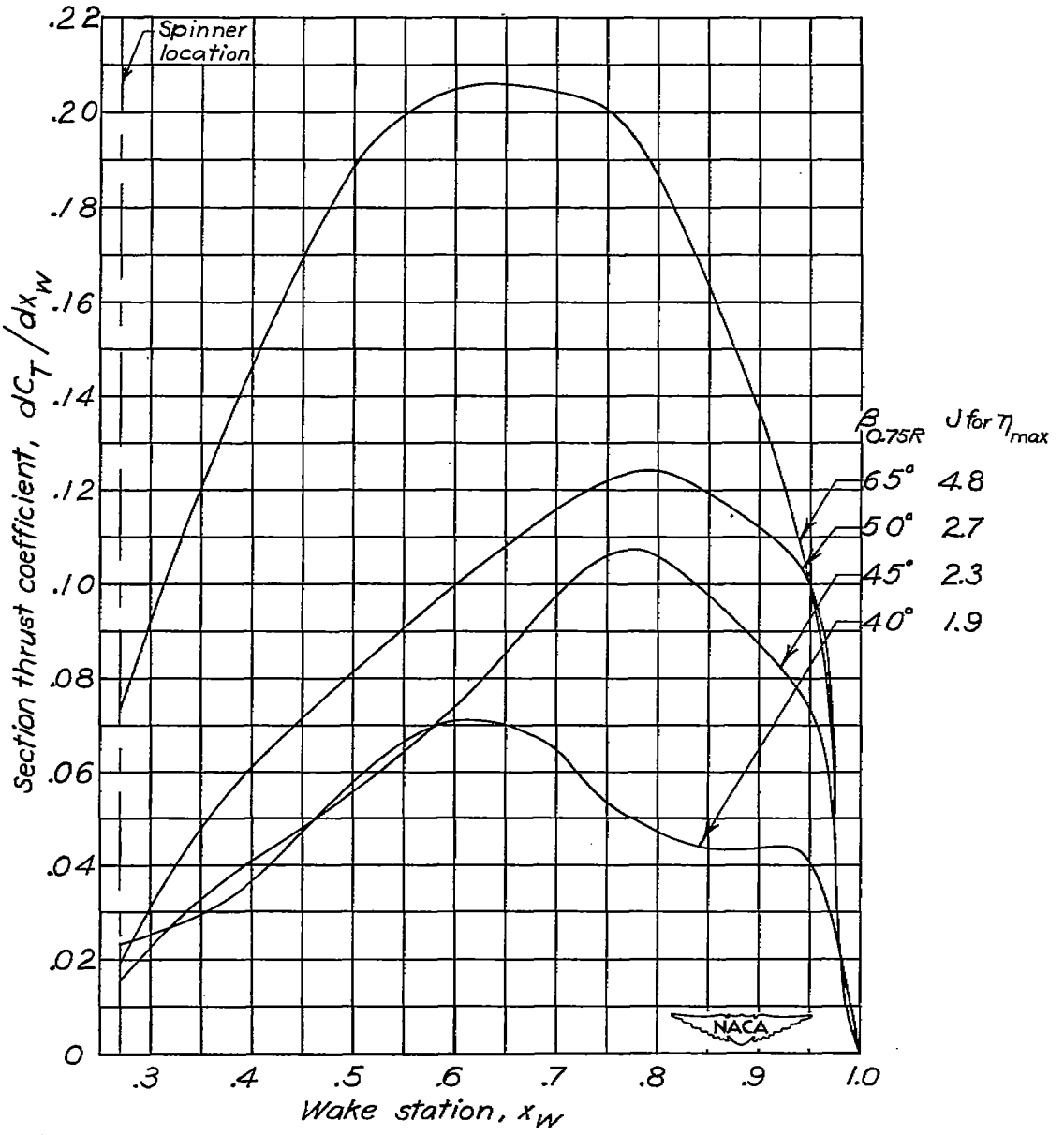

(c) M = 0.53.

Figure 10.- Continued.

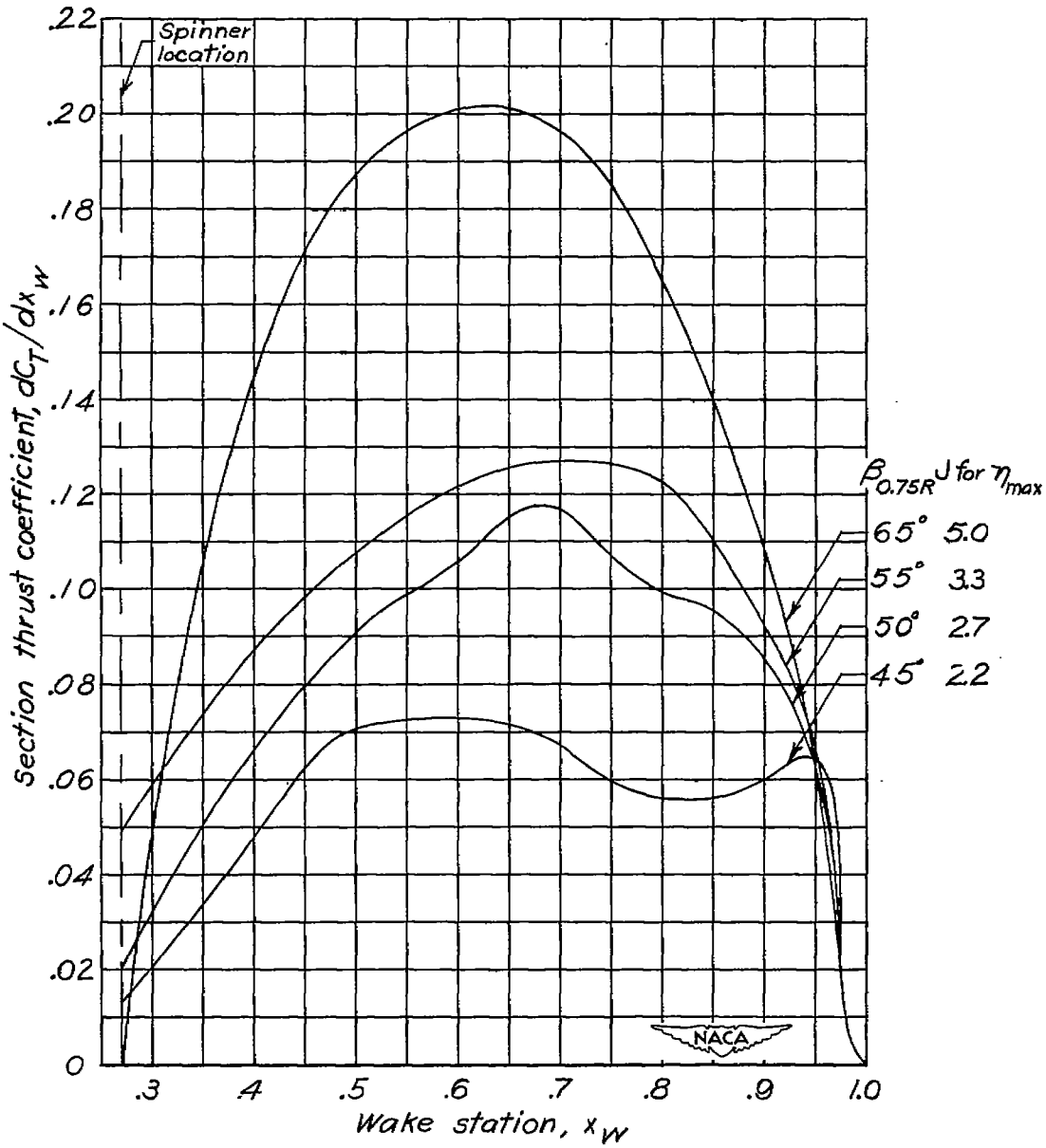

(d) M = 0.60.

Figure 10.- Continued.

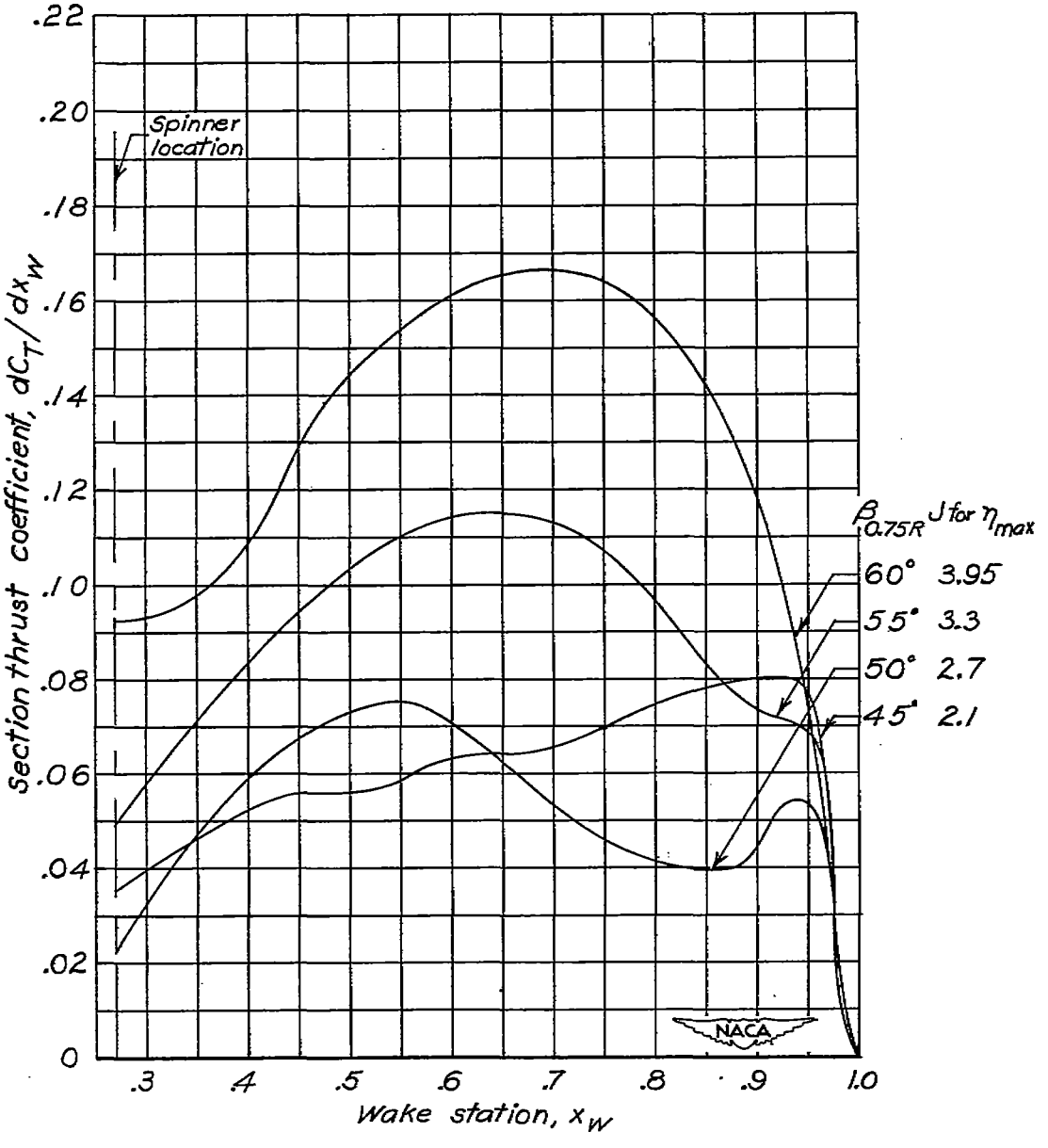

(e) M = 0.65.

Figure 10.- Continued.

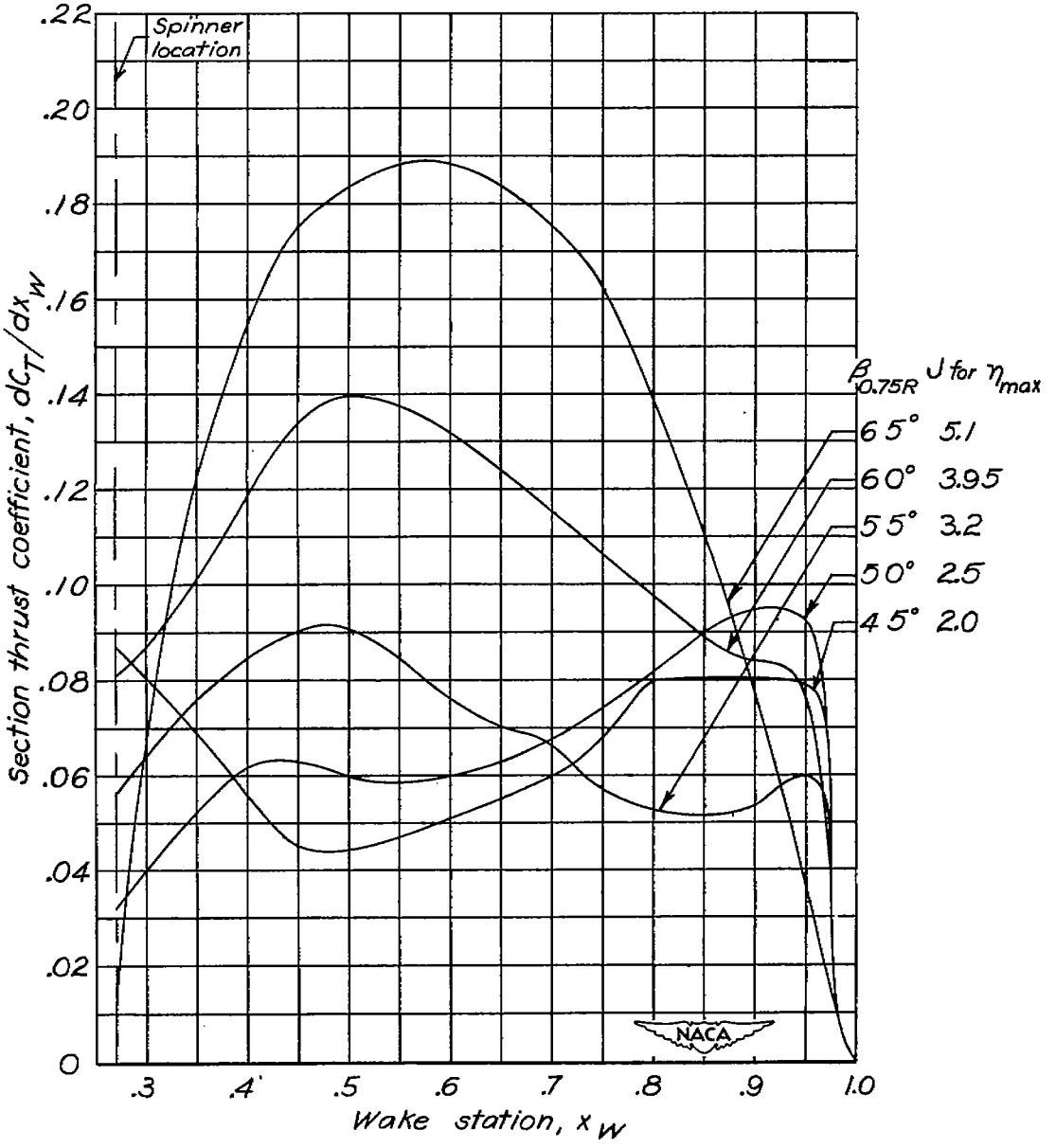

(f) M = 0.70.

Figure 10.- Continued.

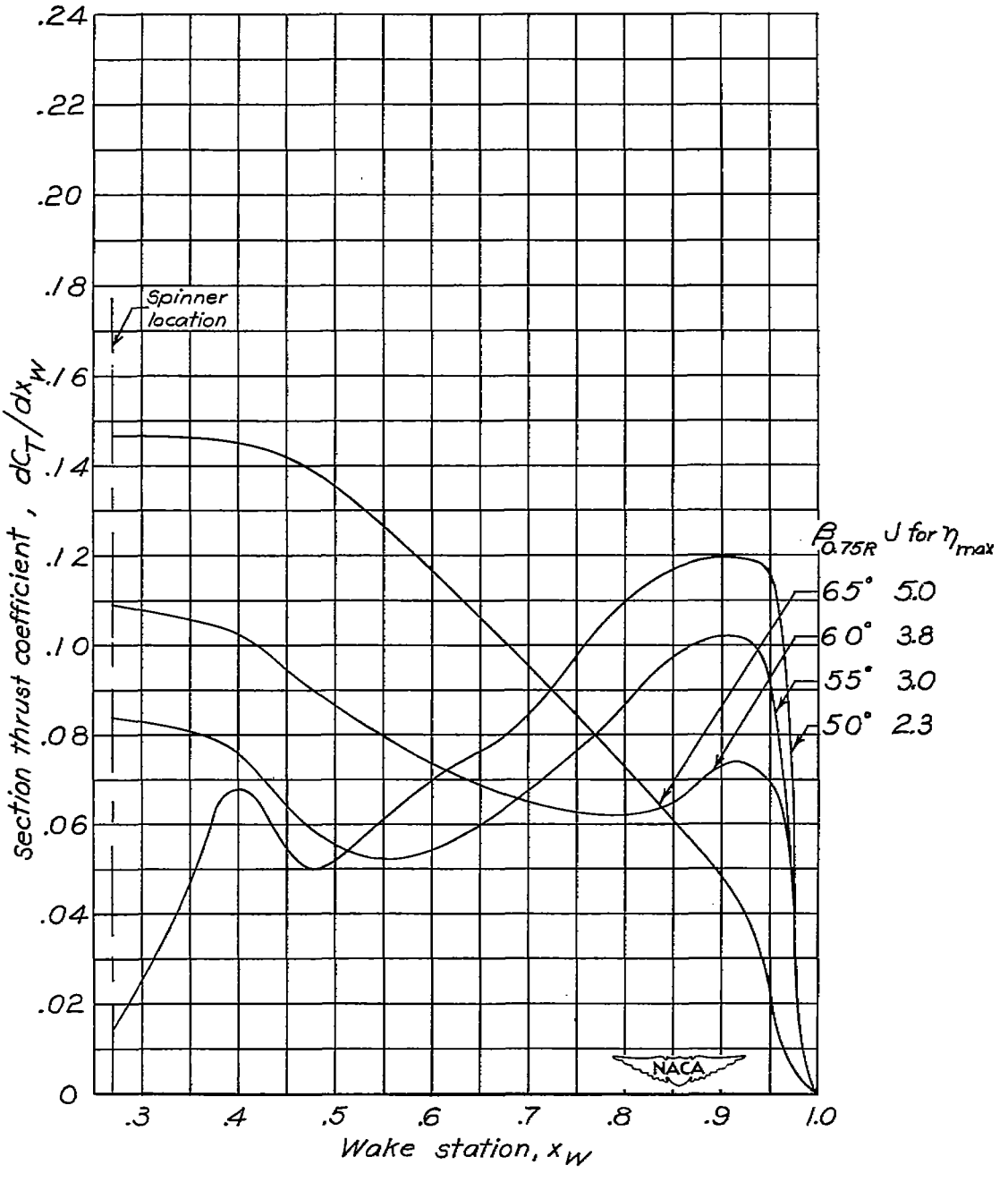

(g) M = 0.75.

Figure 10.- Continued.

[redacted]

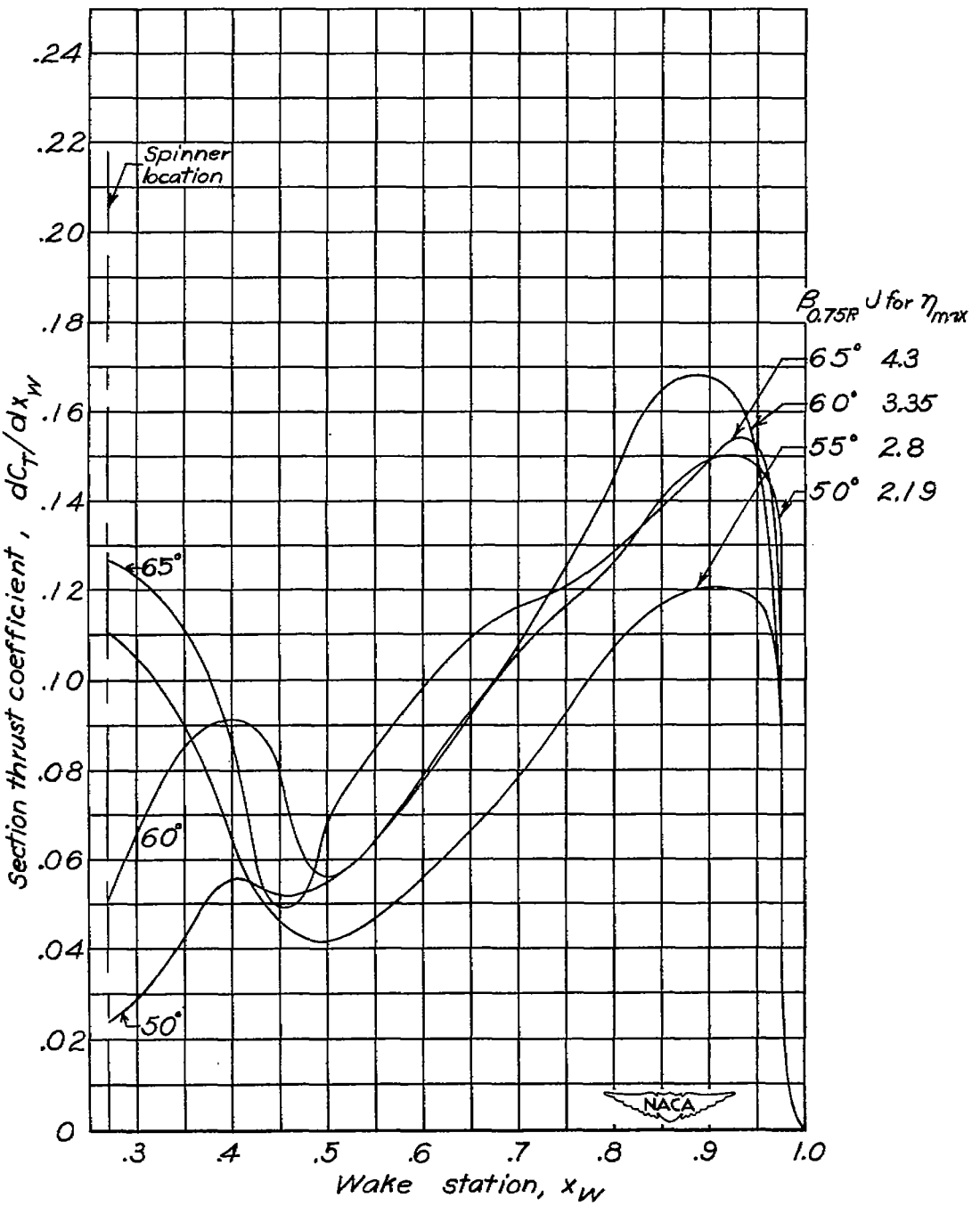

(h) M = 0.80.

Figure 10.- Continued.

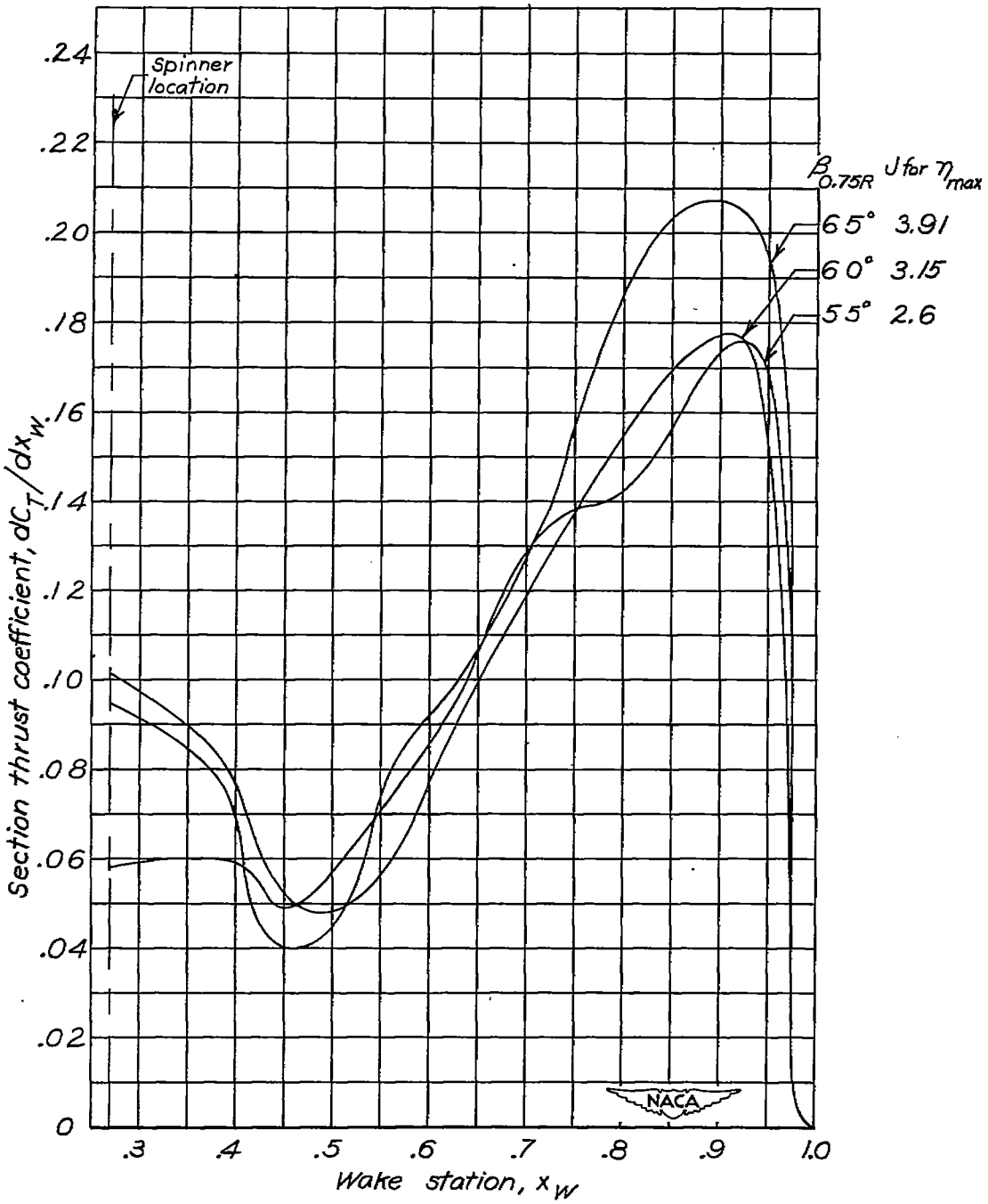

(i) M = 0.85.

Figure 10.- Continued.

[redacted]

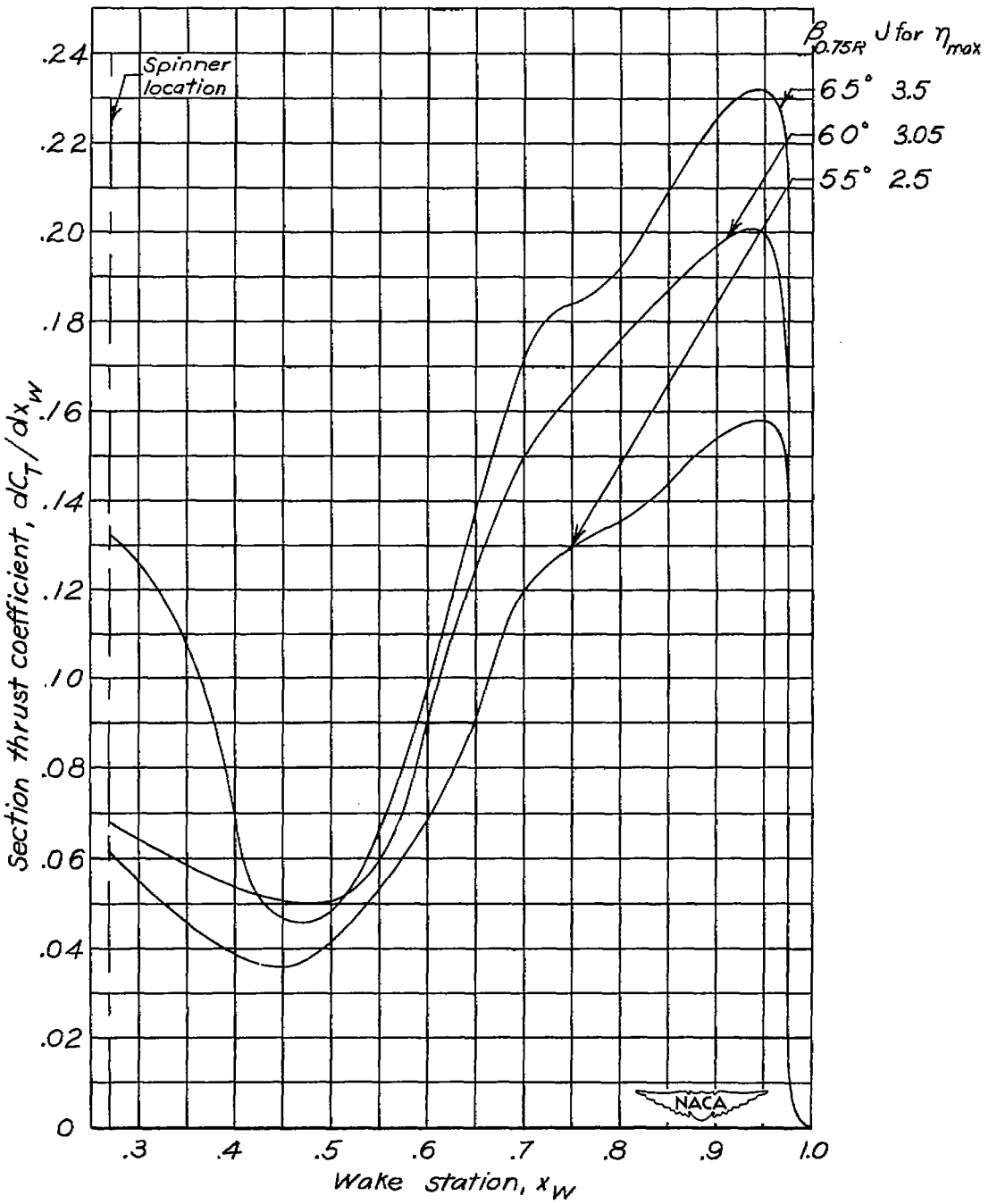

(j) M = 0.90.

Figure 10.- Continued.

[redacted]

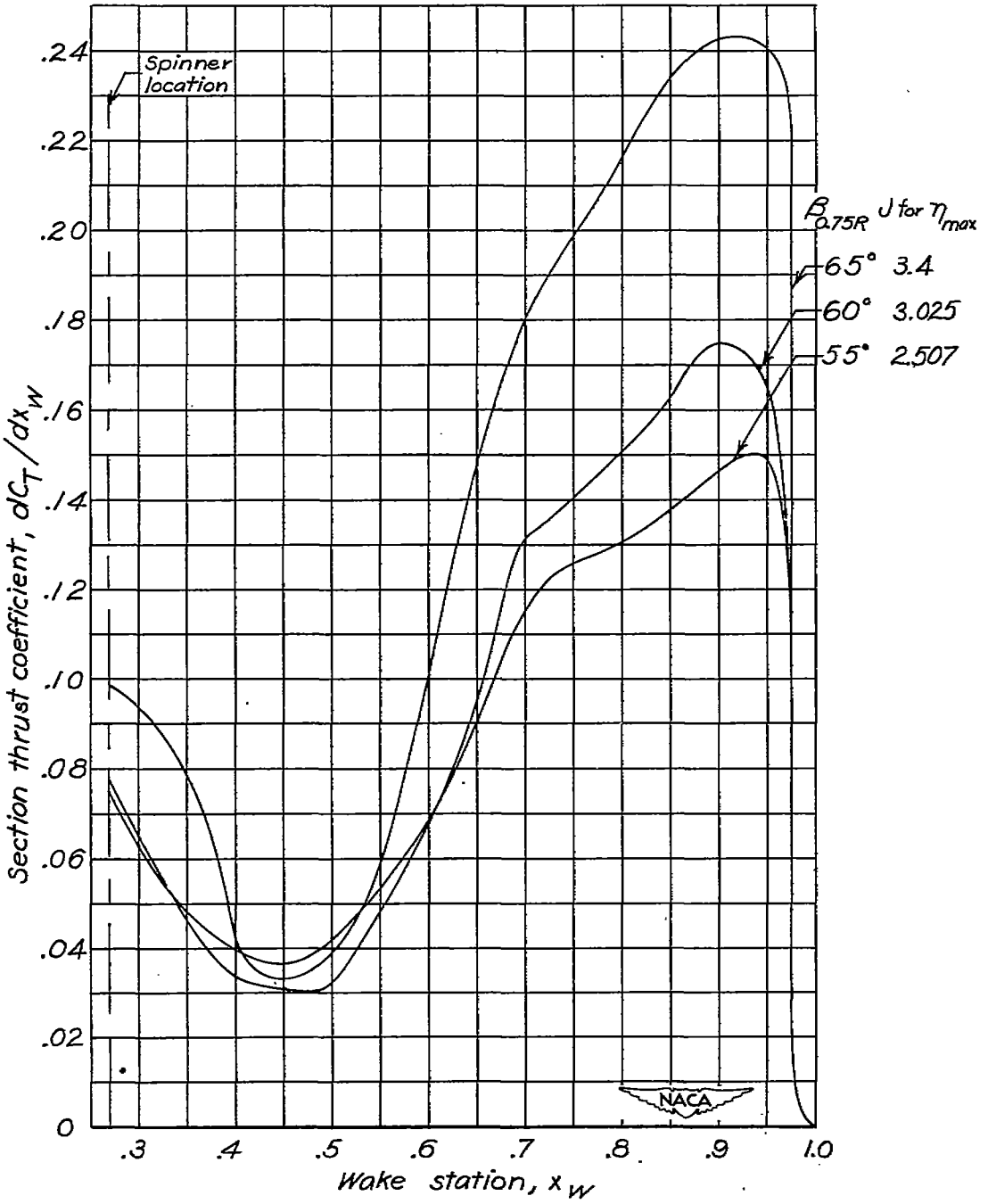

(k) M = 0.925.

Figure 10.- Concluded.

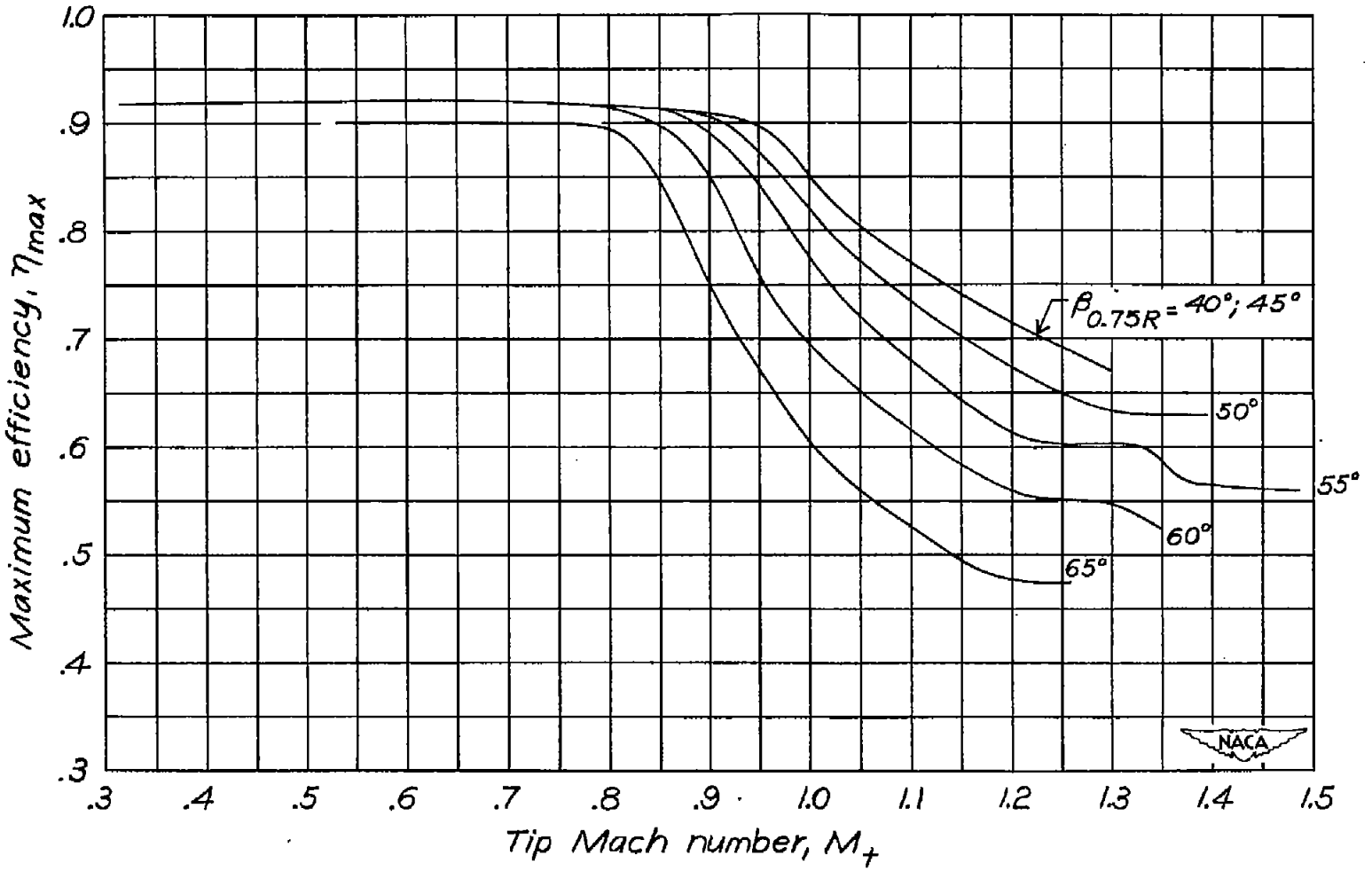

Figure 11.- Effect of tip Mach number on maximum efficiency.
NACA 4-(5)(08)-03 propeller.

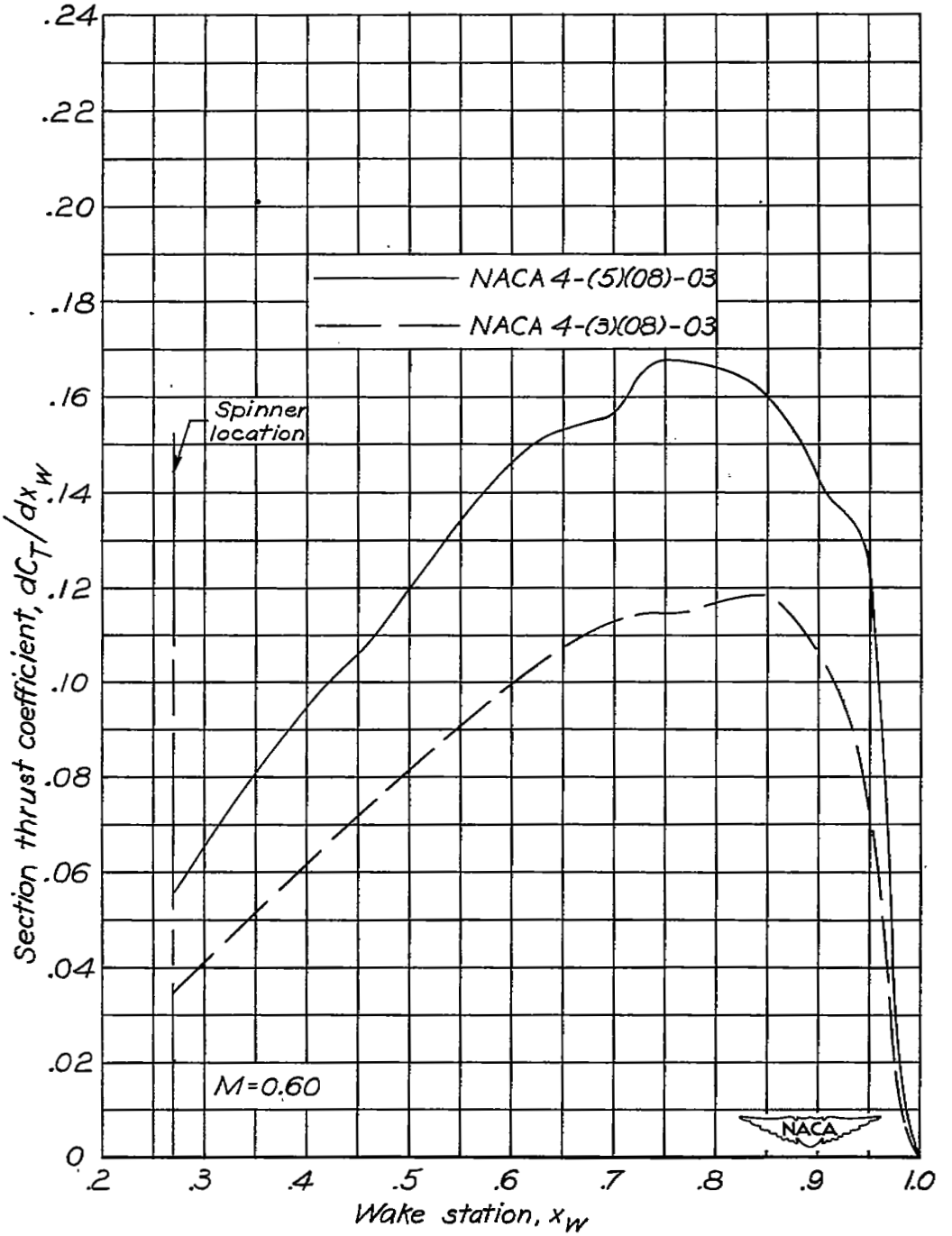

(a) $\beta_{0.75R} = 55°$; J = 3.15.

Figure 12.- Effect of camber on section thrust coefficient.

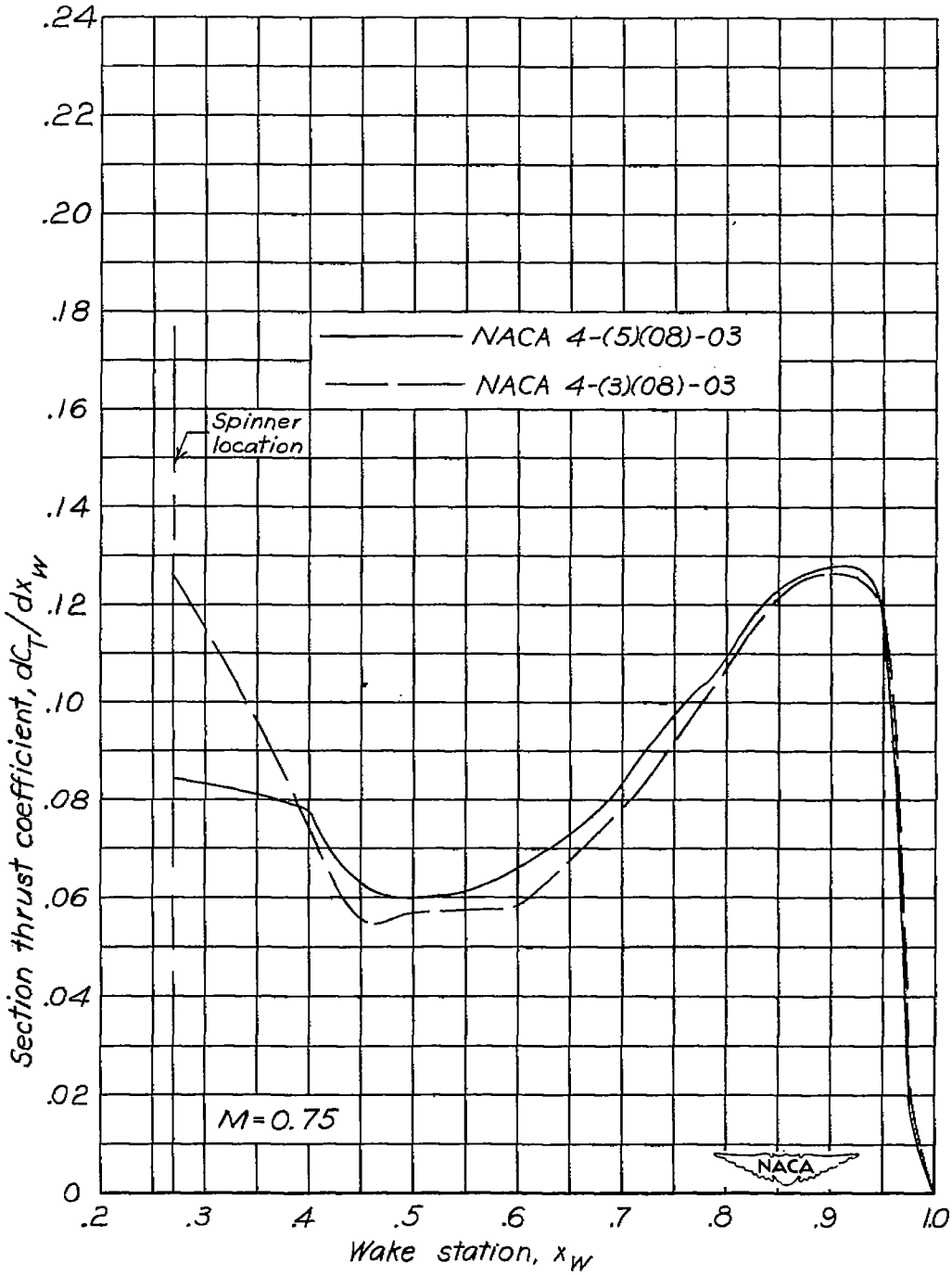

(a) Continued. $\beta_{0.75R} = 55^\circ$; J = 2.90.

Figure 12.- Continued.

[redacted]

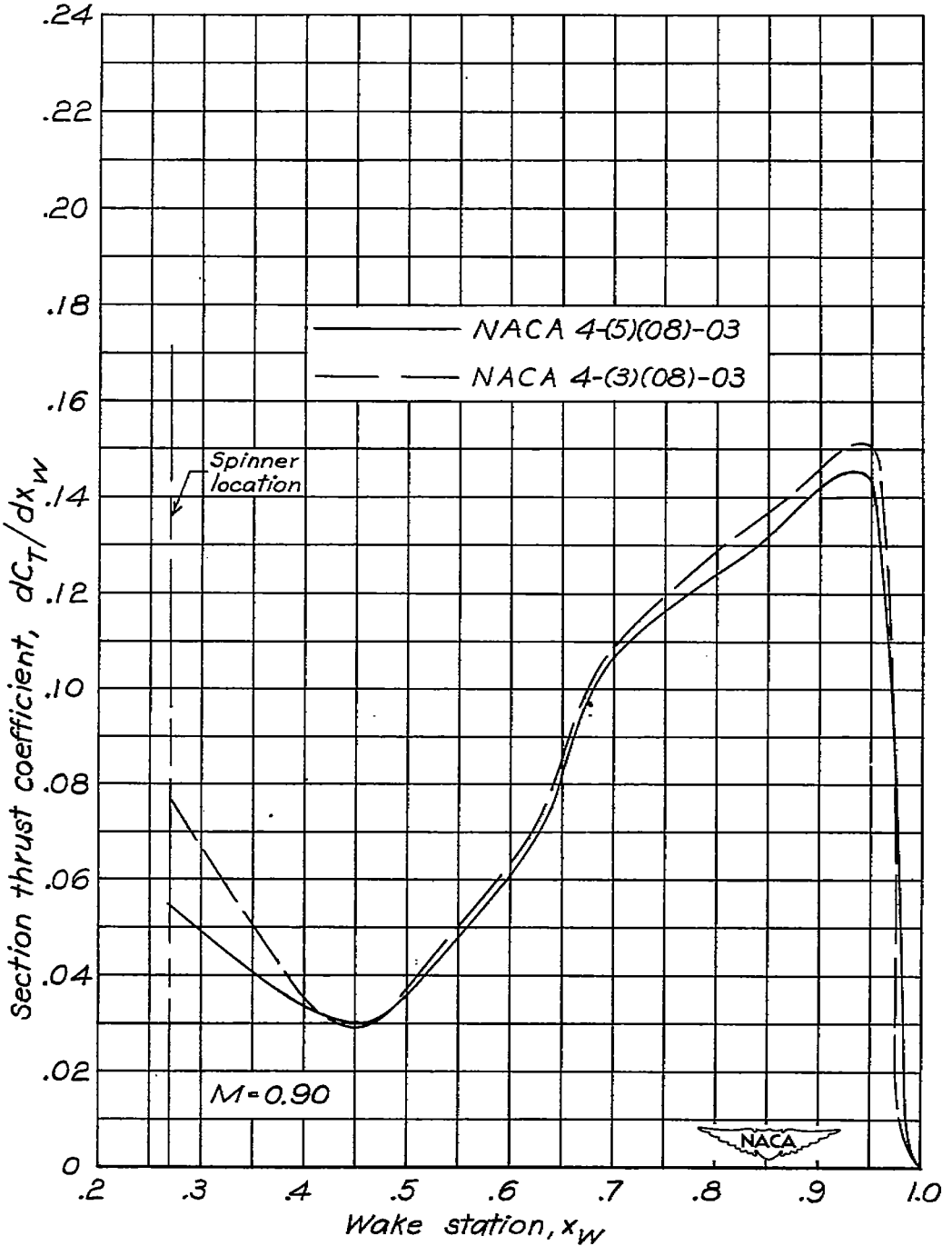

(a) Concluded. $\beta_{0.75R} = 55^\circ$; J = 2.59.

Figure 12.- Continued.

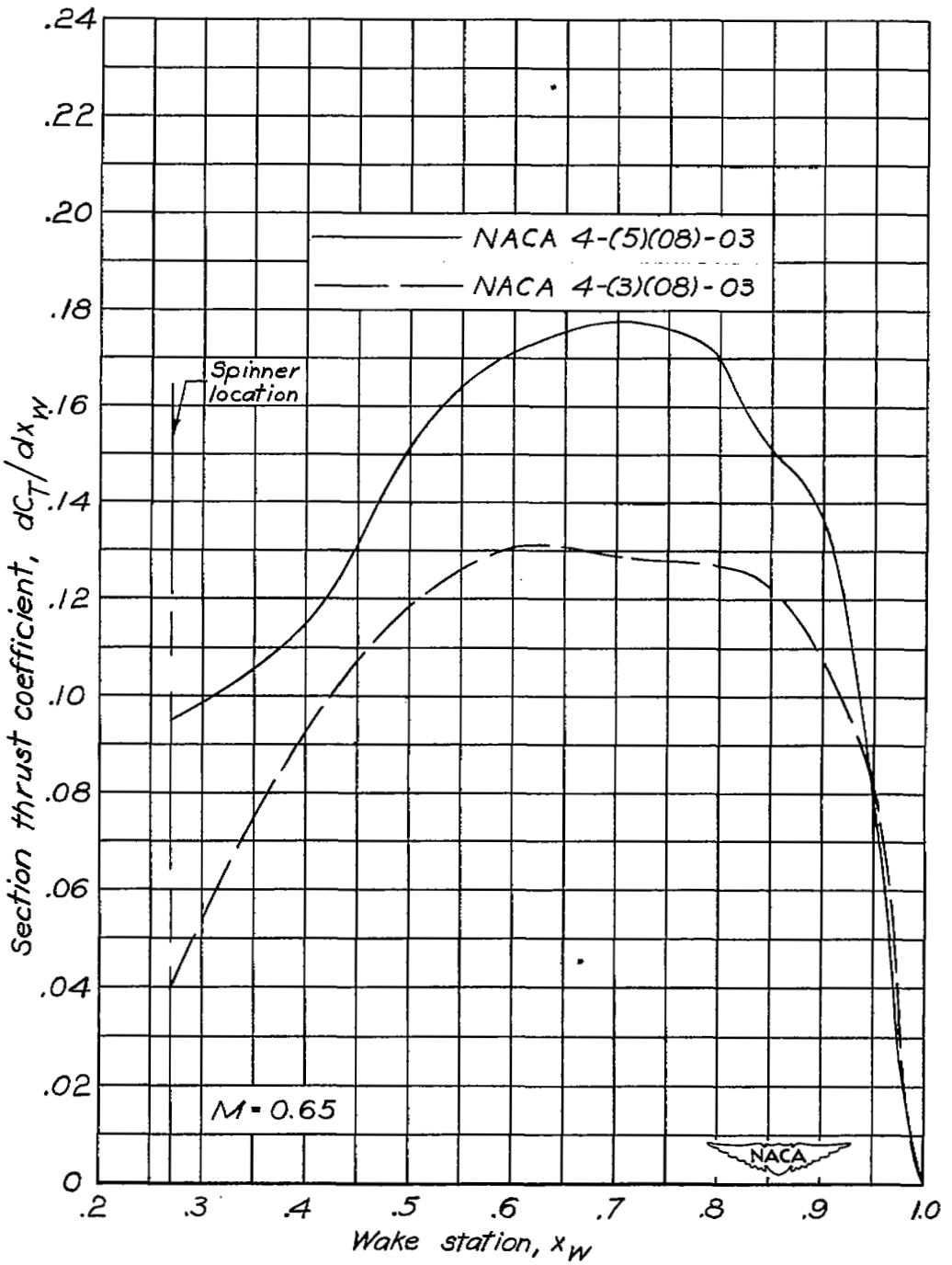

(b) $\beta_{0.75R} = 60^\circ$; J = 3.90.

Figure 12.- Continued.

[redacted]

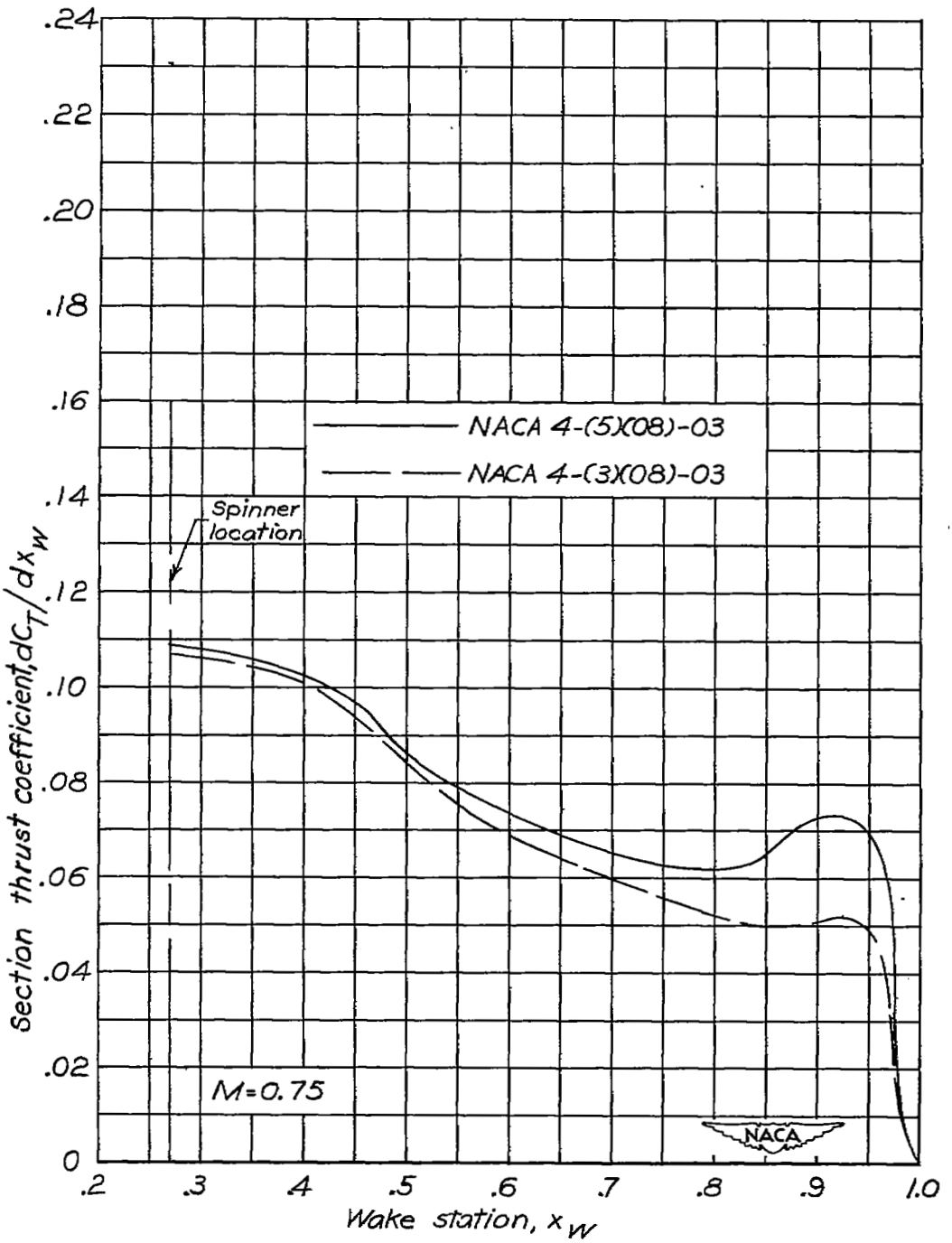

(b) Continued. $\beta_{0.75R} = 60^\circ$; J = 3.80.

Figure 12.- Continued.

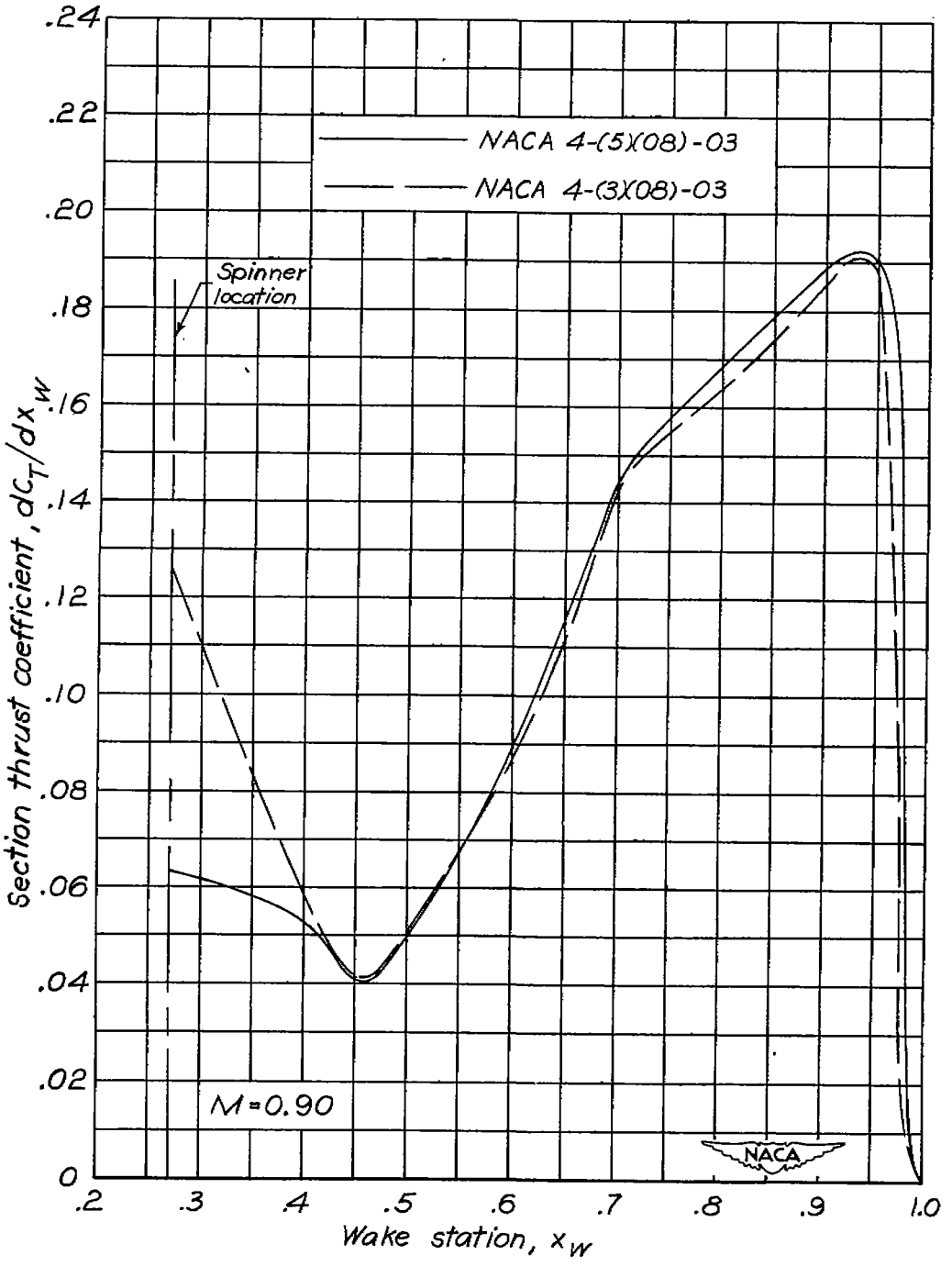

(b) Concluded. $\beta_{0.75R} = 60^\circ$; J = 3.10.

Figure 12.- Continued.

[redacted]

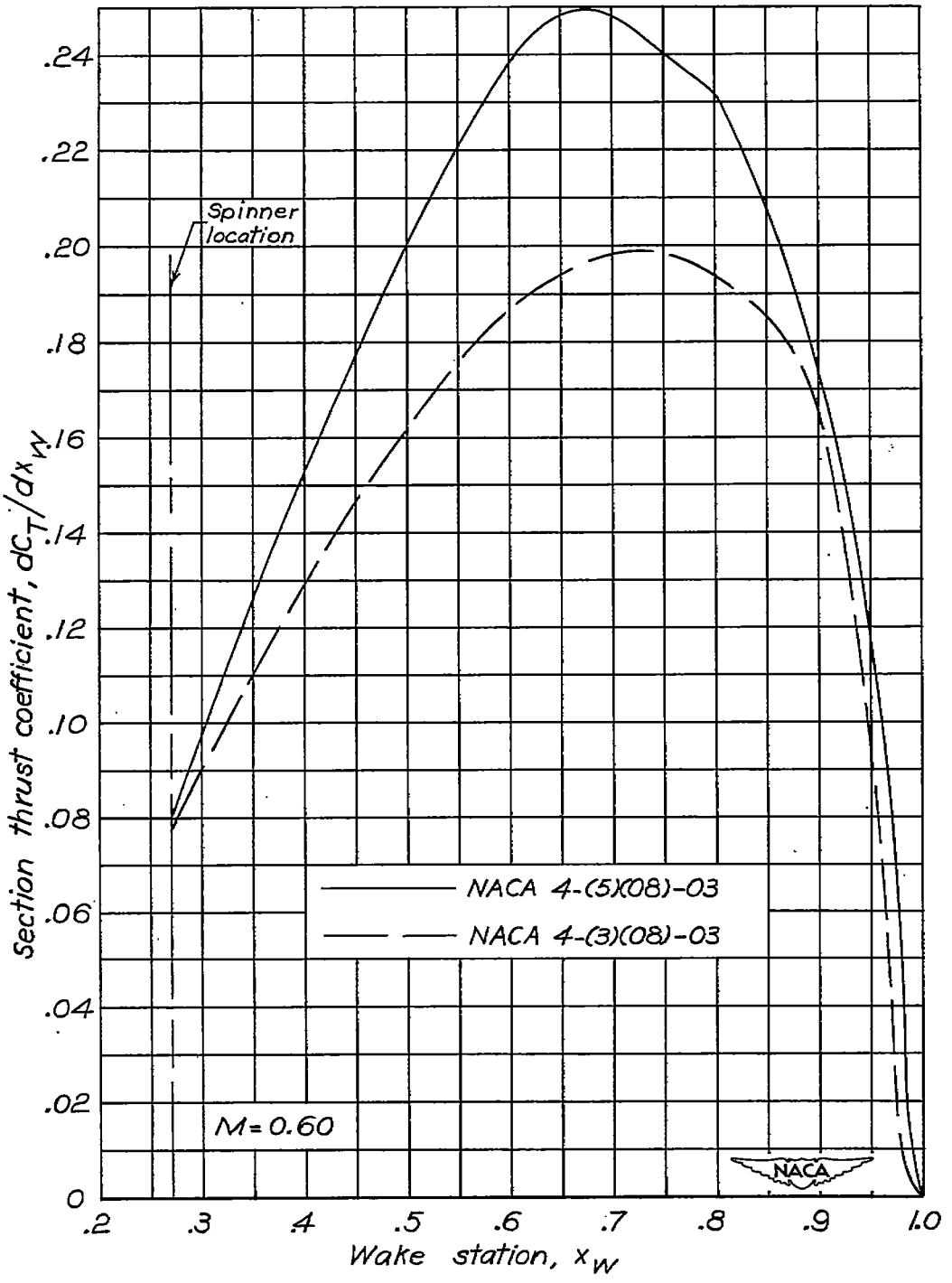

(c) $\beta_{0.75R} = 0.65°$; J = 4.60.

Figure 12.- Continued.

[redacted]

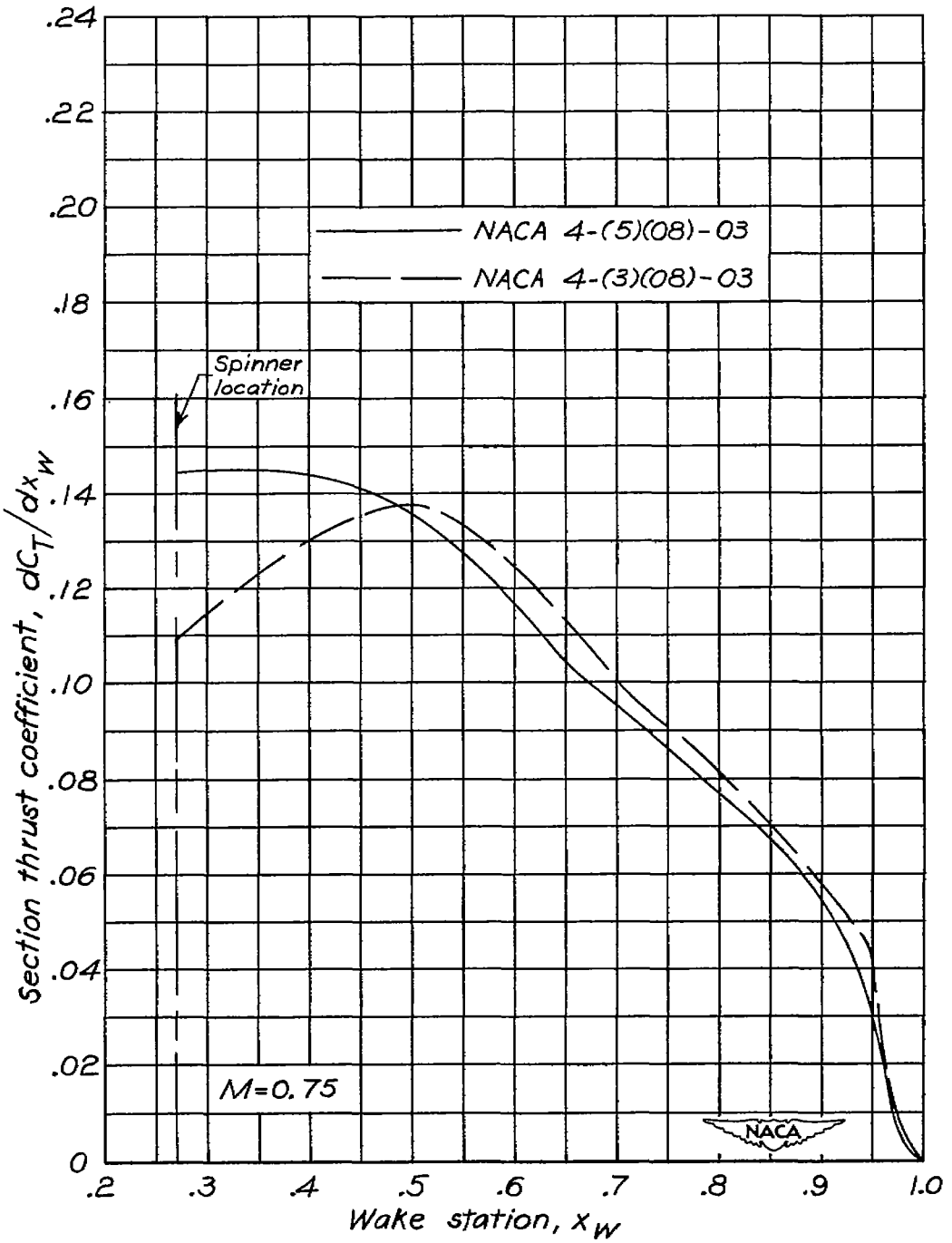

(c) Continued. $\beta_{0.75R} = 65°$; J = 4.95.

Figure 12.- Continued.

[redacted]

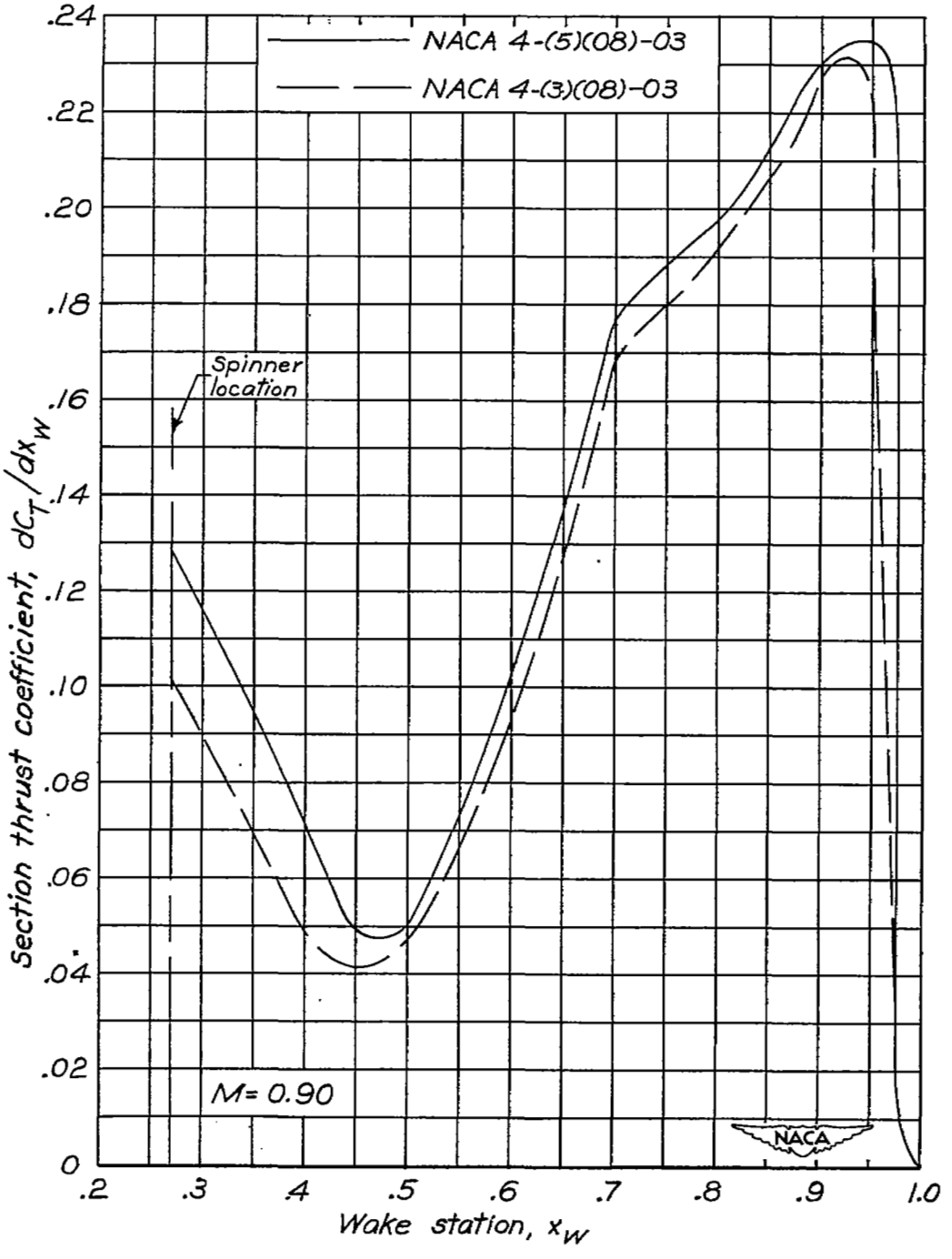

(c) Concluded. $\beta_{0.75R} = 65°$; $J = 3.45$.

Figure 12.- Concluded.

[redacted]

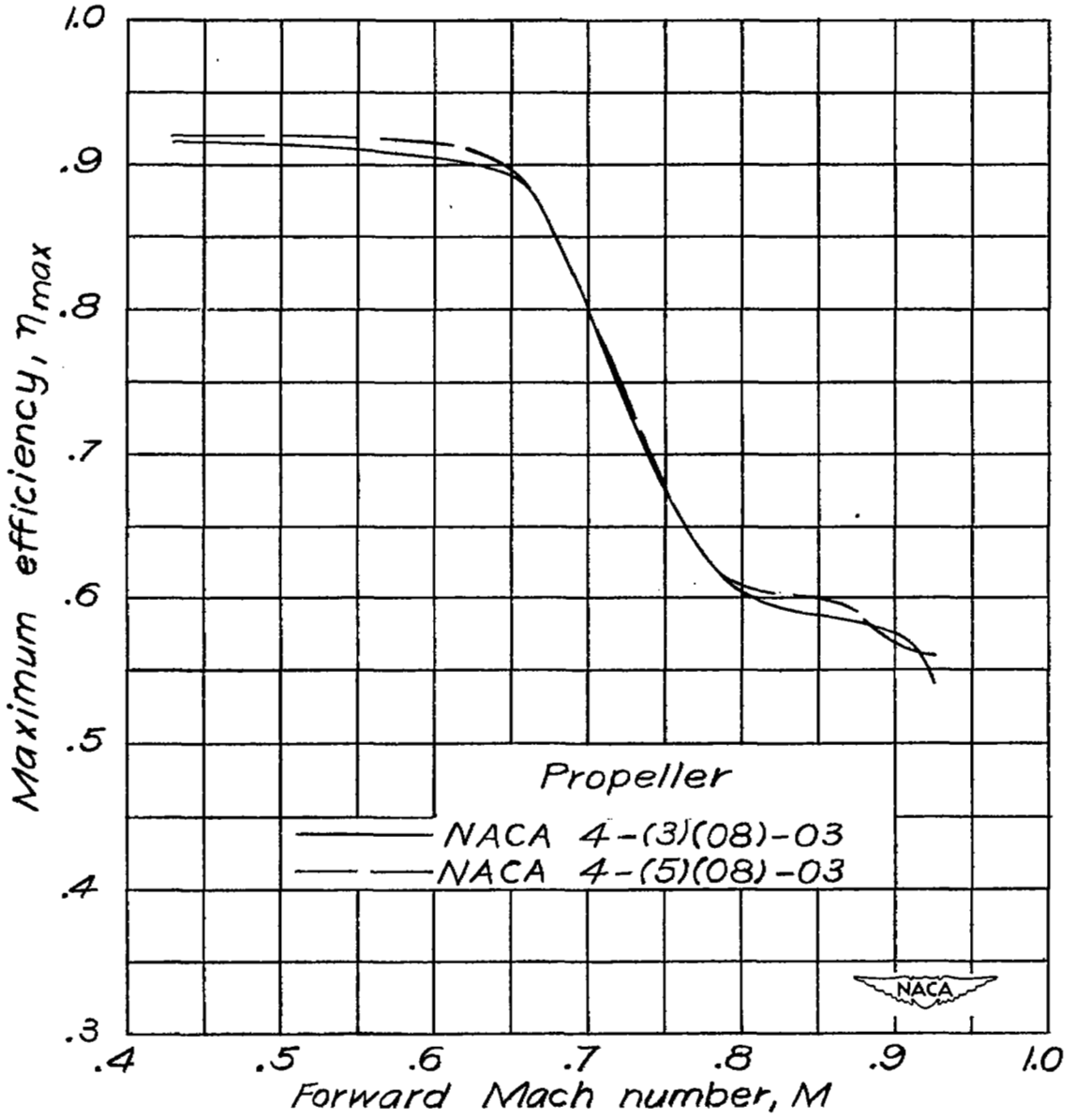

Figure 13.- Effect of forward Mach number on maximum efficiency. $\beta_{0.75R} = 55°$.

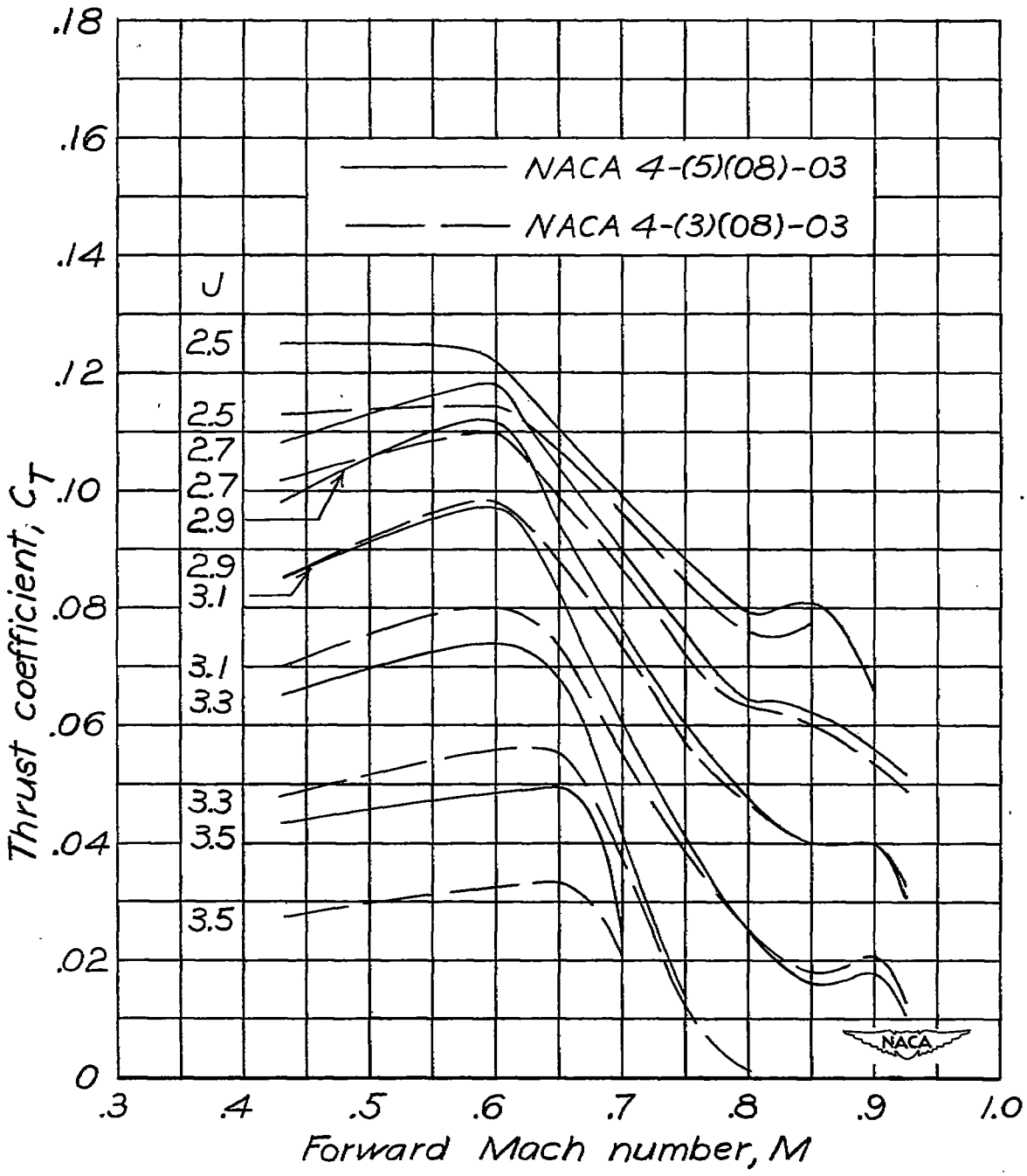

(a) $\beta_{0.75R} = 55°$.

Figure 14.- Effect of camber on thrust coefficient.

[redacted]

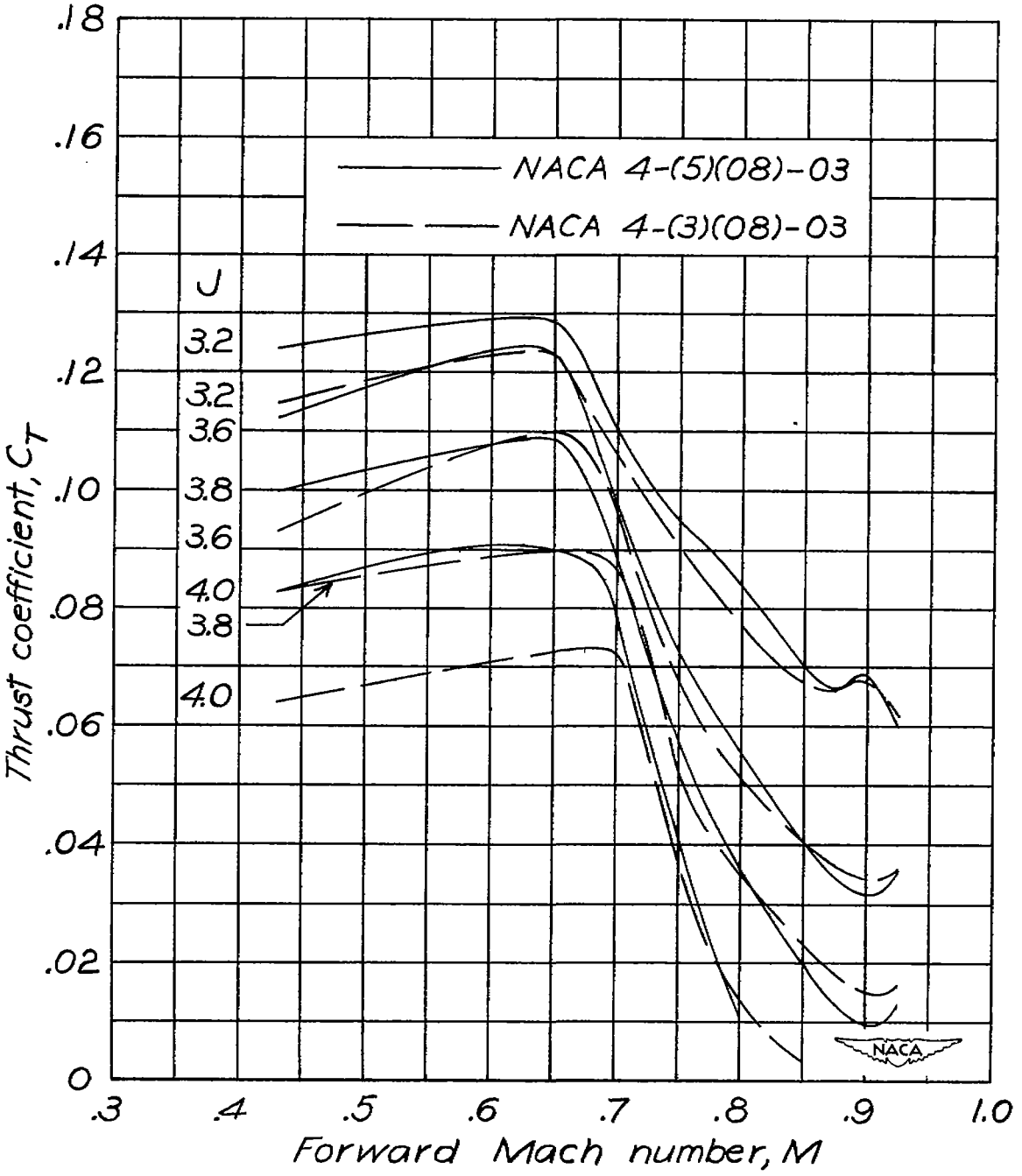

(b) $\beta_{0.75R} = 60^{\circ}$.

Figure 14.- Continued.

[redacted]

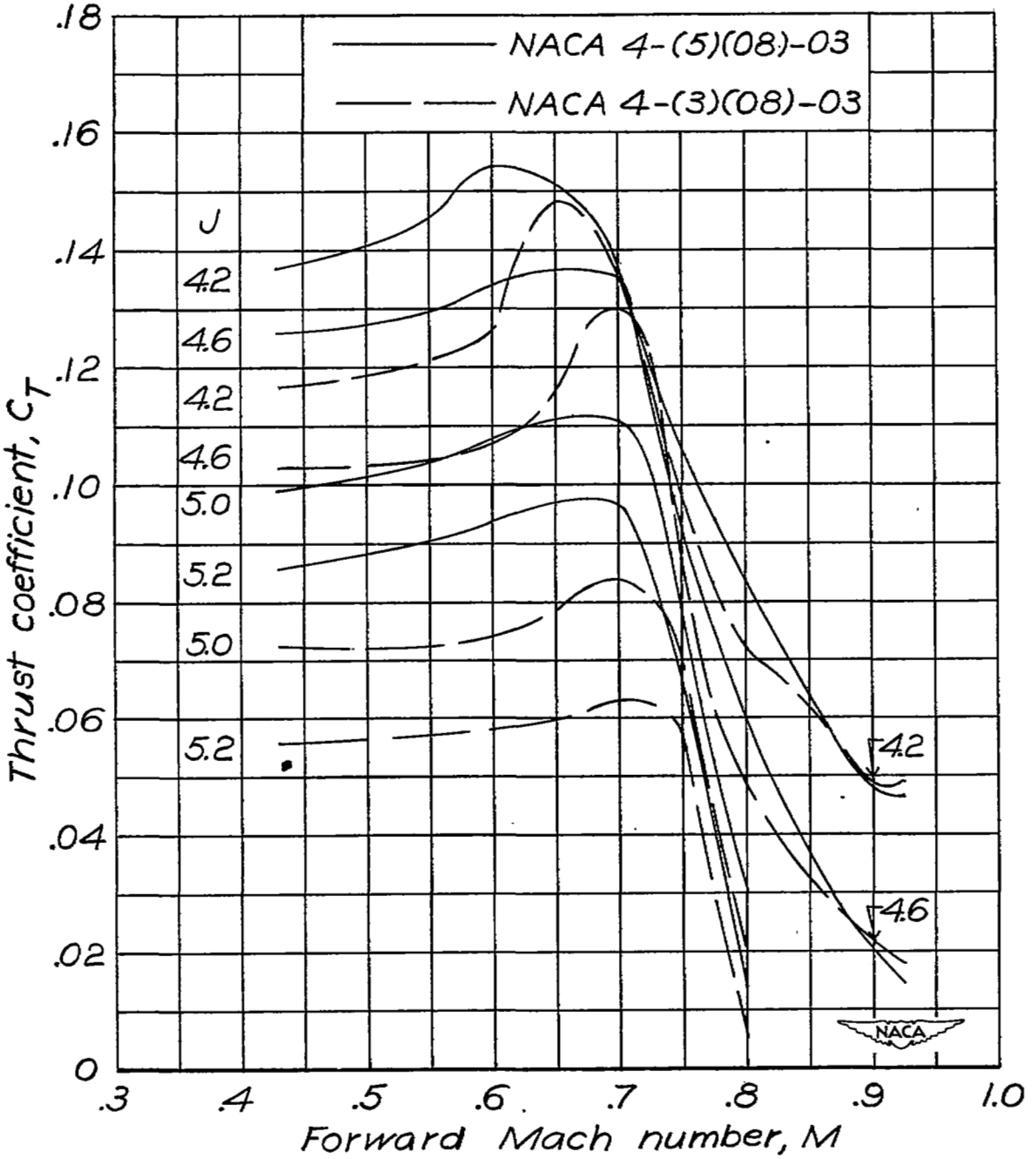

(c) $\beta_{0.75R} = 65°$.

Figure 14.- Concluded.

[redacted]

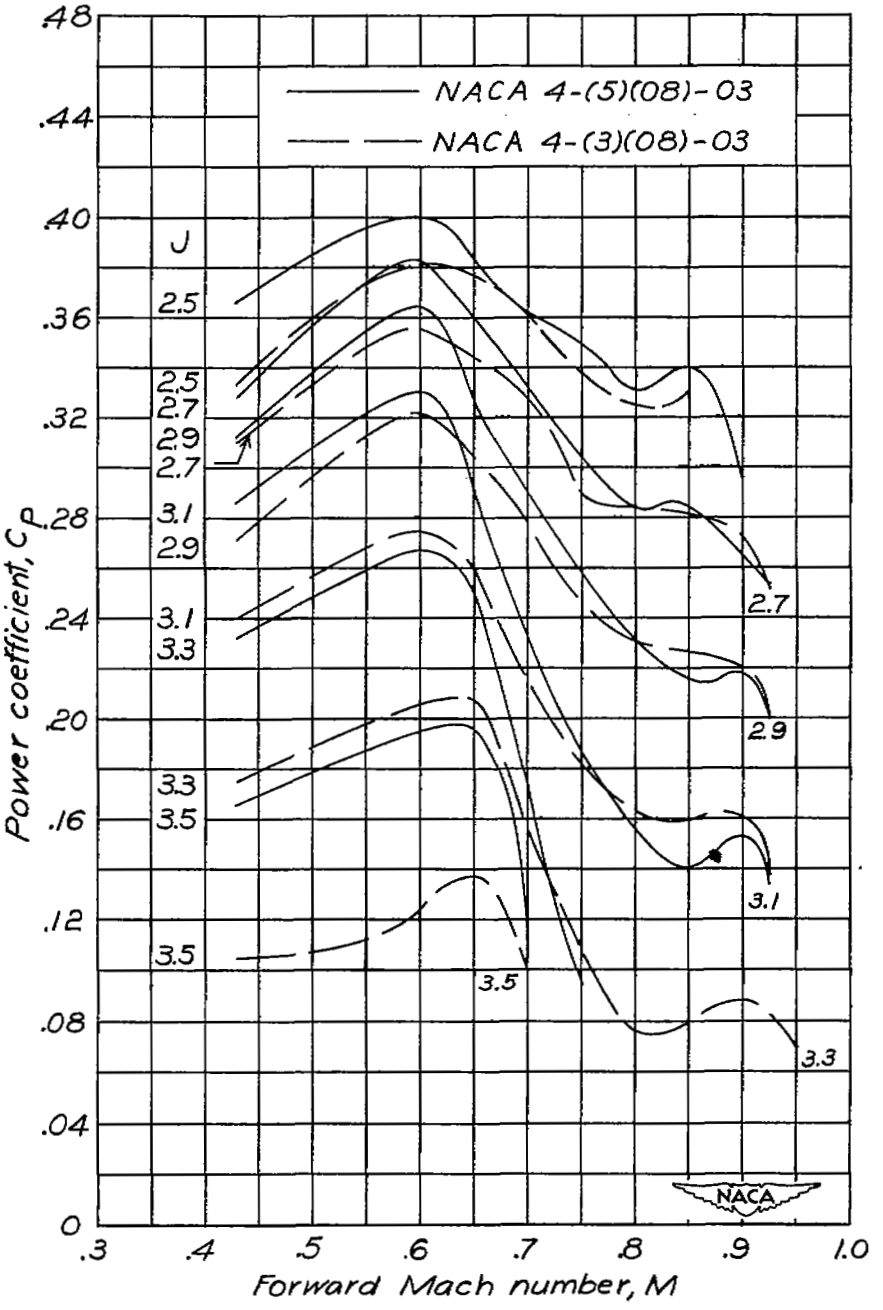

(a) $\beta_{0.75R} = 55^\circ$.

Figure 15.- Effect of camber on power coefficient.